To the Graduate Council:

I am submitting herewith a dissertation written by Latika S. R. Becker entitled "An Investigation of the Interaction of Potassium Seed and Coal Slag in the MHD Power Generator." I recommend that it be accepted in partial fulfillment of the requirements for the degree of Doctor of Philosophy, with a major in Engineering Science.

K. E. Tempelmeyer

Dr. K. E. Tempelmeyer, Major Professor

We have read this dissertation
and recommend its acceptance:

AA Mason

E C Hubschmann

Kenneth R. Kimble

Accepted for the Council:

L Evans Roth

Vice Chancellor
Graduate Studies and Research

Thes
7
.B432
cop.2

AN INVESTIGATION OF THE INTERACTION OF POTASSIUM SEED AND COAL SLAG IN THE MHD POWER GENERATOR

A Dissertation

Presented for the

Doctor of Philosophy

Degree

The University of Tennessee, Knoxville

Latika S. R. Becker

June 1977

1324189

ACKNOWLEDGEMENTS

The author wishes to express her gratitude to her advisor, Dr. K. E. Tempelmeyer, Program Manager, Energy Conversion Division, under whose directions and support the research work was carried out. Appreciation is expressed to Dr. A. A. Mason, Dr. E. C. Huebschmann, and Dr. K. Kimble for serving on the Committee.

The author wishes to express her sincere appreciation to Dr. B. H. Goethert, Dean Emeritus and Dr. J. B. Dicks, Director, Energy Conversion Division for being given the opportunity to associate with the Energy Conversion Division.

This research was supported by the Office of Coal Research, U. S. Department of the Interior, Washington, D. C., under contract number 14-32-0001-1213, as well as the Energy Research and Development Administration, Washington, D. C., under contract number EX-76-C-01-1760.

The assistance of Dr. Joel Muehlhauser, Mr. Mike Beaton, Mr. Jim Whiteford, Mr. Larry Reynolds, the late Mr. Jim Warner and the staff of the MHD laboratory is gratefully acknowledged.

The author wishes to take this opportunity to thank her past advisor Dr. V. T. Chiplonkar for introducing her to the subject of plasma physics and the principles of research work and whose constant encouragement made this research possible.

The author's research effort was greatly assisted by the help of Mrs. Helen Mason, Institute Librarian.

The author is indebted to her parents and her husband Bob for their support and encouragement.

Lastly, thanks also go to Mrs. Gottshall for typing this manuscript.

ABSTRACT

The overall efficiency of an MHD power generator depends strongly on the plasma electrical conductivity σ and magnetic field strength B through an expression σB^2. In order to increase the electrical conductivity of the combustion gas it is necessary to add some easily ionizable material to the fuel or combustion products. This material is usually referred to as seed. Potassium is preferred seed material on economic grounds for the open-cycle MHD system. However, if MHD power generation is to be commercially acceptable, seed recovery efficiencies over 90% are required. The potential loss of potassium seed into slag is a serious problem in open-cycle MHD system with high ash carryover. As a result, the slag/seed interaction and separation process is investigated here.

It has been shown that sulfur compounds react in large amounts with seed to form potassium sulfate (K_2SO_4). Seed is recovered in the form of water soluble component K_2SO_4. If the sulfur free form of seed material is used, then there will be reduction in sulfur dioxide (SO_2) concentrations in the flue gas. Tests were made with K_2CO_3 (potassium carbonate), K_2SO_4 seed and no seed coal. Eastern U. S. coal with 2.5% to 4.5% sulfur was used. All analysis and experimental results presented here correspond to an investigation of potassium seed recovery in a direct coal-fired MHD plant with total ash carryover through the generator.

Experiments consisting of many slag/seed separation and interaction test runs with and without a magnetic field in two different test systems were conducted. Two water cooled separation cyclones were

connected downstream of the generator through a simulated radiant "boiler" flow duct. Samples were taken from the bottom of the cyclones and in the cyclone exhaust. They were chemically analyzed in detail and water washed to determine the potassium seed recovery.

This investigation of potassium seed recovery indicates:

(1) High temperatures and short residence times in the flow train increases the seed recovery.

(2) The simplest method of water washing the slag/seed ash in order to extract the water soluble component in the form of K_2SO_4 can make potassium seed recovery up to 95% possible of the flyash particles.

(3) Loss of potassium in the large slag pieces (chunks) blown away from slag layers on the walls of the system is the most serious problem. However, as the overall potassium seed recovery depends upon the slag layer surface area, large-scale plant with greater volume to surface area ratios can be expected to recover higher seed than small scale plant.

(4) Presence of magnetic field may increase the seed recovery due to the suppression of flow turbulence.

(5) Experimental results show lower potassium absorption in the slag than predicted by equilibrium model. This difference is believed to be due to the kinetics of the process. Rate constants for the various reactions between slag and seed compounds is almost totally unavailable.

TABLE OF CONTENTS

CHAPTER		PAGE
I.	INTRODUCTION	1
	General Background	1
	Literature Review	7
	Current Research	15
II.	EXPERIMENTAL FACILITY	17
	Combustion Chamber and Nozzle	17
	Test System I	17
	Test System II	19
	Mass Flow Rate	21
	Channel	22
	Test System I	22
	Test System II	22
	Radiant "Boiler" Duct	24
	Test System I	24
	Test System II	25
	Cyclone Separators	28
	Test System I	28
	Test System II	28
	Instrumentation	30
	Vidar System	30
	Summary of Test Runs	31
	Sampling Train	31
	Test System I	31

CHAPTER PAGE

Test System II 34

III. SLAG/SEED SEPARATION CYCLONE PERFORMANCE 36

Slag/Seed Separation Concept 36

Cyclone Design 38

Cyclone Operational Reliability 40

Collection Efficiency 43

Characteristics of Collected Particulate Matter 45

Chemical Analysis 48

Analysis by Use of SEM and EDX 50

Formation of Slag/Seed Wall Deposits in the Radiant "Boiler" 55

Calculation of Equivalent Oxides 60

Size Distribution 66

IV. EMISSIONS FROM THE CYCLONE SEPARATION 68

Sampling Techniques and Sampling Calculations 68

Particulate Matter 68

Particulate Emission Calculations and Sampling Procedure 71

Velocity Measurements (EPA Method 2) 75

Calculations 77

Volume of Dry Gas Samples 77

Volume of Water Vapor in the Stack Gas 78

Moisture Content of Stack Gas 78

Particulate Emission Concentration 78

CHAPTER PAGE

Stack Gas Volumetric Flow Rate (EPA Method 2) 79

Isokinetic Variation 80

Characteristic of Collected Particulate Matter at the Exit of the Cyclone 82

Chemical Analysis 82

Analysis by Use of SEM and EDX 87

Calculations of Equivalent Oxides 89

Size Distribution 93

Possible Collection Methods 93

V. SEED RECOVERY 97

Introduction 97

Experimental Measurements 97

Potassium Sulfate (K_2SO_4) Seeding 99

Potassium Carbonate (K_2CO_3) Seeding 103

Effect of Temperature Variation 106

Effect of Magnetic Field 113

Effect of Residence Time in the Flow Train 115

Effect of Particle Size 115

Potassium Balance 120

VI. CONTROL OF SULFUR DIOXIDE EMISSIONS 122

Introduction 122

Sulfur Balance 122

Sulfur Dioxide (SO_2) Reduction 122

VII. DIFFUSION OF POTASSIUM (K) IN SLAG 129

Absorption of Potassium (K) Into Slag 131

CHAPTER PAGE

VIII. SUMMARY AND CONCLUSIONS 140

Analysis of Material Collected from Cyclone 140

Seed Recovery 141

Sulfur Dioxide (SO_2) Control 142

Recommendation for Future Work on the Absorption of Potassium Seed by Slag Compounds 143

BIBLIOGRAPHY 145

APPENDICES 148

APPENDIX A. CHEMICAL ANALYSIS METHODS 149

APPENDIX B. THE SCANNING ELECTRON MICROSCOPE 151

APPENDIX C. MEASUREMENT ACCURACIES 153

VITA 154

LIST OF TABLES

TABLE		PAGE
2.1	Summary of the Water-Cooled Cyclone Tests	32
3.1	Melting Points of Slag Species and Various Potassium Compounds	37
3.2	Heat Loss Results for a Cyclone	42
3.3	Collection of Ash	46
3.4	Composition of Collected Slag/Seed From Test System I and II (With K_2SO_4 and K_2CO_3 Seed)	49
3.5	Comparison of Composition of Collected Slag/Seed With K_2SO_4 and K_2CO_3 Seed in Test System I (B-Field On)	51
3.6	Comparison of Composition of Collected Slag/Seed With K_2SO_4 and K_2CO_3 Seed in Test System II (No B-Field)	52
3.7	Potassium and Sulfate Concentration of Wall Samples in Test System I and II for K_2SO_4 Seeding	57
3.8	Slag/Seed Oxide and Sulfate Composition Calculated From Laboratory Analysis With K_2SO_4 Seed for Test System I and II	64
3.9	Slag/Seed Oxide and Sulfate Composition Calculated From Laboratory Analysis With K_2CO_3 Seed for Test System I and II	65
4.1	Slag/Seed Cyclone Emissions Tests Downstream of the MHD Generator	72
4.2	Slag/Seed Cyclone Emissions Tests Downstream of the MHD Generator	81
4.3	Composition of the Sampled Flyash at the Exit of the Cyclone From Test System I and II (With K_2SO_4 and K_2CO_3).	83

TABLE		PAGE
4.4	Comparison of Composition of Collected Flyash at the Exit of the Cyclone With K_2SO_4 and K_2CO_3 Seed in Test System I ($B \neq 0$) and Test System II ($B=0$)	85
4.5	Potassium and Sulfate Concentration of Samples in Test System I ($B \neq 0$) and Test System II ($B=0$) for K_2SO_4 and K_2CO_3 Seeding	86
4.6	Slag/Seed Oxide and Sulfate Composition Calculated From Laboratory Analysis With K_2SO_4 Seed for Test System I and II	91
4.7	Slag/Seed Oxide and Sulfate Composition Calculated From Laboratory Analysis With K_2CO_3 Seed for Test System I and II	92
5.1	Percentage of Water Soluble Component From Collected Slag and Flyash Samples	98
5.2	Comparison of Composition of Collected Slag/Seed From Test System I and II (With K_2SO_4 Seed and No B-Field)	109
5.3	Comparison of Composition of Collected Slag/Seed From Test System I (B-Field On) and II (No B-Field) With K_2SO_4 Seed	114
6.1	Sulfur Balance (K_2CO_3 Seed)	123
6.2	Removal of Sulfur Compounds in MHD Generation With K_2CO_3 Seed	123
7.1	Dependence of Temperature T on Residence Time τ for 60 K CAL Energy of Activation	133
7.2	Comparison of Experimental Results With Equilibrium Calculations for Potassium Loss	139

LIST OF FIGURES

FIGURE		PAGE
1.1	Reaction of Potassium Seed With Sulfur	3
1.2	Allowable Potassium Seed Loss for MHD Power Generation by Balancing Seed Cost Against Plant Efficiency	4
1.3	The Range of Equilibrium Calculations	9
1.4	Equilibrium Adsorption of Potassium by Coal Ash Slag . .	9
1.5	Diffusion Characteristics	13
1.6	Diffusion Times into Spherical and Flat Plate Geometries	13
2.1	Experimental Test Facility	18
2.2	A Combination of a Combustor - Test System I	20
2.3	A Combination of a Combustor - Test System II	20
2.4	Channel From Both Test Systems	23
2.5	30° Inclined Radiant Boiler, Test System I	26
2.6	A Radiant "Boiler" Flow Duct, Test System II	26
2.7	Schematic of Radiant Boiler, Test System II	27
2.8	Two Water-Cooled Cyclones	29
2.9	Schematic of Particulate Sampling Train, Test System I .	33
2.10	Schematic of Particulate Sampling Train, Test System II	35
3.1	Uncorrected Gas Temperature at Cyclone Entrance	39
3.2	Gas Temperature (Corrected) in the MHD Flow Train System II for a Typical Run	41
3.3	Conversion of Ash in Coal/Seed to Ash + Flyash	44
3.4	Particulate Dust Formed Under MHD Conditions Removed From Bottom of Cyclone, Unwashed (Run 1437)	53

FIGURE PAGE

3.5 Particulate Dust Removed From Bottom of Cyclone, Unwashed (Run 71) 53

3.6 Micrograph of Cyclone-Collected Dust With K_2CO_3 Seeding and Short-Circuit Operation 55

3.7 EDX Analysis With K_2CO_3 Seed for Dust Collected by Cyclone 55

3.8 Interior of Radiant Boiler Showing Slag Coating 58

3.9 Layer Separation in Slag Coating at the Entrance of the Radiant Boiler 59

3.10 An EDX Scan of Layer No. 1 59

3.11 EDX Analysis of Layer at the Entrance of the Radiant Boiler 59

3.12 An EDX Analysis of a Radiant Boiler Slag Layer From Test System I 61

3.13 Layer Separation in the Slag Coating at the Splitter Plate Wall 62

3.14 EDX Analysis of Slag Layer at the Splitter Plate Wall . . 62

3.15 Size Distribution of Cyclone Collected Ash From Both Test Systems 67

4.1 Schematic Illustration of Isokinetic and Non-Isokinetic Sampling. 69

4.2 Sampling Box Assembly Showing Impingers and Filter - Test System II 74

FIGURE		PAGE
4.3	A Sketch Showing Circular Stack Divided Into Six Traverse Points According to EPA Rules	76
4.4	Particulate Dust Formed Under MHD Conditions and Collected at the Exit of the Cyclone by a Fiberglas Filter, Unwashed (Run 1437)	88
4.5	Particulate Dust Collected at the Exit of the Cyclone by a Fiberglas Filter, Unwashed (Run 54) Test System II . .	88
4.6	EDX Analysis With K_2CO_3 Seed for Particulate Collected at the Cyclone Exit	90
4.7	Size Distribution of Flyash Leaving the Cyclone	94
5.1	Particulate Dust From Bottom of Cyclone After Warm-Water Washing (Run 1437)	101
5.2	Particulate Dust From Bottom of Cyclone After Warm-Water Washing (Run 71)	101
5.3	Solid Material Resulting From Water Washing of Dust Taken From Bottom of Cyclone (Run 1437)	102
5.4	EDX Scan of Soluble Dust Taken From Bottom of Cyclone (Run 71) Test System II	102
5.5	EDX Scan of Soluble Dust at the Cyclone Exit (Run 54) Test System II	102
5.6	EDX Analysis With K_2CO_3 Seed for Particulate Collected From the Bottom of the Cyclone (Run 1440) Test System I . . .	104
5.7	EDX Analysis With K_2CO_3 Seed for Particulate Collected at the Bottom of the Cyclone (Run 58) Test System II	104

FIGURE		PAGE
5.8	Formation of Sodium Sulfate From Sodium Chloride and Sulfur Dioxide	105
5.9	Energy Distribution of Molecules	107
5.10	Effect of Temperature on Potassium Seed Recovery. Solid Symbols - B-Field, Open Symbols - No B-Field (K_2SO_4)	110
5.11	Effect of Temperature on Potassium Seed Recovery. Solid Symbols - B-Field, Open Symbols - No B-Field (K_2CO_3)	110
5.12	Comparison of Experimental Results With the Predicted Equilibrium Model	112
5.13	Effect of Flow Residence Time on Seed Recovery	116
5.14	SEM Photo of Cyclone Collected Dust, 6240X (Unseeded Coal Run)	118
5.15	Potassium Recovery at 1400°K, K_2CO_3 Seed With Magnetic Field	121
6.1	Variation of K With S	125
6.2	Effect of Temperature on SO_2 Control, Test System II	125
6.3	Reduction of SO_2	126
6.4	Effect of Velocity on SO_2 Reduction	126
7.1	Diffusion Coefficients of Calcium and Silicon in a Slag	132
7.2	Diffusion Into Spherical Droplet	135
7.3	Diffusion Into Two-Dimensional Wall Thickness	136
7.4	Diffusion Times Into Spherical and Two-Dimensional Surface	137

NOMENCLATURE

A	Cross-sectional area of stack
A_n	Cross-sectional area of the probe inlet
B	Magnetic field
B_{wo}	Moisture content in stack gas
C_s'	Particulate emissions concentration
$\bar{c}$	Mean concentration of diffused specie
C_o	Equilibrium value of the surface concentration
C_p	Pitot tube coefficient
D	Diffusion constant
D_o	Pre-exponential factor
EDX	X-ray energy dispersive
$\bar{h}$	Heat transfer coefficient
ΔH	Average pressure drop across the orifice meter
ℓ	Thickness of the slag layer
$\dot{m}$	Mass flow rate
M_n	Total amount of particulate matter collected
M_s	Molecular weight of stack gas (wet basis)
M_d	Molecular weight of stack gas (dry basis)
M_{H_2O}	Molecular weight of water
P	Pressure
P_{std}	Standard absolute pressure

P_{bar}	Barometric pressure at the outlet of the orifice meter
P_s	Absolute stack gas pressure
ΔP	Velocity pressure
Q	Adsorption energy
$\dot{Q}$	Rate of heat loss by the gas
Q_s	Average volumetric flow rate
R	Ideal gas constant
R	Radius of spherical droplet
SEM	Scanning electron microscope
T	Temperature
T_a	Temperature at the exterior metal wall of the radiant boiler
T_b	Temperature in the ceramic in the radiant boiler
T_c	Temperature at the surface of the cooling tubes in the radiant boiler
T_{gas}	Gas temperature
T_w	Wall temperature
T_s	Stack gas temperature
T_m	Average dry gas meter temperature
T_{std}	Standard absolute temperature
t_r	Flow residence time
t	Time
V_s	Average stack gas velocity
$V_{m_{std}}$	Volume of dry gas sampled and corrected to standard conditions
V_m	Volume measured by the dry gas meter

$V_{n_{std}}$ Volume of water vapor in the stack gas at standard conditions

V_{lc} Total volume of liquid collected in impingers and silica gel

Greek Symbols

η_{MHD} Efficiency of MHD power plant

η_{CONV} Efficiency of conventional steam plant

θ Total sampling time

ρ_{H_2O} Density of water at standard conditions

τ Time of adsorption

τ_o Time of vibration of the constituent molecules

CHAPTER I

INTRODUCTION

General Background

The direct coal-fired open-cycle magnetohydrodynamic (MHD) electrical power generation may play a significant role in the near future in meeting the increasing demands for the electrical power, not only because coal is the most abundant fossil fuel in the U. S. but also because of its high thermodynamic efficiency and that it can considerably reduce air pollution due to sulfur dioxide (SO_2) emissions.

In an MHD power generation plant combustion is carried out at higher temperatures than would normally occur in a conventional steam plant. Temperatures in the range of 2500°K to 3000°K are required. A material with a low ionization potential is added to the combustion gas to achieve the necessary electrical conductivity. This "seed" material (usually a potassium compound) loses its electrons and the combustion gas becomes a weak conductor of electricity. Since it is necessary to employ high temperatures for MHD power generation, to achieve an acceptable degree of ionization in the gas, the thermal efficiency of the MHD generator is potentially higher than that of a conventional plant.

These MHD power generators offer a unique means of controlling sulfur emissions from their effluent gases because of the affinity of the potassium (ionizing additive-seed material) for sulfur. Potassium seed materials added to the fuel react with sulfur dioxide, resulting from

a sulfur impurity from coal, to form potassium sulfate, thus reducing SO_2 concentrations in the flue gas.

Because of their high cost, the seed material must be recovered and recycled back to the MHD generator. Figure 1.1, taken from Reference 1, illustrates the amount of potassium which is needed to react with various amounts of sulfur in the coal. It is observed that the normal seeding range required for MHD is sufficient to react the sulfur dioxide formed in coals having up to 4% sulfur. It is possible to operate on high sulfur coals.

Allowable seed loss for various costs and seed is calculated by using the following equation:

$$\frac{\text{cost of coal}}{\eta_{CONV}} = \frac{\text{cost of coal}}{\eta_{MHD}} + \frac{\text{cost of seed x(\% seed loss) x 0.1}}{\eta_{MHD}}$$

Efficiency of the conventional steam plant η is taken as 40% while for the MHD power plant it is taken as 50%. Figure 1.2(a) and 1.2(b) show a plot of the percent allowable potassium carbonate (K_2CO_3) loss as a function of the coal cost for various costs of K_2CO_3 and for an overall plant thermal efficiency of 50%. Figure 1.2(a) corresponds to no sulfur content in the coal and Figure 1.2(b) is for high sulfur content coal. Figure 1.2(c) illustrates for different percent of sulfur content in the coal, the MHD efficiency which needs to be achieved if the cost of coal is \$33/metric ton and the cost of K_2CO_3 is \$1.21/Kg. From these plots, it is seen that for recent costs of coal at \$27.5/metric ton and

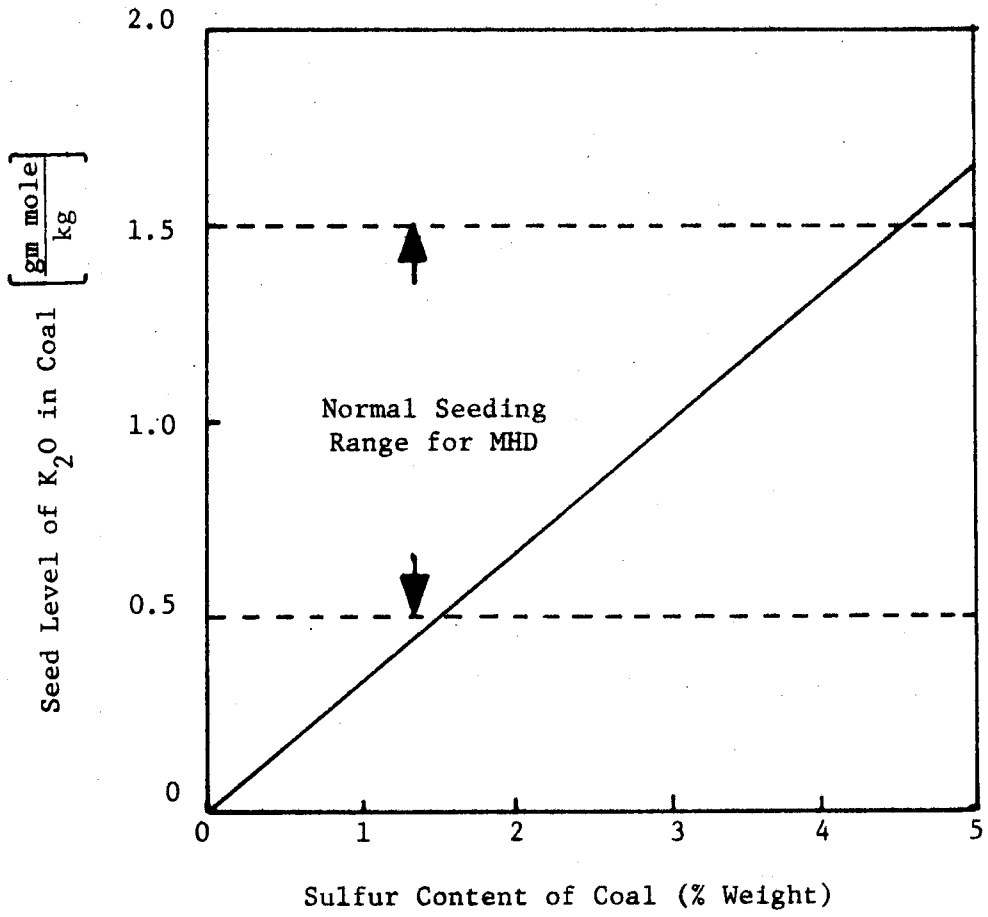

Figure 1.1. Reaction of Potassium Seed With Sulfur (Ref. 1).

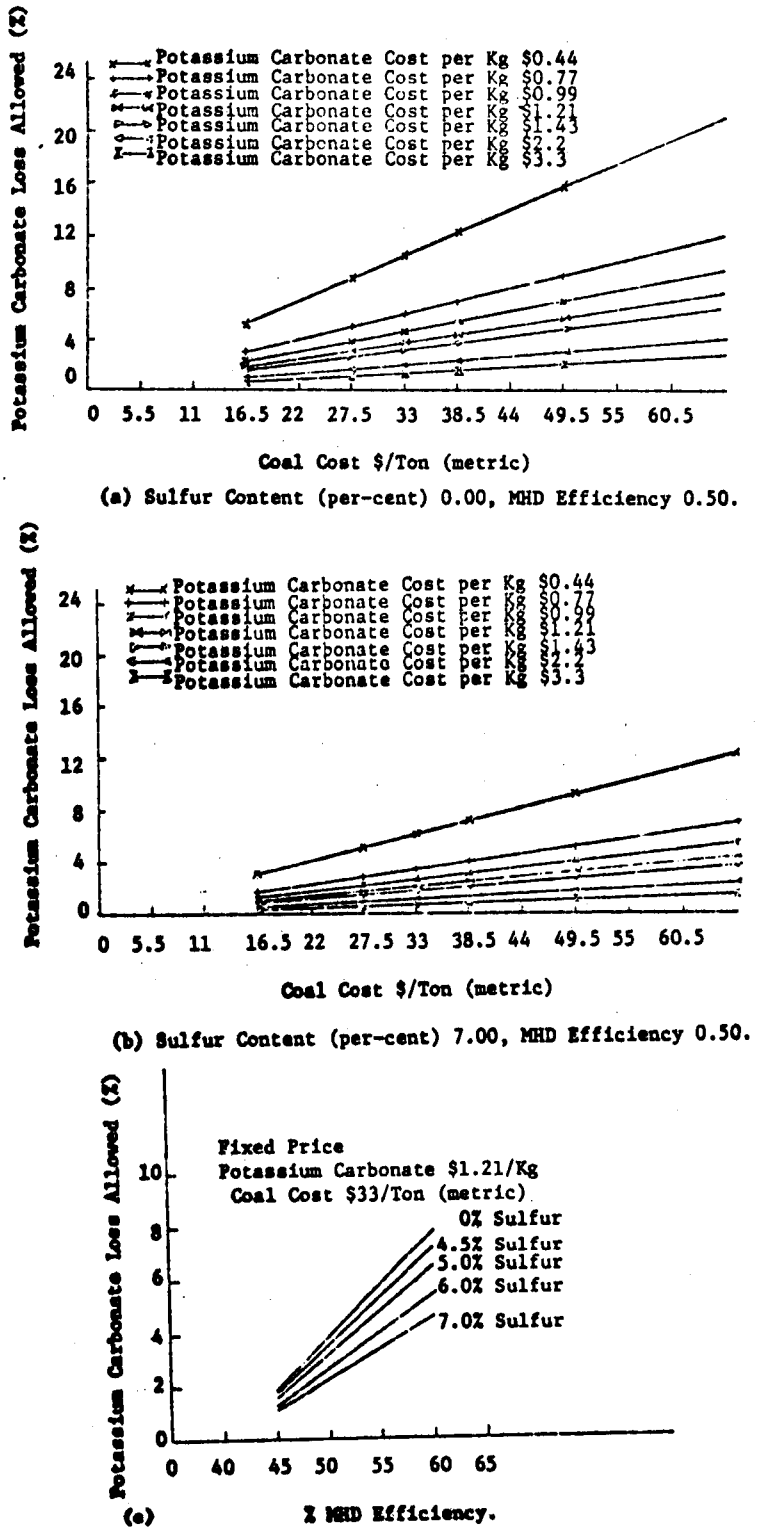

Figure 1.2. Allowable Potassium Seed Loss for MHD Power Generation by Balancing Seed Cost Against Plant Efficiency (Referred to η 40%).

K_2CO_3 at 99¢/Kg the "breakeven" point corresponds to about 4% K_2CO_3 loss for no sulfur coal and about 2% to 3% K_2CO_3 loss for high sulfur coal, if the MHD efficiency is 50%. As cost of K_2CO_3 increases for the fixed price of coal, allowable loss for K_2CO_3 is narrowed down to about 1%. In order for MHD power generation to be cost effective over a conventional steam plant, the seed material added to the combustion gas must be recovered and recycled at least in these amounts.

The experimental investigation presented in this dissertation is directed toward an understanding of the coal slag/seed interaction, and improving the recovery of seed from eastern coal for the high-temperature MHD flow. Western Kentucky coal with normally 3% sulfur was used in this investigation. By mannually controlled weighing seed was mixed in the coal in the ratio of 4.55 kg. of seed to 45.5 kg. of coal.

It is necessary to consider the interaction of the coal slag and seed. It is anticipated that under some conditions of temperature and pressure in the generator, seed compounds may also mix and/or combine with the coal slag.

The major constituents of coal slag are Al_2O_3 (Alumina), SiO_2 (Silica) and iron oxides. It has been predicted[2] that at the high operating temperatures for the MHD power generation, slag/seed interaction will result primarily from the formation of potassium metasilicate (K_2SiO_3), potassium aluminate ($K_2Al_2O_3$), potassium alumina silicate ($KAlSi_3O_8$), and potassium sulfate (K_2SO_4).

Therefore, one major problem to commercially develop MHD power generation is to understand the slag/seed interaction and devise the means

to recover seed considering the rate of reaction and the slag/seed separation process. All of the analyses and experimental results presented here correspond to the operational mode of total ash (slag) carryover through the generator. The results given here, however, are useful to estimate potassium seed losses with any degree of ash carryover.

A slag/seed separation using a concept of high ash carryover is adopted here.

It is believed that the coal slag having components such as Al_2O_3, SiO_2, iron oxides and CaO (Calcia) are solidified at about 1700^oK to 1900^oK and the potassium sulfate (K_2SO_4) becomes solid at about 1400^oK. So a substantial fraction of the slag will be condensed above this (1400^oK) temperature with only a few percent K (potassium) absorbed in it. Thus, a coal-fired plant could be provided with a means of separating slag from the system at a point in the system where the temperature is above the temperature of condensation of the seed but below the temperature of condensation of other compounds. Thus, the potassium may be separated and recovered from the coal slag downstream of the generator using water cooled cyclones which operate in this temperature range. This promotes the formation of potassium sulfate, the reduction of sulfur emissions and easing the potassium seed recovery.

Details of this concept will be found in Chapter III.

Literature Review

There are two major concepts for coal-fired MHD generators. The first proposes removal of a large portion of the coal slag at the exit of the combustor and prior to adding the seed material. Bienstock, et al.[1], and Hals, et al.[3], have predicted that the use of combustor sub-systems rejecting up to 95% of the coal ash may allow very high levels of seed recovery and extremely effective removal of sulfur from the exhaust products. The second concept proposed by Dicks and others[4], involves passing of all of the ash (coal-slag products) through the system and to carry out the slag/seed separation at the downstream of the generator. This current research involves the second approach. The problems introduced by high carryover rates of ash and seed at high temperatures required in the process include (1) the absorption of the seed by the slag and (2) corrosive effects of the mineral matter in the coal on metals and refractories.

M. A. Styrikovich, et al.[5], used potassium carbonate as seed material in the U-25, which was injected as 50% aqueous solution and dispersed directly to the combustion chamber to the input of the MHD generator. U-25 is the natural gas fired MHD plant but is considering the use of alternative fuels such as liquid fuel and perhaps coal. They used a hydromechancial system, which consisted of the foam apparatus, the two-stage turbulent gas washer, and the cyclone drop extractor to recover the seed material. The tests showed 99% removal of the seed was possible. In these tests there was no significant amount of ash.

There are two considerations in the estimation of seed absorption by slag, namely, equilibrium effects and kinetic or rate effects.

A computer thermodynamic program was assembled in The University of Tennessee Space Institute, (UTSI)[6], to calculate the equilibrium absorption of potassium seed in the slag. The thermodynamic data were obtained from the JANAF tables. Some important condensed phase species are silica (SiO_2), potassium metasilicate (K_2SiO_3), alumina (Al_2O_3), mullite ($Al_6Si_2O_{13}$), and iron oxides, as well as potassium sulfate (K_2SO_4). The range of some equilibrium calculations is shown in Figure 1.3[6]. The values shown in the figure correspond to various assumptions for chemical and thermodynamic properties. The range of the detailed and complete equilibrium calculations made by personnel at the U. S. Bureau of Mines[2] are also shown in this figure. All of these results indicate significant potassium absorption at equilibrium.

Some years ago, experimental equilibrium absorption coefficients of the seed in the slag in static tests were made in England[7]. They indicated that slag/seed separation is feasible, depending on seed content and slag content, in the range of temperatures 2100°K-2200°K. This temperature range is somewhat higher than previously estimated by Crawford et al.[6], at UTSI.

Figure 1.4 from Reference (7) indicates the fraction of added seed absorbed as a function of temperature. The calculations are based on seed absorption measurements up to 1923°K, with extrapolation to higher temperatures.

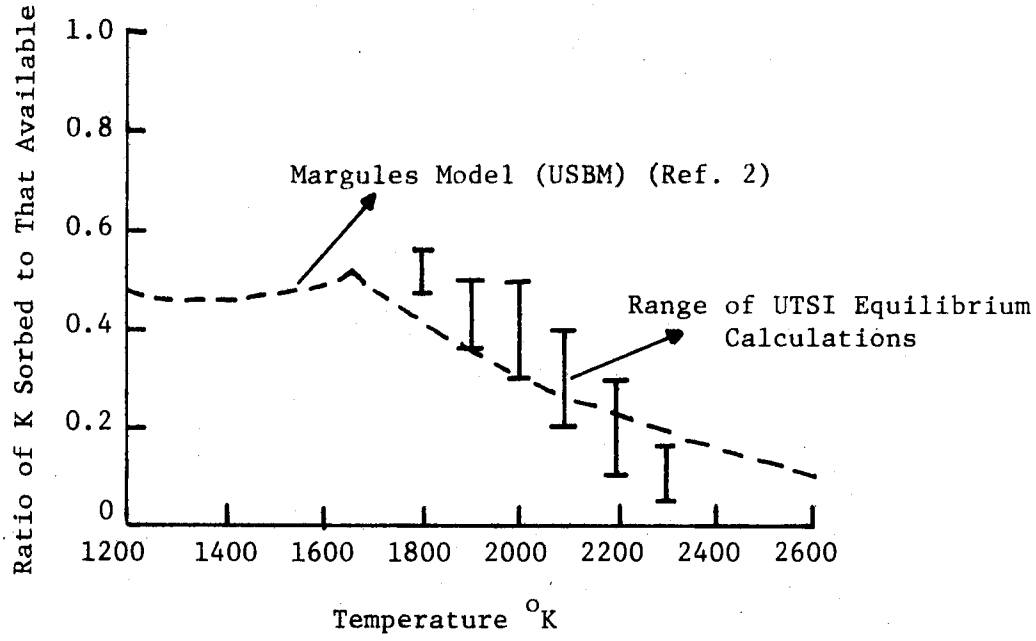

Figure 1.3. The Range of Equilibrium Calculations.

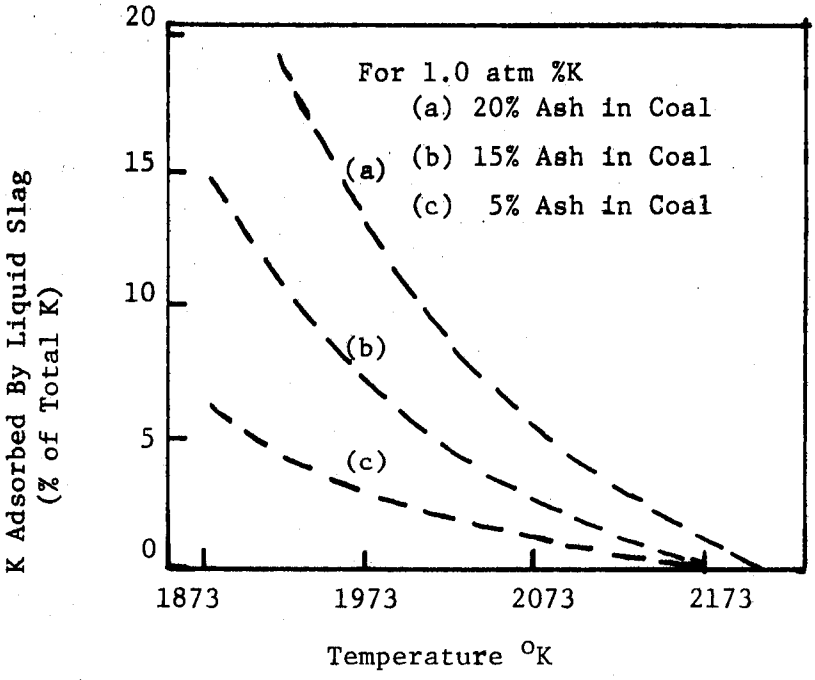

Figure 1.4. Equilibrium Adsorption of Potassium By Coal Ash Slag (Ref. 7).

In most existing MHD test equipment, it is not likely that equilibrium exists because of the small scale. Previous experimental studies carried out at UTSI on the interaction of potassium seed material with the slag (at lower temperatures) is not in agreement with equilibrium calculations[6]. The reason for this discrepancy between theory and experiment may lie in the thermodynamic data and reasoning. The thermodynamic properties at high temperatures for many species such as potassium metasilicate are estimated in the JANAF tables rather than measured. However, kinetic or rate effects may also be responsible for these differences.

Further progress on the economic analysis and optimization of the overall design of a MHD plant requires data from which the expected seed loss to the slag may be estimated under varying operating conditions. That is, the difficulty of separation of seed from slag will depend to a large extend on how rapidly the seed is sorbed by the slag in the MHD system. Previous experiments favor physical absorption. Simple diffusion models may be derived. If it is assumed that the surface absorbed potassium sulfate or a new chemical compound formed from it diffuses into the slag, the mean concentration of the diffused specie $\bar{c}$ in the spherical droplet of slag to the equilibrium value of the surface concentration of potassium on the surface of the coal slag C_0 would be (8), from Fick's law,

$$\frac{\bar{c}}{C} = 1 - \frac{6}{\pi^2} \sum_{n=1}^{\infty} \frac{1}{n^2} \exp\left[-(n^2\pi^2 Dt/R^2)\right] \qquad (1.1)$$

with initial and boundary condition,

$c = 0$ for $0 < r < R$ and $t = 0$,

$c = C_0$ for $r = R$ and $t > 0$,

and equation $\frac{\partial(c/C_0)}{\partial t} = \frac{D}{r^2} \frac{\partial}{\partial r} \left(r^2 \frac{\partial(c/C_0)}{\partial r} \right)$

where R is the radius of the spherical droplets, D is the diffusion constant and t is time.

In the discussion of the slag/seed interaction, one point which has to be looked upon is the two-dimensional wall deposits. One disadvantage of having slag in the generator flow and deposited on the generator walls is that the seed material in the slag layer may chemically interact with slag and become difficult to recover. If it is assumed that the surface absorbed K_2SO_4 or a new chemical compound formed from it diffuses into the slag layer, then the mean concentration of the diffused specie $\bar{c}$ to its equilibrium value, C_0 in the case of two-dimensional wall deposit would be (8),

$$\frac{\bar{c}}{C_0} = 1 - \frac{8}{\pi^2} \sum_{n=1}^{\infty} \frac{1}{(2n-1)^2} \exp \left\{ - \left[(2n-1)^2 \pi^2 Dt/4\ell^2 \right] \right\} \quad (1.2)$$

with initial and boundary condition,

$c = C_0$ for $0 < x < \ell$ at $t = 0$,

$c = 0$ for $x = 0$ and $x = \ell$ at $t > 0$,

and D and t has the usual meaning,

ℓ is the thickness of the deposit. Simple expression for diffusion coefficient is given (9) as:

$$D = D_o \exp(-Q/RT). \tag{1.3}$$

Mori and Hijikata[10] from their analytical study of diffusion suggested that in the boundary layer adjacent to the condensing surface under a condition of thermal equilibrium, small droplets of condensing vapor exit and diffuse to the surface. For their numerical example, air was taken as a non-condensable gas and K_2SO_4 was used as a condensing material.

Equations (1.1) and (1.2) suggest the form of the diffusion kinetics and is shown in Figure 1.5 as a function of the parameter Dt/L^2 where L=R and L=4ℓ respectively. If all factors are equal, it is observed that diffusion into slag droplets in the combustion gas stream would be faster than into the slag layer on wall (6). Diffusion coefficient data for various materials into coal slag are not available but they are probably in the range of 10^{-7} to 10^{-9} $cm^2/sec.$ at temperatures of MHD generator. The calculated values of $\bar{c}/C_0$ as a function of time is given in Figure 1.6 for diffusion coefficients in this range assuming a mean particle radius of 5 microns and a wall deposit thickness of 0.1 cm. It is observed that potassium will diffuse into spherical droplets more easily than into wall layers. Thus, one might expect to find most of the potassium associated with flyash dust particles and less associated with the wall layers. Equation (1.3) shows that higher the temperature T the greater the diffusion coefficient which suggest that if this type of

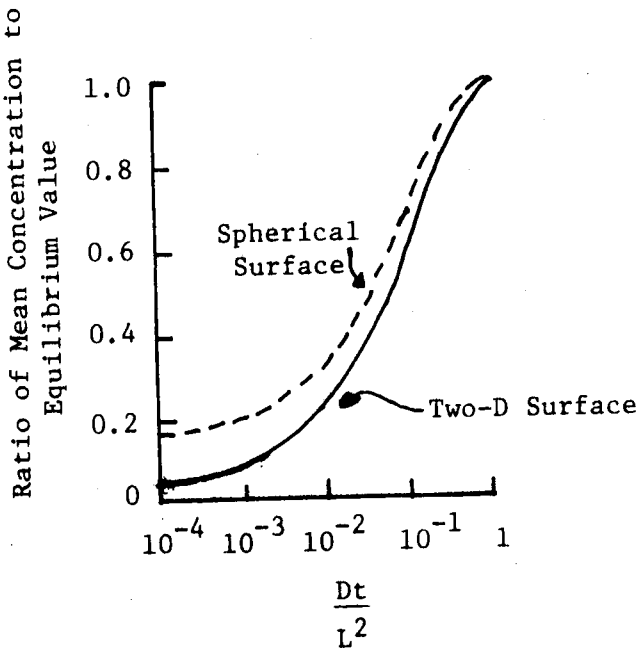

Figure 1.5. Diffusion Characteristics.

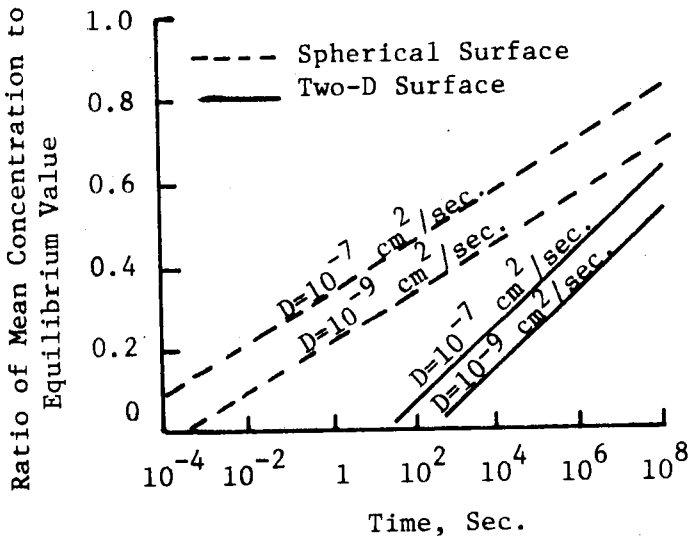

Figure 1.6. Diffusion Times into Spherical and Flat Plate Geometries.

kinetic process occurs (described above), it may be possible to carry out the slag/seed separation at lower temperatures than initially anticipated because the diffusion constant will decrease with decreasing separation temperature. As a result, seed may be readily absorbed into spherical slag droplets on the surface at low temperature; the seed will not diffuse into the slag as effectively as it would at high temperature and may be recovered by water washing. Equation (1.3) also suggests that the adsorption energy Q is the all-determining factor for the diffusion coefficient D. The adsorption energy in the case of physical adsorption is, generally, lower than the energy involved in the process of chemisorption. The heat of sorption governs the length of time adsorbed molecules will stay at the surface before re-evaporating (11). The time of adsorption τ is given by equation derived in 1924 by Frenkel[11] as:

$$\tau = \tau_o \exp (Q/RT) \qquad (1.4)$$

where,

Q and T has usual meaning and τ_o is the time of vibration of the constituent molecules or atoms of the adsorbing surface. For adsorbents having high melting points and close packing (such as coal slag having major constituents as aluminum oxide (Al_2O_3) and silicon oxide (SiO_2)), the calculated value for τ_o is of the order of 10^{-14} seconds (11). Equation (1.4) suggests that the value of τ increases very rapidly with an increase in the value of heat of adsorption.

An extensive literature survey is made on the diffusion coefficient data for materials into coal slag and the results were obtained using these above equations connecting the experimental temperature will be found in Chapter VII. These theoretical equations derived elsewhere (not in this dissertation) are utilized in forming an analytical model for this experiment.

Current Research

In this experiment, the coal slag/seed separation tests, with and without a magnetic field, were conducted by means of two water-cooled separation cyclones connected to the generator through a water-cooled diffuser and a radiant "boiler" flow duct. Details of the experimental facility with two test systems are discussed in Chapter II.

Tests were made with (1) coal seeded with potassium carbonate, (2) coal seeded with potassium sulfate and (3) unseeded coal.

The coal slag/seed separation cyclone performance and the composition of the collected material are reported in Chapter III.

Isokinetic sampling measurements made at the exit of the cyclone in order to sample the particulate matter leaving the cyclone are explained in Chapter IV. It also contains a discussion of the potassium recovery and the particulate removal techniques using baghouses or high energy water scrubbers and an electrostatic precipitator (ESP) employed for the collection of fine particulate which exits the cyclone.

Warm water washing is applied to recover the potassium sulfate from slag/seed ash collected by the cyclone downstream of the MHD generator. The composition of the samples is obtained by chemical analysis and by

the use of a scanning electron microscope and an energy dispersive x-ray analysis. These topics are covered in Chapter V.

This investigation also reports in Chapter V the influence on the potassium seed recovery from the ash of (1) the temperature of the combustion gases at entrance of the slag/seed separation cyclones, (2) the residence time in the flow train, (3) the effect of a magnetic field, (4) the size of the particles, and (5) the geometry of the flow train.

An understanding of these factors will enable us to get an idea of the reaction rates and having comparisons with the theoretical calculations of the equilibrium theory on the absorption of seed by coal slag.

Calculations are presented in Chapter VI for the control of sulfur dioxide (SO_2) emissions from the flue gas in the operation of an MHD generator.

Chapter VII discusses the diffusion coefficient data for the materials into coal slag compounds.

Finally, discussion is presented in Chapter VIII on the conclusions drawn from these experiments of coal slag and seed interaction in the coal-fired open-cycle MHD power generation.

CHAPTER II

EXPERIMENTAL FACILITY

The experimental investigation of the slag/seed interaction was accomplished in the University of Tennessee Space Institute MHD facility. Tests were carried out in two systems of the MHD laboratory. The test configuration consisted of a combustor, a nozzle, a channel, a radiant "boiler" flow duct and two cyclone separators (Figure 2.1). All components of these test systems were water cooled. The cooling water was provided by pumping water from a nearby reservoir through the system. A high pressure water pump, pumps the water from a storage tank (7000 gallons) to the experimental area.

At the existing flame temperature of 3100°K (a theoretical determination) very little ionization takes place in an unseeded combustion gas. As a result, the potassium seed material is added to the coal.

Combustion Chamber and Nozzle

Test System I

The combustion chamber assembly consisted of an injector head, a cylindrical and two conical sections. The hopper cylindrical section was 38 cm. inside diameter and 10.2 cm. in length. The conical sections made up of copper were 20.3 cm. long and were 38 cm. in diameter at the end where the cylindrical section was welded and 17.8 cm. at the small end. One of the small ends connected to a nozzle at the exit of the combustor and an injector head at the entrance was bolted to the other.

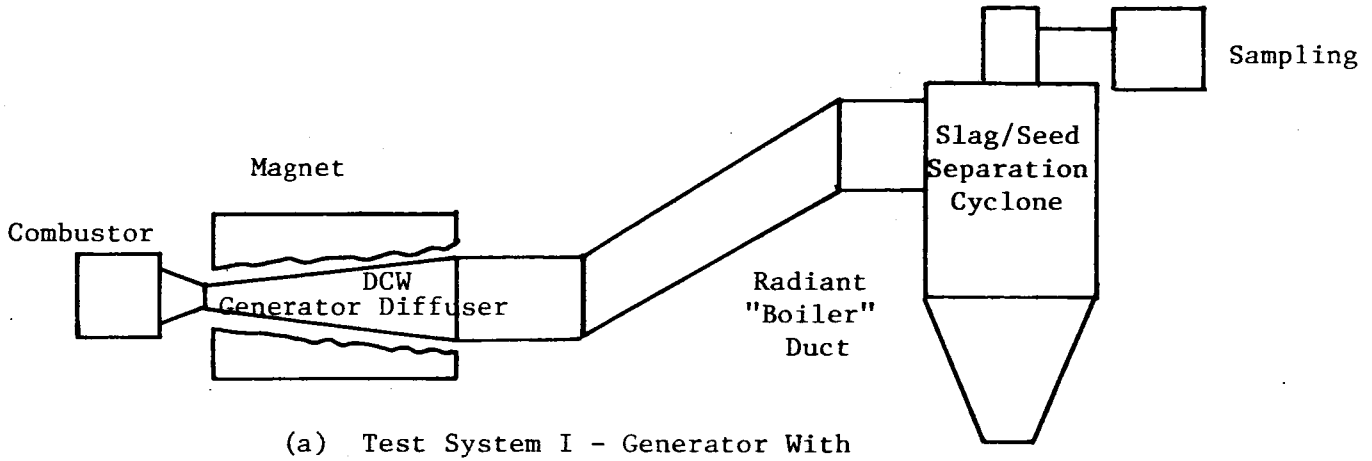

(a) Test System I - Generator With B-Field.

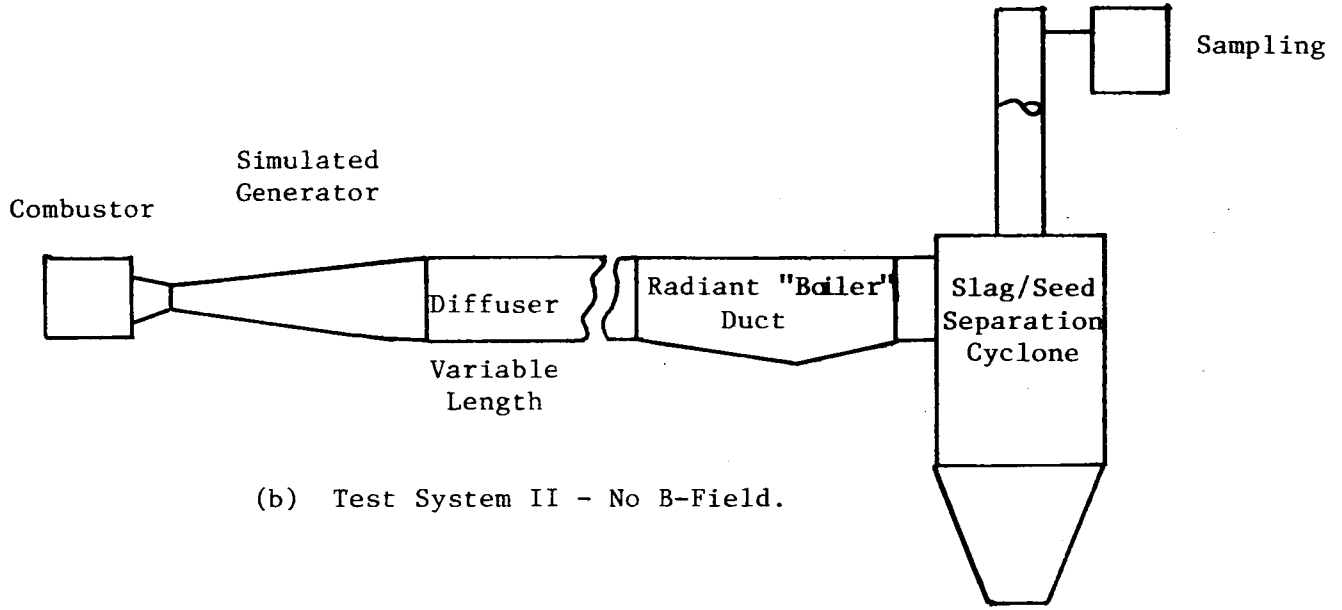

(b) Test System II - No B-Field.

Figure 2.1. Experimental Test Facility.

A converging nozzle section and then a diverging nozzle section transition was achieved between the circular cross-section of the combustion chamber (Figure 2.2) and the rectangular cross-section of the MHD channel. The mach number at the exit of the nozzle was 1.4 and was produced from the diverging section.

Test System II

The combustion chamber used consists of four segments, an injector head, a cylindrical chamber, and two end plates; a head adapter plate and nozzle adapter plate (Figure 2.3). The cylindrical section was 38.7 cm. inside diameter and 38 cm. long. The end plates were 5 cm. thick, were 26.6 cm. in diameter at the large end and 17.8 cm. at the small end, and serve the purpose of adapting the cylindrical section to the injector head at the entrance, and to the nozzle at the exit of the combustion chamber.

The 5 cm. thick, stainless steel injector head was bolted to the combustor. The fuel, oxidizer, propellant and coal with seeding agent were injected into the combustion chamber through six kerosene ports, two oxygen lines, one propane line, and one coal and seed line through the injector head.

The seed material was mixed in the coal in the ratio of 4.55 Kg. of seed to 45.5 Kg. of coal. Potassium sulfate (K_2SO_4) was introduced in the system at a rate of 10% by weight of the coal flow.

Due to the hydroscopic nature of potassium carbonate, the coal/seed mixture packs and thus blocks the coal transport line. A small amount of

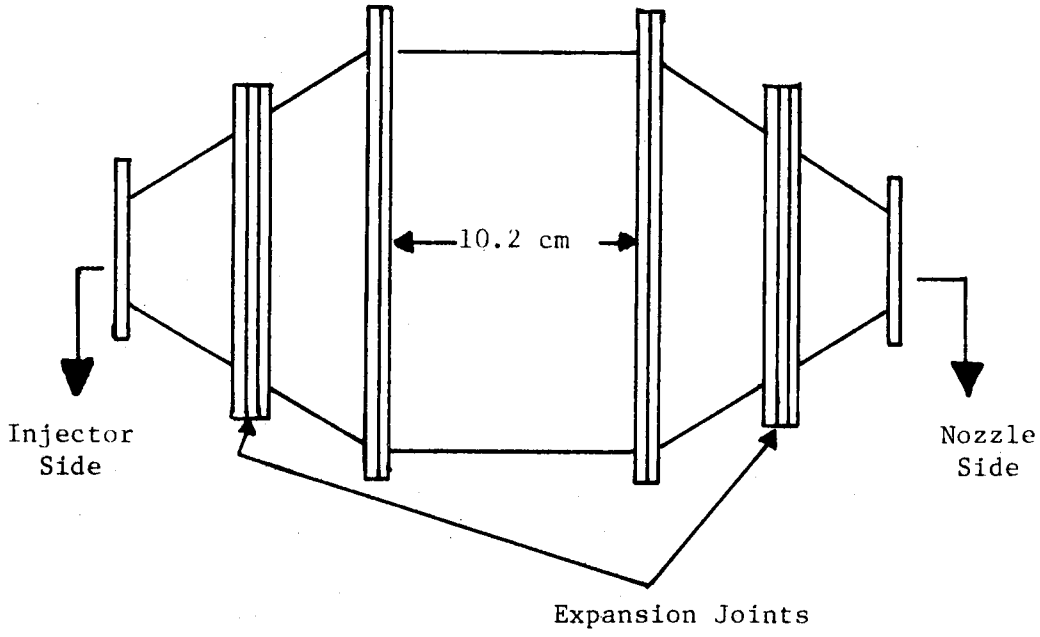

Figure 2.2. A Combination of a Combustor - Test System I.

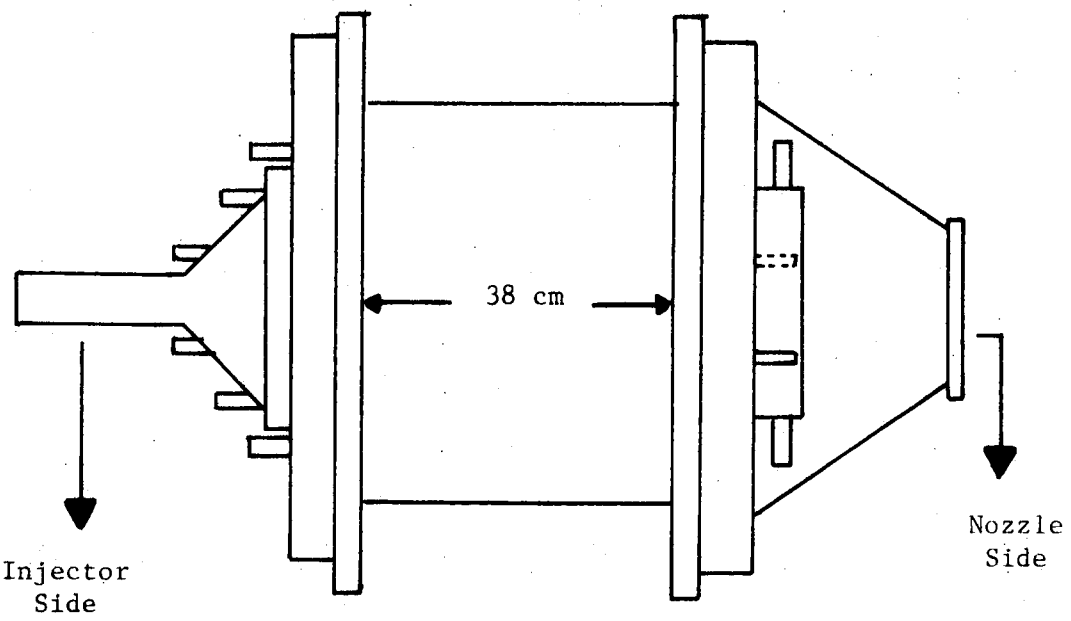

Figure 2.3. A Combination of a Combustor - Test System II.

water absorbing material such as magnesium carbonate ($MgCO_3$; 1% by weight) was added to seeded coal (with K_2CO_3) in order to prevent caking and blocking of the coal flow to the combustion chamber.

Propane was initially ignited with the spark plugs. The liquid fuel (kerosene) was used to ignite the coal and its flow subsequently terminated when coal burning was established after approximately thirty seconds in Test System II and about one minute in Test System I.

The water cooled, stainless steel nozzle in two sections was bolted to the downstream end of the combustion chamber. With the inside dimensions of 12.8 x 16 cm. from the inlet of one section it converged to a 5 x 9.6 cm. at the inlet of the second section and then diverged at the outlet of the nozzle.

Mass Flow Rate

Average coal/seed flow rate was determined by finding its weight differences for every second of running.

Absolute pressure P and the pressure differential ΔP across the known orifice in the oxygen line were measured by means of strain gage pressure transducers in order to determine the oxygen flow rate. The formula used in calculating the oxygen flow rate was,

$$\dot{m}_{O_2} = .04(\Delta P_{O_2} \times P_{O_2})^{1/2} \text{ kg/sec.} \qquad (1.5)$$

Channel

Test System I

In this system a diverging diagonal conducting wall channel (12), made up of copper, was used (Figure 2.4 (a)). The overall length of the channel was one meter and it had dimensions of 5 cm. x 10.2 cm. at the entrance and 5 cm. x 30.5 cm. at the exit. There were seventy-one copper electrodes, each 2.54 cm. thick and water-cooled and were inclined at 60° relative to flow axis. The insulation between electrodes was plasma sprayed alumina.

At the channel exit was connected through a transition piece to two constant area spacers, each 25.4 cm. long and with a dimension of 5 cm. x 30.5 cm., were connected to the channel exit. Each had ten, water-cooled, straight to flow electrodes.

The magnetic field over the active channel in this test system was provided by an electromagnet of strength 2 tesla. The pole pieces were 91 cm. long.

Test System II

A simulated MHD channel was used in this system (Figure 2.4 (b)). It was made from carbon steel and had a total length of one meter. The side walls measuring in height 10.2 cm. from the inlet (nozzle end) diverged to a 30.5 cm. at the outlet (the diffuser portion). It's geometry was the same as in Test System I but it had smoother walls. At the channel outlet, a constant area spacer (30.5 cm. x 30.5 cm. long) was used to connect the channel into the diffuser section. The water cooled diffuser length was varied by adding or subtracting 30.5 cm. long constant area spacers.

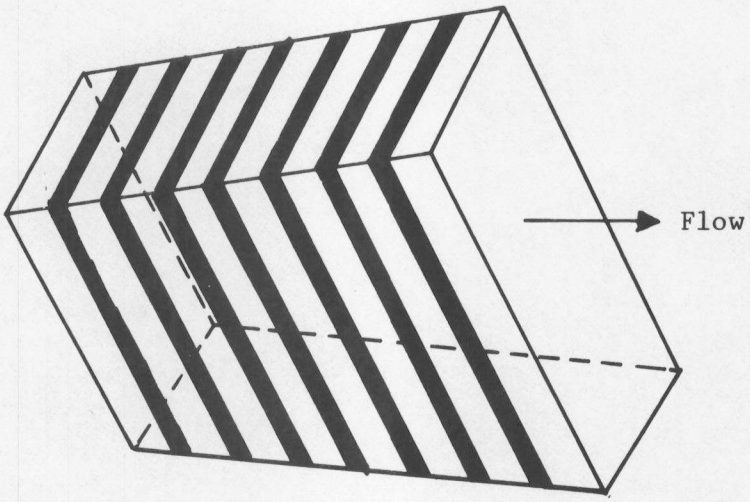

(a) DCW MHD Channel - Test System I.

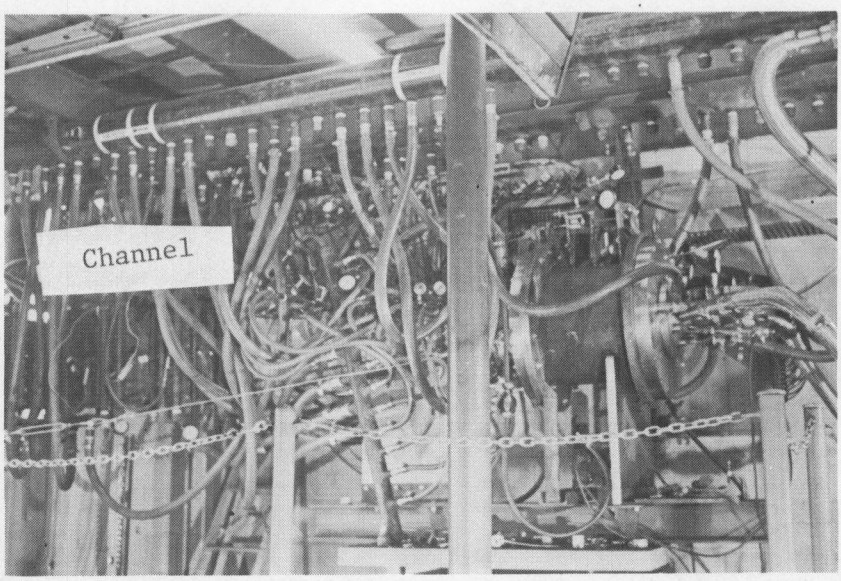

(b) Simulated Channel - Test System II

Figure 2.4. Channel From Both Test Systems.

The channel was assembled without the individually insulated electrodes as required in the MHD power generation and it was smooth and it simulated a channel with the internal dimensions of the water cooled MHD generator channel in order to carry out the slag/seed separation processes at the downstream of the generator without a magnetic field.

Radiant "Boiler" Duct

Test System I

The 2.3 meter long radiant "boiler" flow duct (simulating a radiant boiler in a large system) in this test system had dimensions of 17.8 cm. wide x 38.4 cm. high at the inlet where the end of the constant area spacer was flanged and 35.6 cm. wide x 44.8 cm. high at the exit. Steel water cooled tubes having a diamter of 1.3 cm. were placed against each wall of the radiant boiler and the space between the tubes was filled with a morganite concrete.

The flow was directed upward at an angle of 30° in order to attach the boiler to the water cooled cyclones described in the next section. In this test system, the condensed slag layer flows smoothly covering the walls.

Since an unusual accumulation (several centimeters thick) of ash layer occurred in the downstream part of the radiant "boiler" due to upward flow of the slag-ladden combustion gases in this test system, Test System II was built.

K-type (Cr-Al) thermocouples were used to measure the two side wall temperatures of the radiant "boiler."

The exit of the radiant "boiler" (Figure 2.5) was connected through a transition section (the splitter plate) to two water cooled cyclones. A Pt-Pt/ 10% Rd thermocouple was inserted into the flow at the end of the transition piece to measure the cyclone entrance temperature.

Test System II

The radiant "boiler" flow duct (Figure 2.6) was constructed with steel with dimensions of 10.2 cm. x 35.6 cm. at the side of the constant area spacer and 40.6 cm. x 49 cm. at the outlet. The overall length of the radiant "boiler" was 1.22 meters. The radiant boiler consisted of a bank of 304 stainless steel 1.3 cm. water cooled tubes placed against each wall. The space between the tubes was packed with an alumina based ceramic in order to avoid the metal surface of the wall of getting hot which would destroy the radiant "boiler."

Altogether there were twelve thermocouples installed in the radiant "boiler" for the measurement of temperatures; (1) at the exterior metal wall (T_a), (2) in the ceramic (T_b), and (3) at the surface of the cooling tubes (T_c). A schematic is shown in Figure 2.7. The cross-section of the wall of the radiant "boiler" shows the locations of the thermocouples. Thermocouples used were of K-type (Cr-Al).

A splitter plate was used to divide the flow into two cyclones and connected at the outlet of the radiant "boiler." It had dimensions of 13.3 cm. by 48 cm. at the entrance. The splitter plate end was split into two parts each having the size of 16.8 cm. and connected to two cyclone separators. At the end of the splitter plate, an S-type thermocouple (Pt-Pt/10% Rd) was inserted into the flow such that a temperature at the cyclone entrance was measured.

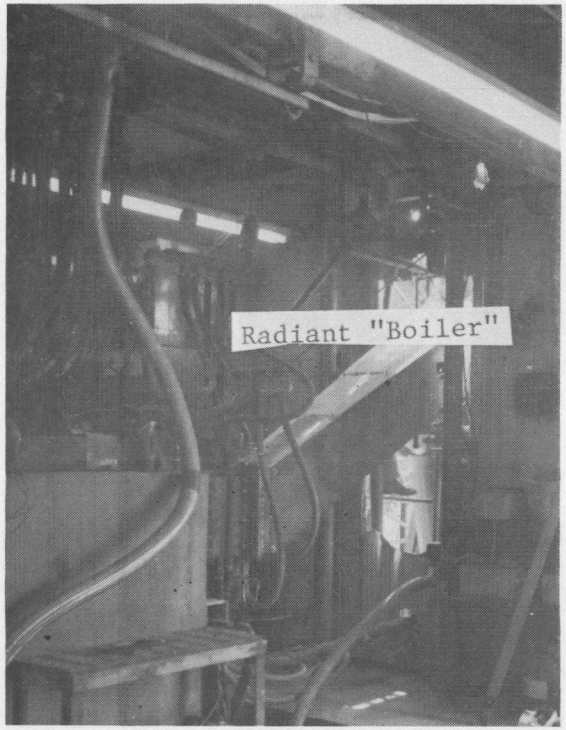

Figure 2.5. 30° Inclined Radiant Boiler, Test System I.

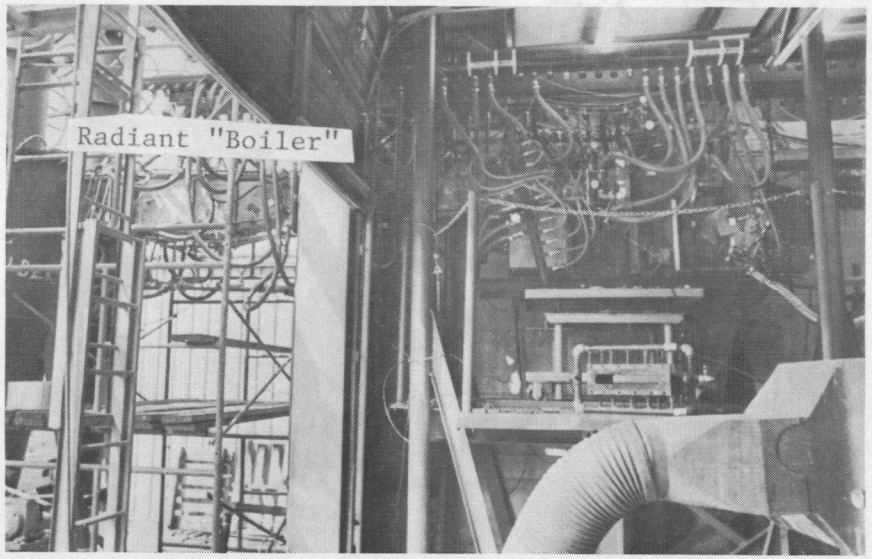

Figure 2.6. A Radiant "Boiler" Flow Duct, Test System II.

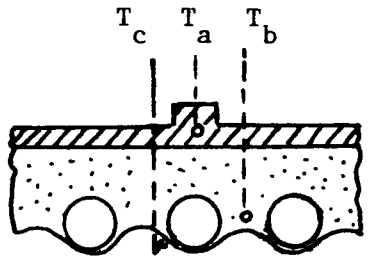

Cross Section

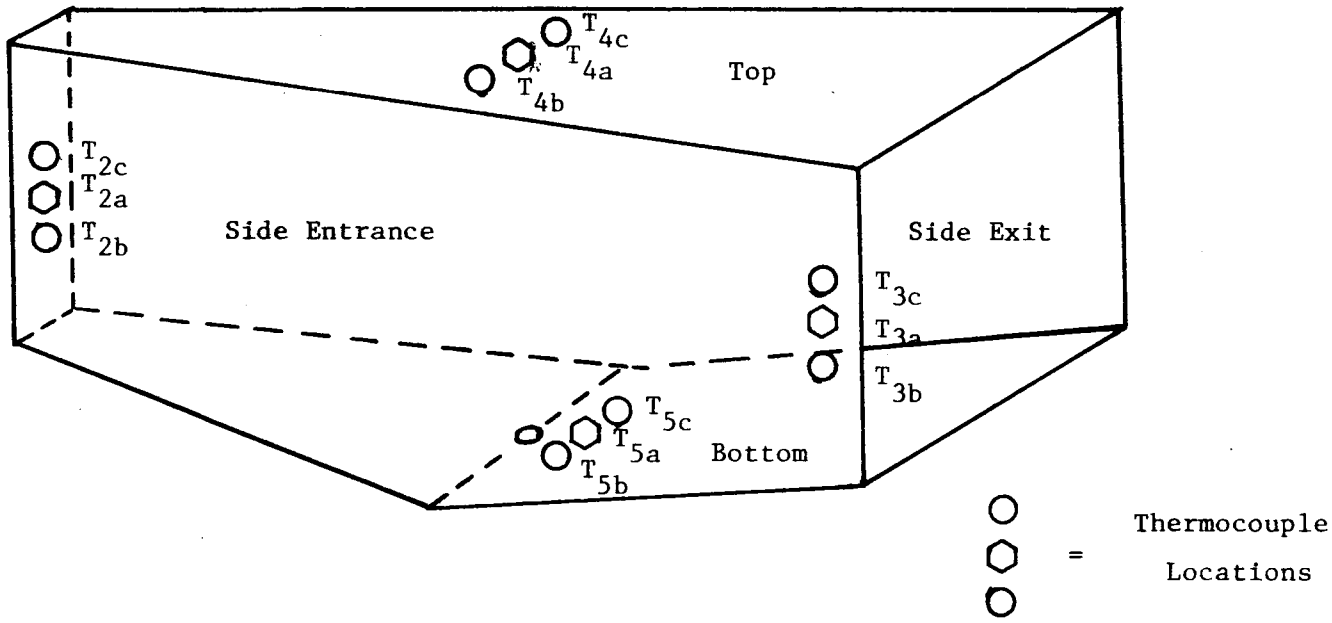

Figure 2.7. Schematic of Radiant Boiler, Test System II.

Cyclone Separators

Test System I

In this test system two water cooled cyclones were attached to the exit of the radiant "boiler." Their short exhaust stacks did not contain any flow straighten means as was done in the Test System II (Figure 2.8). The dimensions of these two cyclone separators will be discussed in the Test System II.

In this test system, the wall temperature of the cyclone body was measured by K-type (Cr-Al) thermocouple. Swirl flow existed at the cyclone exit.

Test System II

The exit of the radiant "boiler" was connected through the splitter plate to two water cooled cyclones with extended stacks, so that the cyclonic flow was straightened (Figure 2.8). The overall height of the cyclones was about 5 meters. The 38.7 cm. in diamter flow straightener having eight 0.3 cm. thick and 71 cm. long vanes was placed at a height of 1.5 meters from the top flange over the cyclone body in the stack extension. This helped significantly in eliminating the swirling motion of the flowing gas which occurred in the Test System I. Thus, having a smoothed flow in the exhaust stack resulted in a more uniform velocity in order to make more accurate sampling measurements across the 35.6 cm. diameter exhaust stack. While the cyclone body was of 76 cm. in diameter, it was tapered toward the bottom having 15 cm. diameter slag tap. The cover bolted to the slag opening was removed manually after every test to collect the solidified slag for sampling.

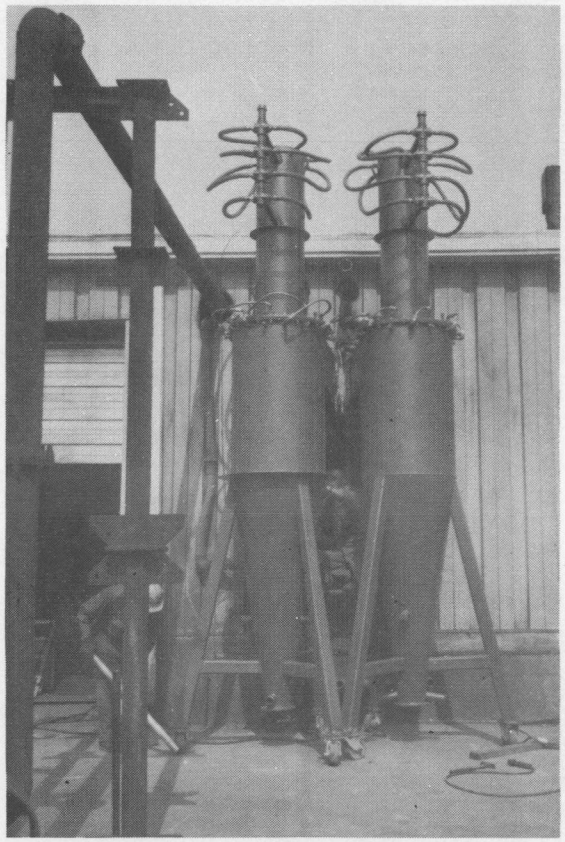

Test System I - Without Extension.

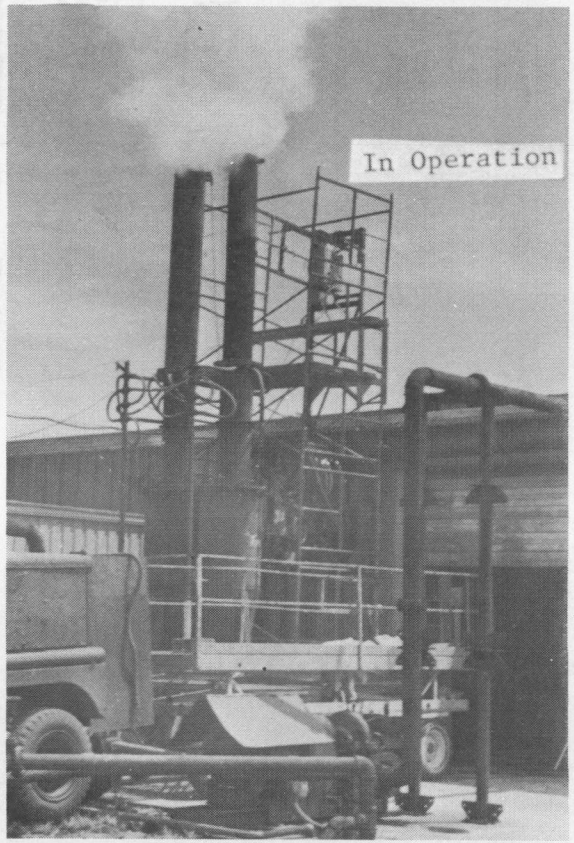

Test System II - With Extension and a Flow Straightner.

Figure 2.8. Two Water-Cooled Cyclones.

Instrumentation

Primary parameters of the combustion chamber, which are coal and seed flow rate, oxygen flow rate, and total chamber pressure, were displayed by mounted panel meters as well as recorded on a Vidar.

Strain-gage pressure transducers were used to measure pressure inside the channel, constant area spacers and in the combustion chamber. The pressure differential in the cooling water manifold, connected to each component in the system, was determined before the test run by dial pressure gages. A temperature change in the cooling water manifold (tubes) was measured by T-type (Cu-C) thermocouples and recorded on the Vidar. In addition, all temperatures measured by thermocouples in the system, such as wall temperature, stack gas temperature, entrance to slag/seed separation cyclone temperature, etc., were recorded on the Vidar.

Vidar System

The Vidar Digital Data Acquisition system is a multi-channel system which sequentially scans, measures, and prints out data from each channel. The input voltage signal on each channel, which was scanned by the Vidar 606-03 scanner, was read by the Vidar 502 B integrating digital voltmeter.

The printer records data on a paper tape at a speed of 30 lines/sec. Since the number of channels utilized in this experiment was about sixty, the total scan time was about two seconds. One complete scan is called a data set. Each scan was repeated in the intervals of ten seconds in

this experiment. A digital clock in the system provides the time to the printer and initiates the scan sequence.

The data set consisted of weight of the coal, temperatures and pressures in the component of the system as described in each section of this chapter.

Summary of Test Runs

This experiment was conducted for two different flow rates. It included a number of test runs using potassium sulfate (K_2SO_4) and potassium carbonate (K_2CO_3) seed with no seed. Summary of these runs for both test systems is tabulated in Table 2.1.

Sampling Train

Test System I

The particulate matter leaving the cyclone was sampled by an assembled sample train consisting of a 1 cm. diameter sampling probe and a fiberglas thimble filter (Figure 2.9). The sampling probe was aligned with the cyclonic flow at a location of the exhaust duct. A manually controlled pulley type traverse mechanism was used to traverse the probe in and out of one cyclone exit stack of 35.6 cm. in diameter. The first three impingers, filled with distilled water backed by the dry fourth one in order to collect any liquid carryover, were installed in the particulate sampling line downstream of the filter. Four impingers were placed in the ice bath. An Iron-Constantan thermocouple was used to measure the stack gas temperature. At the downstream of the impinger box, there was dry gas meter and vacuum pump.

TABLE 2.1. SUMMARY OF THE WATER-COOLED CYCLONE TESTS.

Test System	Test Run	Date	Time On Coal, Min.	Seed Type	Mass Flow Rate Kg/Sec. $\dot{m}_{coal}$	$\dot{m}_{O_2}$	$\dot{m}_{total}$	Cyclone Ent. Temp. ^{o}K	Sample Weight Kg. Cyclone Left Side	Sample Weight Kg. Cyclone Right Side
I	1431	6/16/75	6.0	K_2SO_4	0.203	0.203	0.491	1350	-	-
I	1437	7/08/75	20.0	K_2SO_4	0.164	0.414	0.578	1360	6.11	7.80
I	1440	7/15/75	6.17	K_2CO_3	0.155	0.273	0.428	1400	4.97	5.68
I	1447	7/25/75	12.17	None	0.191	0.332	0.523	1360	11.90	9.23
II	54	8/02/76	20.00	K_2SO_4	0.194	0.341	0.535	1600	6.45	6.02
II	57	8/04/76	29.00	K_2SO_4	0.195	0.345	0.540	1630	15.06	22.30
II	58	8/18/76	49.5	K_2CO_3	0.155	0.305	0.460	1740	36.73	37.00
II	62	8/23/76	30.0	K_2CO_3	0.164	0.314	0.478	1740	20.65	22.5
II	64	8/25/76	19.0	K_2CO_3	0.4205	0.350	0.555	1740	16.90	16.65
II	66	8/31/76	18.0	K_2CO_3	0.20	0.359	0.559	1700	21.73	16.08
II	67	9/07/76	16.5	K_2SO_4	0.211	0.373	0.584	1700	18.10	16.5
II	68	9/09/76	17.0	K_2SO_4	0.314	0.573	0.887	1950	42.40	47.7
II	69	9/13/76	17.0	K_2CO_3	0.277	0.555	0.832	1820	26.88	30.06
II	70	9/15/76	18.0	None	0.305	0.591	0.896	1560	19.75	16.88
II	71	10/20/76	16.0	K_2SO_4	0.218	0.423	0.641	1690	9.50	10.0

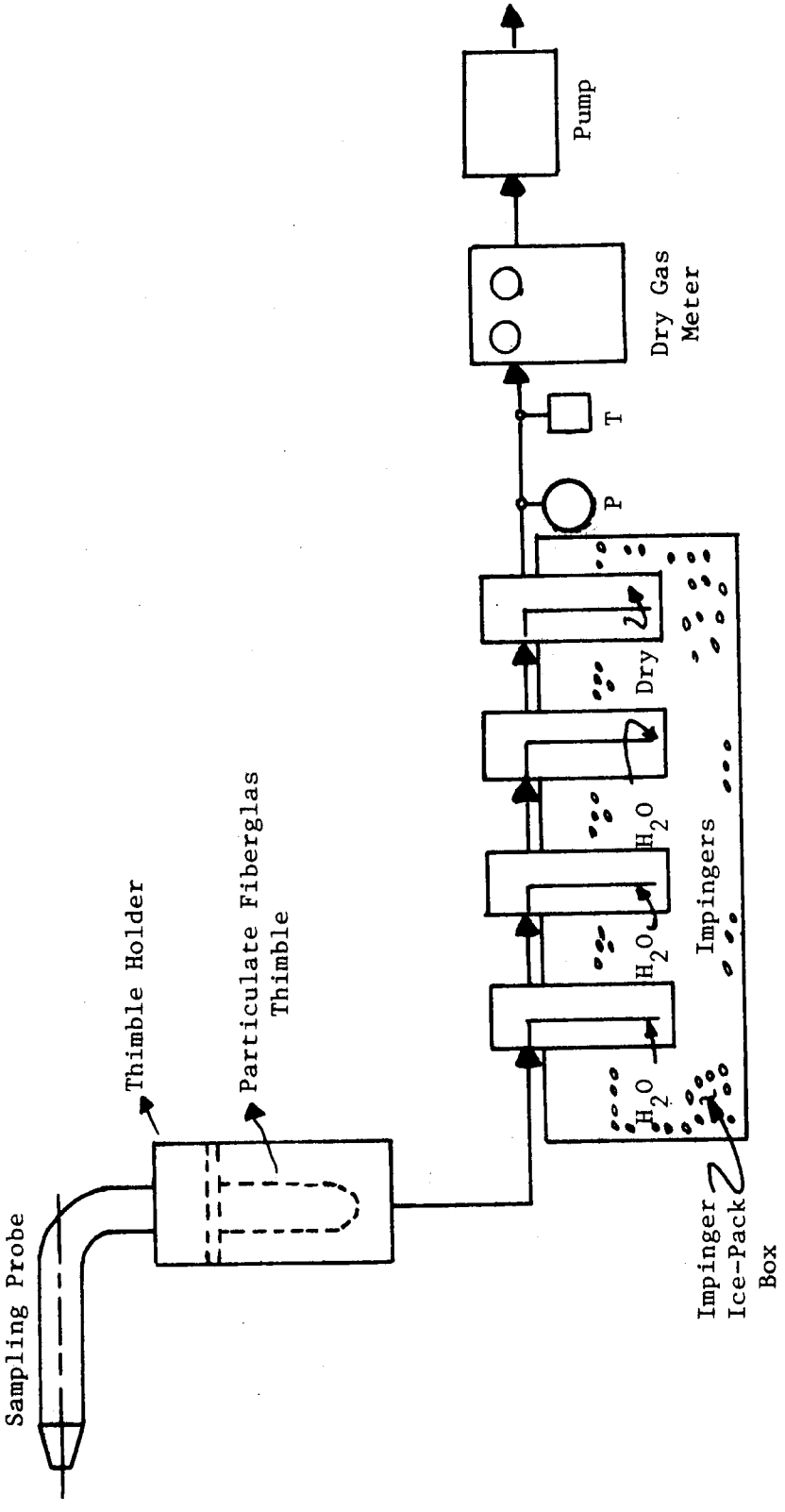

Figure 2.9. Schematic of Particulate Sampling Train, Test System I.

Test System II

The RAC (Research Appliance Company) train stack sampler, developed by the Emissions Testing Branch of the Office of Air Programs, EPA, was used for the isokinetic sampling of particulate matter at the cyclone exit in the test system experiment. The sampling train (Figure 2.10) consisted of a stainless steel sampling probe along with a pitot tube for monitoring gas velocity during sampling. A Chromel-Alumel thermocouple was attached to the probe bundle for acquiring the stack gas temperature. The sample box had heated a portion for the filter (fiber-glas), and an ice bath portion for the impingers. An automatic stack traverse mechanism was used to traverse the probe in and out of the one 35.6 cm. diameter cyclone stack. The umbilical cord connected the sample box with the meter case which consisted of two magnehelic gages to measure the pressure differential in the stack, vacuum pump, dry gas meter, thermocouples and electrical controls for sampling.

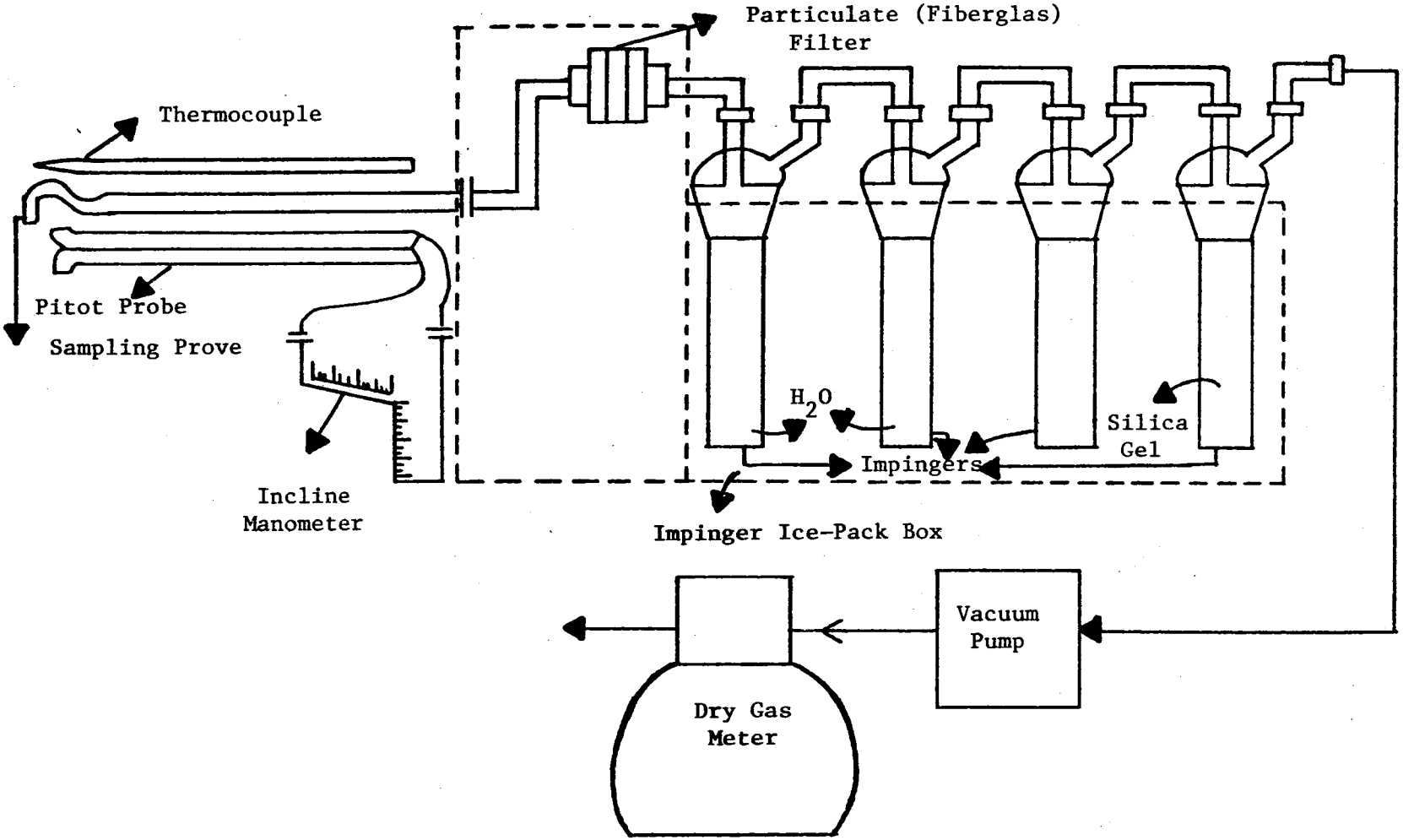

Figure 2.10. Schematic of Particulate Sampling Train, Test System II.

CHAPTER III

SLAG/SEED SEPARATION CYCLONE PERFORMANCE

Slag/Seed Separation Concept

If MHD power generation is to be economically feasible, it is necessary to understand the complexity of coal slag/seed interactions and develop ways to recover the seed from the system. A concept of slag/seed separation is investigated here in which the seed is separated from the slag downstream of the MHD generator. In this operation all of the ash passes through the system.

Table 3.1 presents the melting points (M.P.'s) of the slag species including the M.P.'s of various potassium compounds. This table illustrates that a substantial condensation of the slag would occur above the temperature at which the potassium sulfate or other potassium compounds would condense. Therefore, to separate the potassium seed from the coal slag or ash, the combustion products could be passed through water cooled cyclones whose temperatures are low enough to allow a significant amount of slag to condense but still high enough to be above the condensation temperature of potassium sulfate.

Thus, high ash carryover systems control sulfur emissions by forming potassium sulfate which may be selectively separated from the slag in specific temperature ranges downstream of the MHD generator.

The calculation of the residence time of the combustion gas shows that it is of the order of milliseconds in the combustor and MHD generator. With the cyclone separator attached to the downstream end of the genera-

TABLE 3.1 MELTING POINTS OF SLAG SPECIES AND VARIOUS POTASSIUM COMPOUNDS

COMPOUND	MELTING POINTS (M.P) ^{o}C
Al_2O_3	2045
SiO_2	1713
MgO	2800
FeO	1420
Fe_2O_3	1565
CaO	2580
K_2CO_3	891
K_2SO_4	1069
K_2S	840
K_2O	d 350
$KAlSiO_4$	ca 1800
$KAlSi_3O_8$	1400 - 1300
K_2SiO_3	976

d = Decomposes

ca = Calculated

tor, the residence time is about 1.5 seconds. It is expected that these times should have a significant influence on the slag/seed interaction and separation processes.

Cyclone Design

In order to investigate the feasibility of slag/seed separation and to obtain experimental data concerning slag/seed interaction, two water cooled slag/seed separation cyclones were designed and built at UTSI and used in Test System I and Test System II. A description of these two systems is given in Chapter II. The cyclones were connected to the MHD generator by means of a "radiant boiler" which served only as a water cooled flow duct. The gas temperatures that were measured at the cyclone entrance in the first system were in the range of 1350°K to about 1500°K. The corresponding measurement in the second system was 1600°K to 1950°K.

No difficulties were experienced in the operation of the water cooled cyclones. Their wall temperatures near the entrance reached equilibrium values near 900°K after a few minutes of operation. Figure 3.1 indicates the gas temperature at the cyclone entrance for both test systems. Due to the malfunction of the thermocouple in the cyclone wall in the tests of Test System II, no data of cyclone wall temperature was available. The temperature of the gases leaving the cyclone was approximately 500°K in Test System I and in the range of 800°K to 1000°K in Test System II.

As will be shown later, the cyclone separators effectively captured all particles larger than five microns in diameter (its design limit).

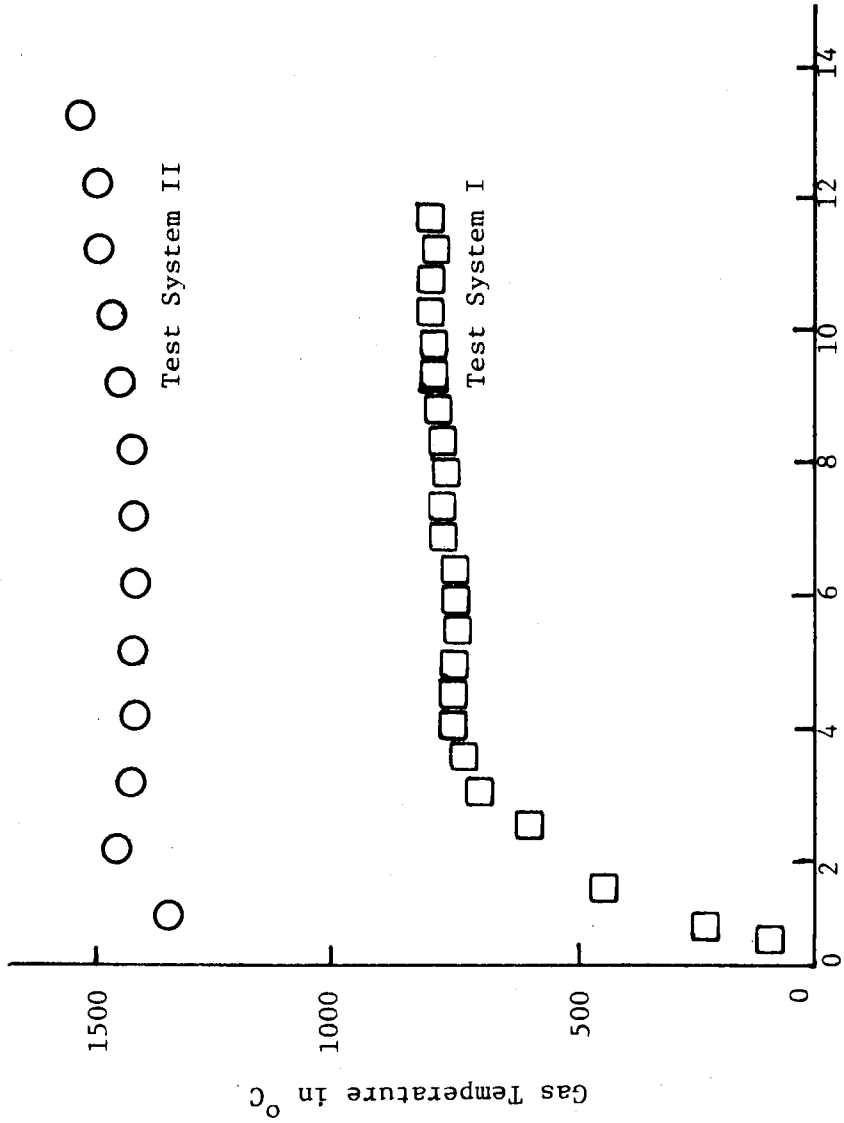

Figure 3.1. Uncorrected Gas Temperature at Cyclone Entrance.

Temperatures of the exhaust gases were measured at the entrance of the cyclone and at the stack. The temperatures were measured by means of Pt-Pt/10% Rd thermocouples at the entrance and Cr-Al thermocouples at the exit of the cyclone (Figure 3.1). The combustion gas temperatures in the other systems of the flow train were calculated from the temperature changes and the flow rates of the cooling water. The measured and calculated temperature distribution for a typical run in Test System II is given in Figure 3.2 clearly showing the agreement, indicating that the cooling performance of the cyclone was satisfactory.

Table 3.2 represents the rate of heat loss by the gas in one of the cyclones and the overall heat transfer coefficient for the cyclone. These data may be useful in designing future cyclones and operating cyclones in different temperature ranges.

Cyclone Operational Reliability

On the walls at the cyclone entrance and the splitter plate area, which divides the flow into two cyclones, some slag accumulation occurred during the operation but there was no visible erosion after four to six hours of operation with the longest single run being fourty-nine minutes.

In Test System II a flow straightener having long vanes was placed in the stack in order to eliminate the swirling motion of the flowing gas which occurred in Test System I. Its operation was reliable except at the end of the series of runs when the mass flow rate of coal and temperature were increased which caused bending of the vanes in the flow straightener.

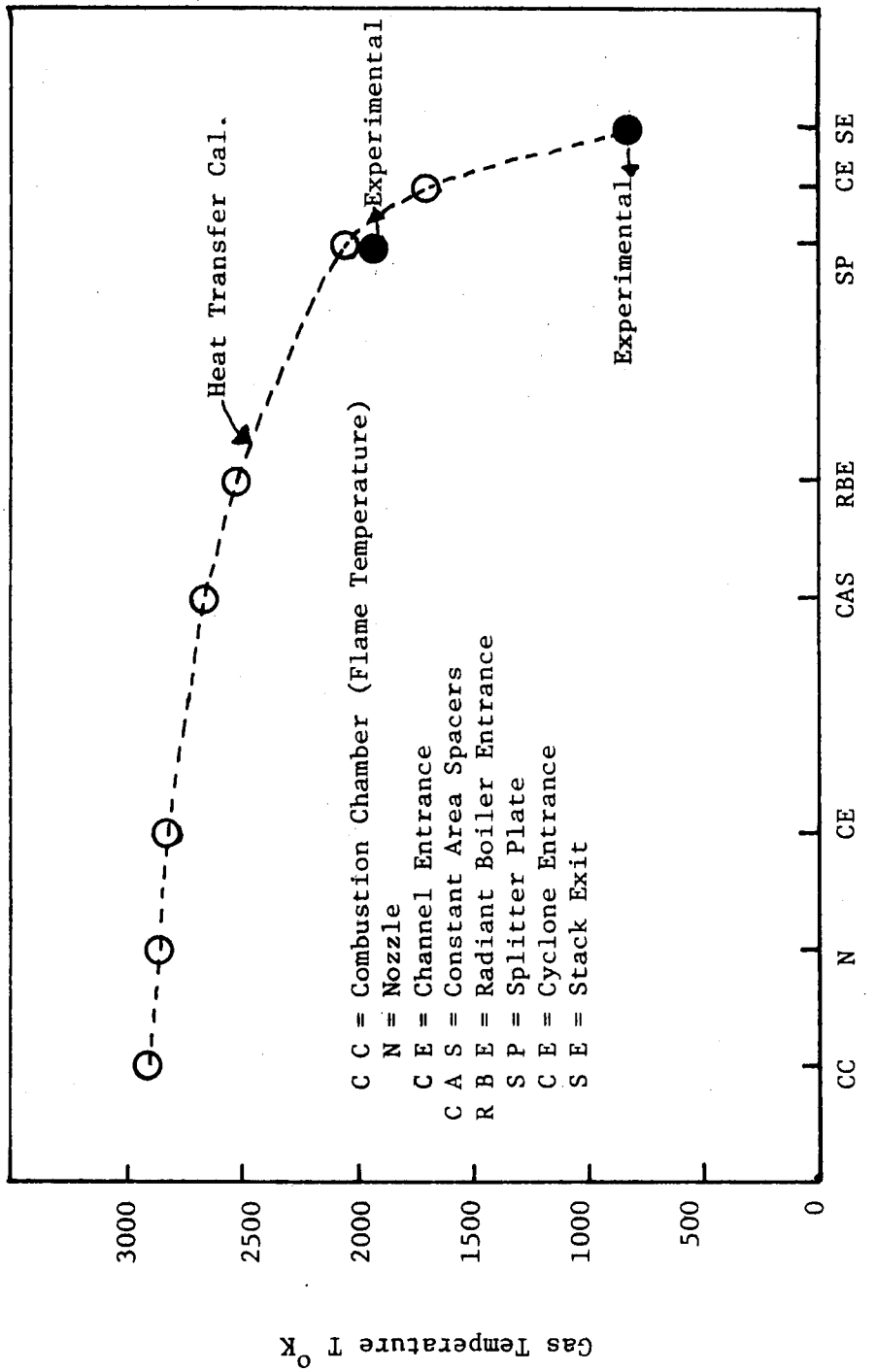

Figure 3.2. Gas Temperature (Corrected) in the MHD Flow Train System II for a Typical Run.

FIGURE 3.2. HEAT LOSS RESULTS FOR A CYCLONE

(T_{wall} = Temperature of the Cyclone Wall = 800°K)

Run	T_{gas} °K	$Q_{Cyclone}$ MW	$\bar{h}$ MW/M^2 °K
54	1236	562.3	0.13
57	1260	576.2	0.13
58	1273	604.4	0.13
62	1282	601.7	0.13
64	1330	659	0.13
66	1301	640.3	0.13
67	1295	666.3	0.14
68	1516	1208.9	0.17
69	1423	980.5	0.16
71	1304	697.1	0.14

In Test System I, the upward flow of the slag ladden combustion gases in the radiant "boiler" duct caused an unusual accumulation of slag several centimeters thick. This accumulation could have eventually caused a shutdown in the operation of the system. Slag accumulations did not occur in the radiant "boiler" or on the splitter plate of Test System II which provided for a straight flow path into the cyclone. It is believed that this flow train configuration will not cause slag layer accumulations.

As the combustion gas temperature was varied from run to run, the thickness of the slag accumulation in the radiant "boiler" and other parts of the flow train varied. At high temperatures and high mass flow rates of coal, the slag layer thickness decreased and the cyclones collected large slag pieces which appear to have been blown away from the system wall. This resulted in an apparent cyclone collection efficiency (Figure 3.3) higher than 100%. When low temperature runs were subsequently made, the layers would again thicken resulting in an apparent low cyclone collection efficiency. Thus, any proper measurement of the collection efficiency of the cyclones needs to be made after equilibrium layers have been established. The actual cyclone collection efficiency was about 80% to 85% when a large number of runs are considered.

Collection Efficiency

The coal fired for these tests was from Western Kentucky, an Eastern coal having about 2.5% to 4.5% content of sulfur, and about 16% to 25%* ash. The control of flyash is one of the major problems in the operation

*With the exception of one run.

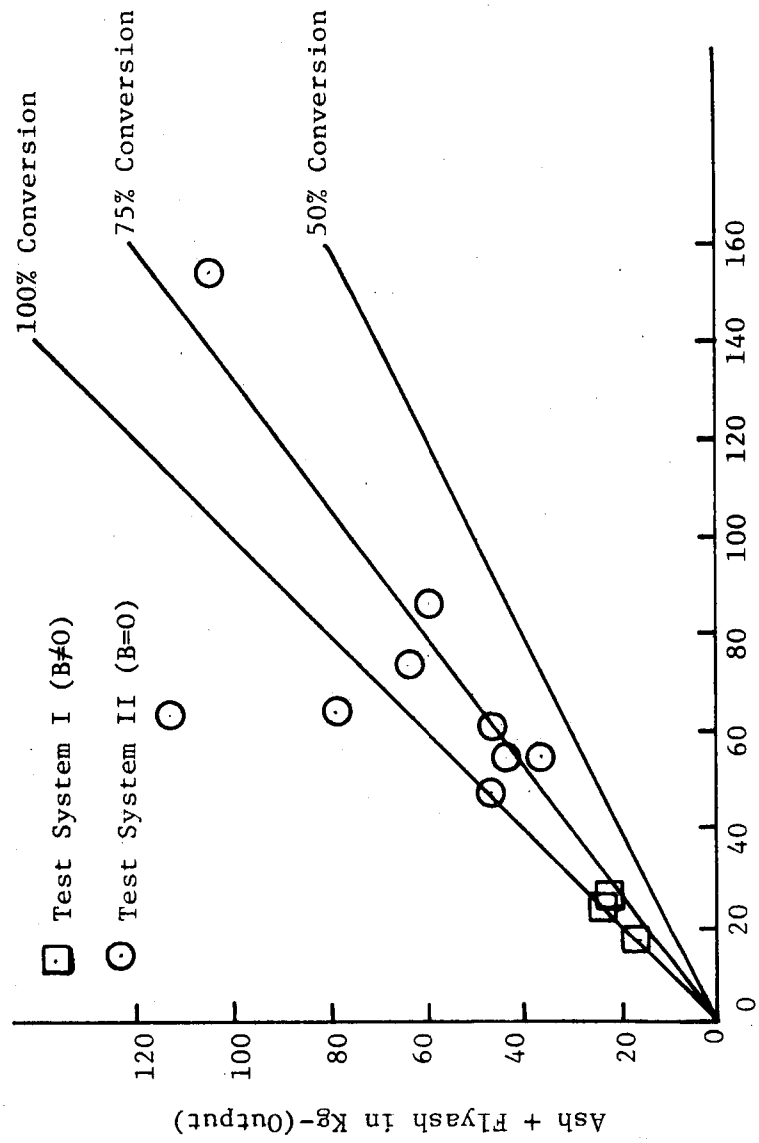

Figure 3.3. Conversion of Ash in Coal/Seed to Ash + Flyash.

of direct-fired MHD power plants. During this experiment most of the coal ash is found to be converted to slag layers and flyash.

Table 3.3 summarizes calculations of ash collection by the cyclones. The coal ash input was based on the percentage of ash in the coal used in the runs and the calculated firing rate. The ash output corresponds to the total ash collected at the bottom of the cyclone and at the exit of the cyclone. The mass flow rate for seed was 10% of that for the coal. Figure 3.3 (page 44) shows the plot of points calculated in Table 3.3. The tests indicate that collection efficiency of the slag/seed separation cyclones varied from about 70% to 95% over a wide range of test conditions. Wide scatter of these data is primarily due to the slag layers in the system being thinned or thickened as the temperature level in the system was varied. Overall it is believed that the collection efficiency of the cyclones is about 85% with the bulk of material having sizes of 5 microns and above. Later discussion will give additional details about the sub-micron size material which leaves the cyclone.

Characteristics of Collected Particulate Matter

This section discusses the experimental data obtained on the slag/seed interaction as well as the slag/seed separation processes. Slag samples were systematically removed from the bottom of the cyclones in the two test systems as described in Chapter II.

The slag material collected by the cyclones was removed after each run and weighed. In addition, slag samples were taken at various locations in the system. Particulate sampling measurements were also made

TABLE 3.3. COLLECTION OF ASH.

Test System	Test Run	Run Time	Entrance Temperature	$\dot{m}_{Coal}$	% Ash in Coal	Coal Ash/ Seed Input	Ash + Flyash Collected By Cyclone Output, Kg
		(mins.)	(^{o}K)	(Kg/Sec)		(Kg)	
I	1437*	20	1360	0.164	14.69	28.85	20.17
I	1440*	6.17	1400	0.155	17.58	15.78	15.75
I	1447	12.17	1440	0.191	17.58	24.51	23.31
II	57	29	1630	0.195	16.04	88.15	55.81
II	67	16.5	1700	0.211	22.58	47.25	46.33
II	71	16	1690	0.218	16.04	54.55	34.75
II	58	49.5	1725	0.155	32.93	155.15	100.99
II	64	19	1740	0.205	23.79	55.47	42.20
II	66	18	1700	0.200	27.99	60.46	49.04
II	68	17	1950	0.314	20.03	64.08	115.26
II	69	17	1835	0.277	22.89	64.74	78.94
II	62	30	1740	0.164	16.04	73.75	61.81

*Magnetic Field On.

by the sampling train in the exit of one of the cyclone separators. Details will be found in Chapter IV.

The particulate matter collected by the cyclones consisted of fine dust and "chunk-like" pieces or "clinkers" which had sizes from a few millimeters to a few centimeters. In general, about 50% of the weight of the material caught by the cyclone was fine dust and 50% was chunk-like pieces. Table 2.1 (page 32) presents a summary of these results. During the test runs, the cyclones collected dust and chunk material at a rate of about 1 kg./min. to 2 kg./min. in Test System I and at a rate of about 1.5 kg./min. to 6 kg./min. in Test System II. It will be seen in Chapter V that the potassium recovery is greater when the collection rate is low.

Some of the collected samples such as (1) flyash sampled in the stack and (2) ash recovered at the bottom of the cyclone, were treated by two warm water washings to determine what portion of the slag would be soluble in water without extensive treatment. When the wash water was evaporated to recover the soluble component in the dust from the bottom of the cyclone and from the stack or chunks, a white or colorless crystal-like material was obtained which in weight was almost equal to the weight loss produced by water washing. These test results on the seed recovery are covered in detail in Chapter V. The composition of the unwashed, washed and evaporated samples was obtained by chemical analysis and by the use of a scanning electron microscope (SEM) and an x-ray energy dispersive analysis (EDX) (Appendix B). The methods used for chemical analysis are described in Appendix A. The chemical analyses of the slag

samples were carried out by a commercial chemical laboratory. This chapter discusses the composition and characteristic of the unwashed sample taken from the bottom of the cyclone, while Chapter IV will contain a discussion on the composition and characteristic of the unwashed cyclone effluent.

Chemical Analysis

Table 3.4 summarizes the chemical composition of the collected slag/seed samples from Test System I and II for the dust and the chunk material collected at the bottom of the cyclone. Tests were made with potassium sulfate seed, potassium carbonate seed with and without a magnetic field. Test results indicated that the composition of the dust sample from Test System I had a slightly lower percentage by weight potassium (K) than from that of Test System II. However, the potassium content in the chunk material taken from Test System II was two times greater than that which was taken from Test System I. Perhaps the reason for this is the geometry of the two systems was different. In Test System I the unseeded coal flow impacted the inclined radiant "boiler" flow duct and an unusual slag accumulation occurred at the entrance of the radiant "boiler." The thermal conduction in this radiant "boiler" was higher than that of the radiant boiler in Test System II. Temperatures at the entrance of the slag/seed separation cyclone in Test System I was lower (range $1350^{o}K$ - $1500^{o}K$) than in Test System II (range $1600^{o}K$ - $1950^{o}K$). This may be the cause of the variation in the composition of the samples from two systems. Table 3.4 also gives the chemical composition of the collected slag/seed samples when K_2CO_3 seed was used. It shows lower percent-by-weight potassium from Test

TABLE 3.4. COMPOSITION OF COLLECTED SLAG/SEED FROM TEST SYSTEM I AND II (WITH K_2SO_4 AND K_2CO_3 SEED)

Specie	Dust Sample				Chunk Sample			
	K_2SO_4 Seed		K_2CO_3 Seed		K_2SO_4 Seed		K_2CO_3 Seed	
	B=0 Run I-1431	B=0 Run II-67	B≠0 Run I-1440	B=0 Run II-58	B=0 Run I-1431	B=0 Run II-67	B≠0 Run I-1440	B=0 Run II-58
K	12.65	19.8	13.20	18.70	6.70	16.10	1.20	15.30
Si	11.5	11.67	14.40	9.80	16.30	18.20	19.8	18.68
SO_4	19.14	18.25	20.15	17.64	1.77	4.40	2.74	2.63
K_2SO_4	28.19	33.11	29.42	32.00	3.21	7.98	2.64	4.77
Al	8.78	7.05	4.68	4.68	17.06	11.63	13.89	12.87
Fe	9.24	7.66	8.40	14.60	11.76	9.84	9.10	10.70
Cu	0.13	0.025	0.18	0.019	0.04	0.014	0.09	0.007
Ca	1.75	1.04	1.86	1.17	3.07	2.24	2.50	2.77
Na	0.50	0.33	0.40	-	0.32	0.36	0.42	-

Numbers Are In Percent-By-Weight.

System I than that from Test System II, mostly for the chunk material (by a factor of 15). This could be due to the presence of the magnetic field in Test System I and/or the geometry of the MHD flow train.

Table 3.5 and 3.6 give comparisons of the composition of the collected slag/seed samples with K_2SO_4 and K_2CO_3 seed in Test System I (with B-field). These tables suggest there is no significant change in the flyash composition when K_2CO_3 seed was used. As expected, there is a difference in the composition of the chunk material from Test System I and Test System II and this difference is probably due to the different flow train geometry and the presence of the magnetic field. Thus, one might expect that there would be a significant effect by the magnetic field on the slag/seed interaction process which will be explained in detail in Chapter V.

Analysis by Use of SEM and EDX

Figure 3.4 shows a scanning electron micrograph (SEM) with 1000X magnification of the dust material removed from the bottom of the cyclone in Test System I. Energy dispersive x-ray (EDX) analysis for this sample is also shown. This test was carried out with K_2SO_4 seed, with the MHD generator magnetic field on. Figure 3.5 represents similar results for an unwashed dust sample from the bottom of the cyclone in Test System II with K_2SO_4 seeding and no magnetic field, but a higher temperature at the entrance of the cyclone than in Test System I.

Scanning electron microscope analysis of other runs with potassium carbonate seeding yielded micrographs similar in appearance to those shown for K_2SO_4 seeding. The similarity in appearance of slag/seed dust caught

TABLE 3.5. COMPARISON OF COMPOSITION OF COLLECTED SLAG/SEED WITH K_2SO_4 AND K_2CO_3 SEED IN TEST SYSTEM I (B-FIELD ON)

Specie	Cyclone Dust		Cyclone Chunks	
	Seed K_2SO_4	Seed K_2CO_3	Seed K_2SO_4	Seed K_2CO_3
K	17.20	13.20	1.42	1.20
Si	11.00	14.40	18.90	19.80
SO_4	21.09	20.15	1.68	2.74
K_2SO_4	38.26	29.42	3.05	2.67
Al	7.41	4.68	14.29	13.89
Fe	6.86	8.40	7.28	9.10
Cu	0.18	0.18	0.05	0.09
Ca	1.07	1.86	1.86	2.50
Na	0.58	0.40	0.52	0.42

TABLE 3.6. COMPARISON OF COMPOSITION OF COLLECTED SLAG/SEED WITH K_2SO_4 AND K_2CO_3 SEED IN TEST SYSTEM II (NO B-FIELD)

Specie	Cyclone Dust		Cyclone Chunks	
	Seed K_2SO_4	Seed K_2CO_3	Seed K_2SO_4	Seed K_2CO_3
K	17.30	18.70	18.50	15.30
Si	11.66	9.80	16.49	18.68
SO_4	14.94	17.64	4.46	2.63
K_2SO_4	27.10	32.00	8.09	4.77
Al	6.49	4.68	12.61	12.87
Fe	7.69	14.60	9.69	10.70
Cu	0.023	0.019	0.015	0.007
Ca	1.42	1.17	2.21	2.77

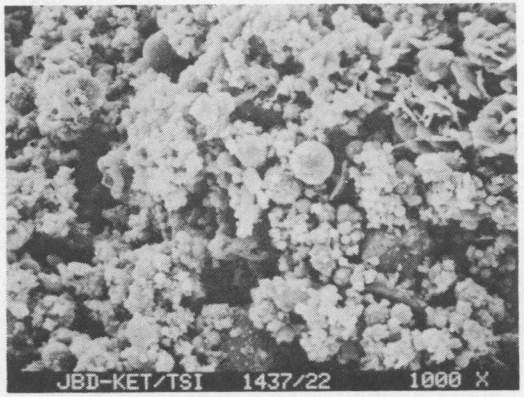

1 cm = 10μ

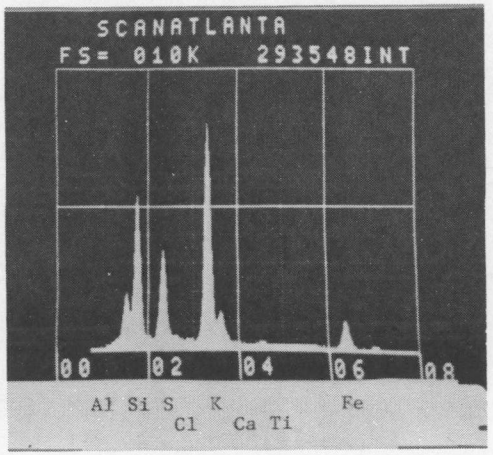

(a) SEM Photo of Cyclone Collected Dust, 1000X.

(b) EDX Scan.

Figure 3.4. Particulate Dust Formed Under MHD Conditions Removed From Bottom of Cyclone, Unwashed (Run 1437).

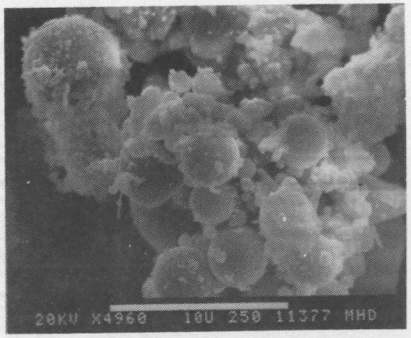

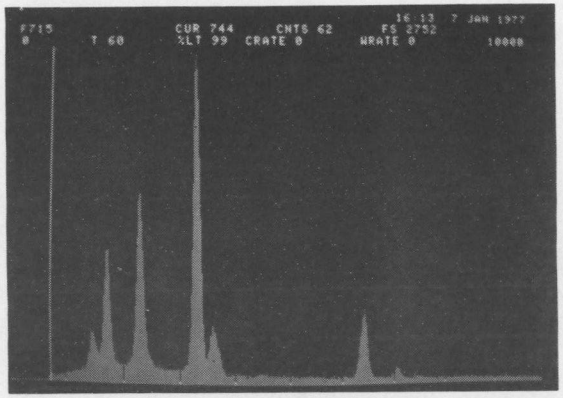

(a) SEM Photo of Cyclone Collected Dust, 4960X.

(b) EDX Scan.

Figure 3.5. Particulate Dust Removed From Bottom of Cyclone, Unwashed, (Run 71).

by the cyclone from tests with K_2CO_3 seeding at 10,000X is illustrated in Figure 3.6. Table 3.5 (page 51) and Table 3.6 (page 52) compare the chemical composition with the two different seed materials.

Figure 3.7 gives an EDX scan for K_2CO_3 seed for both test systems. An EDX scan for all these test runs, made with K_2SO_4 and K_2CO_3 seed, with magnetic field (Test System I) and without magnetic field (Test System II), indicates the existence of the elements in the slag/seed material collected by the cyclone as: aluminum (Al), silicon (Si), sulfur (S), potassium (K), calcium (Ca), iron (Fe), titanium (Ti) and some traces of chlorine (Cl). These elements were also found in the samples which were chemically analyzed.

When viewed at high magnification on the SEM, a spherically shaped particle from a micrograph of the dust material collected by the cyclone seemed to be covered with a rather dense layer of crystal like material which could be said to consist of potassium and/or sulfur as viewed from EDX.

Formation of Slag/Seed Wall Deposits in the Radiant "Boiler"

During the performance of tests, slag deposits occurred on the "boiler" flow duct tubes whose temperature ranged from $300^{o}K$ to $350^{o}K$. The space between the cooling water tubes and the metal of the radiant "boiler" is filled with an alumina based ceramic. The ceramic was exposed to the highest gas temperatures in the boiler which ranged from $1000^{o}K$ to $2000^{o}K$.

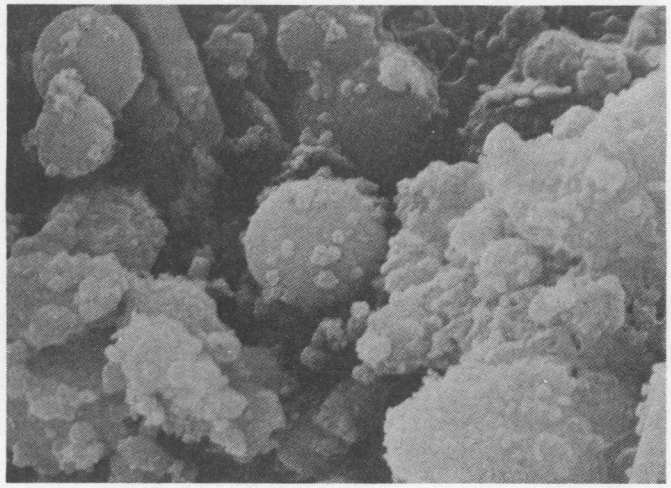

10,000X.

Figure 3.6. Micrograph of Cyclone-Collected Dust With K_2CO_3 Seeding and Short-Circuit Operation.

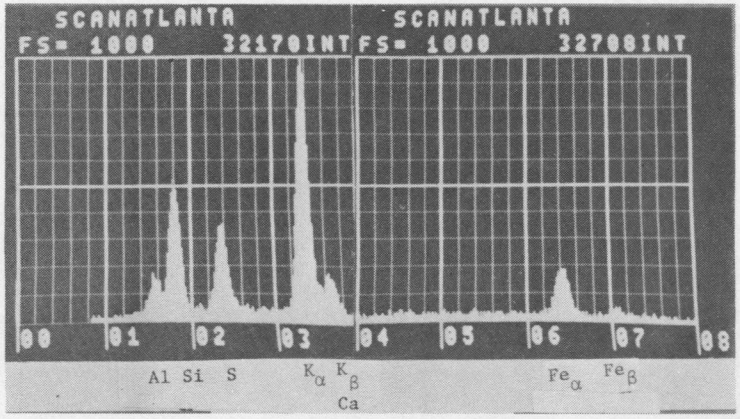

(a) Test System I - Unwashed Dust.

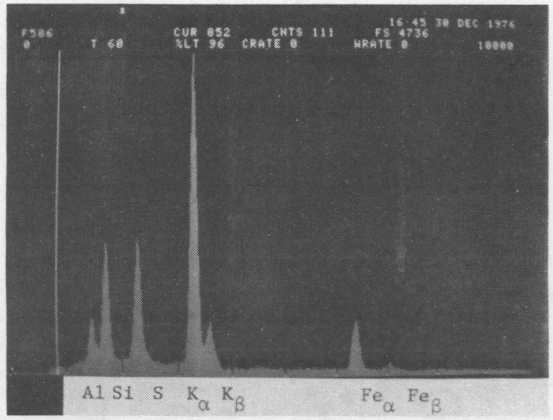

(b) Test System II - Unwashed Dust.

Figure 3.7. EDX Analysis With K_2CO_3 Seed for Dust Collected by Cyclone.

Table 3.7 presents the potassium and sulfate concentration of the radiant "boiler" wall samples from both test systems. Inspection shows that the samples removed from the walls at the MHD generator exit (Test System I), which is the radiant boiler entrance, and at the exit of the radiant boiler, have about the same chemical composition and is believed to be that of the chunk material blown from the walls (Table 3.4, page 49). In Test System II, the potassium concentration in the slag layers on the splitter plate, which leads to the entrance of the slag/seed separation cyclone, is less than at the entrance of the radiant "boiler." The temperature of the slag layers at the entrance of the radiant boiler probably is lower than the layers in the stagnation region of the splitter plate. Figure 3.8 shows a photograph of the slag coating on the interior of the radiant "boiler" looking upstream into the MHD channel (Test System I).

Figure 3.9 illustrates the layer separation in the slag coating on the walls of the radiant "boiler" entrance in Test System II. Layer one in Figure 3.10 at the side of the plasma surface having components that of the slag/seed as: Al, Si, K, and Fe, and it is at the temperature of about $1600^{o}K$ where as layer five and six are in the ceramic having a temperature of about $400^{o}K$ to $600^{o}K$. It is noticed that there are significant variations of concentration of K and S in these layers which indicates that the potassium seed is condensed on the wall (Figure 3.11). The metal surface was at $200^{o}K$. The relationship between slag/seed composition and relative thickness of the deposit is related to the slag layer temperature. This loss of seed affects the recovery of potassium downstream of the generator as will be seen later. Slag layer separation

TABLE 3.7. POTASSIUM AND SULFATE CONCENTRATION OF WALL SAMPLES IN TEST SYSTEM I AND II FOR K_2SO_4 SEEDING

Wall Samples	Test System I		Test System II	
	No B-Field		No B-Field	
	% K	% SO_4	% K	% SO_4
Radiant Boiler Entrance	6.90	0.29	11.30	1.70
Radiant Boiler Exit	7.65	0.31	11.30	0.29
Splitter Plate Stagnation Area	NO DATA		7.59	2.76

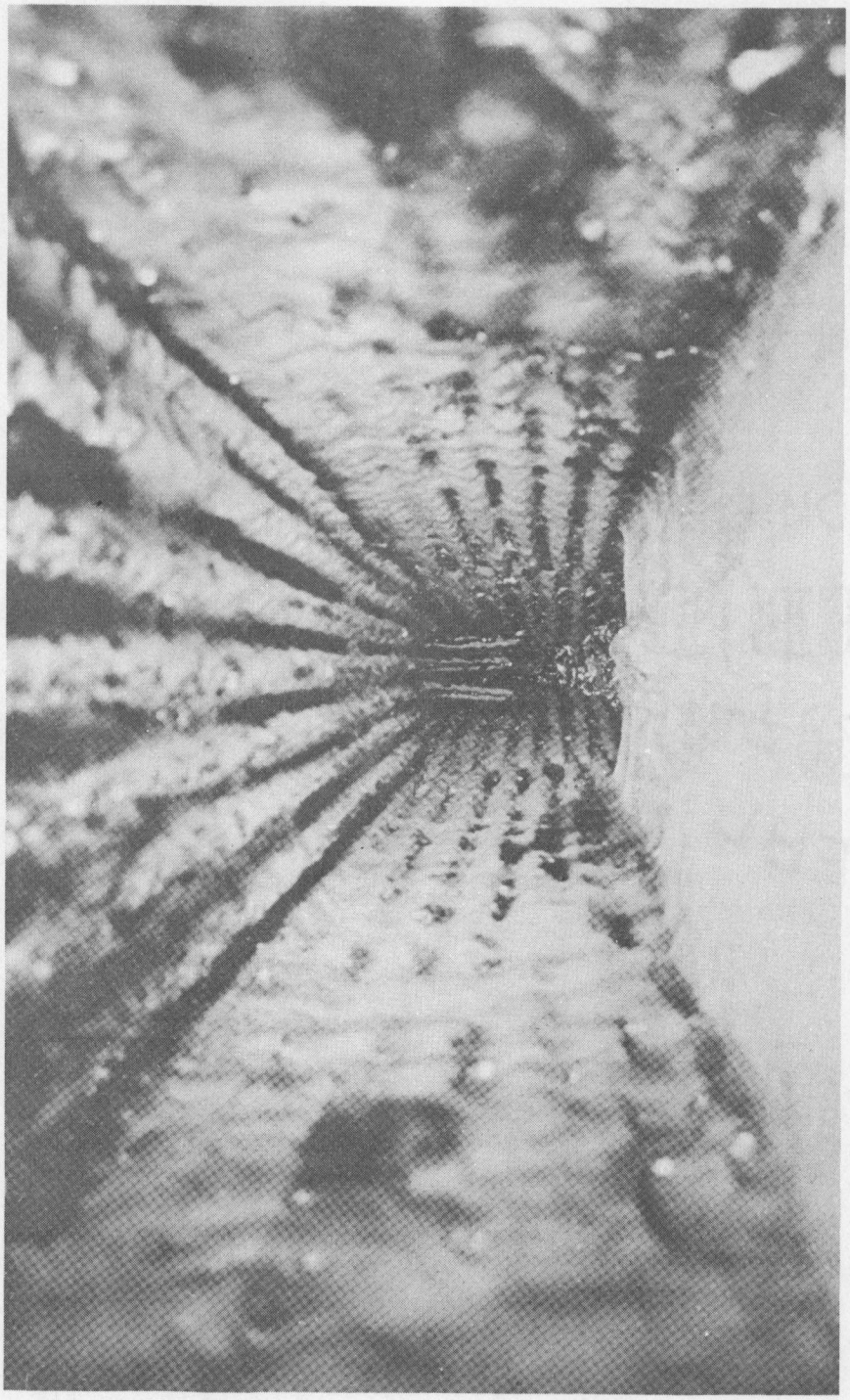

Figure 3.8. Interior of Radiant Boiler Showing Slag Coating.

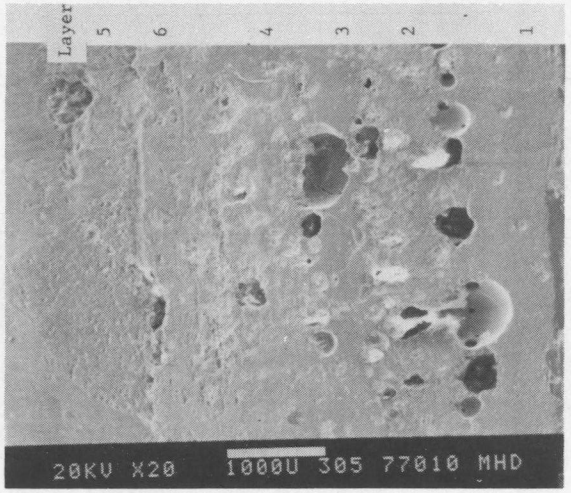

Figure 3.9. Layer Separation in Slag Coating at the Entrance of the Radiant Boiler.

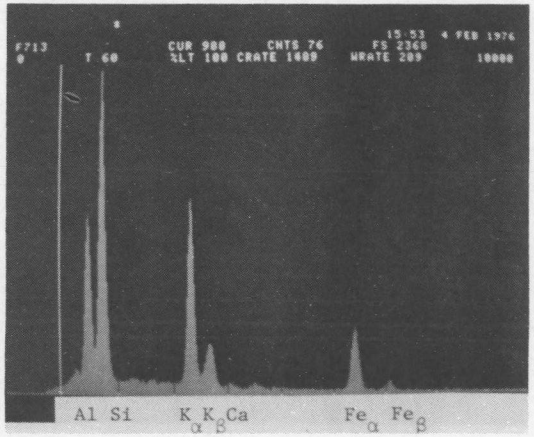

Figure 3.10. An EDX Scan of Layer No. 1.

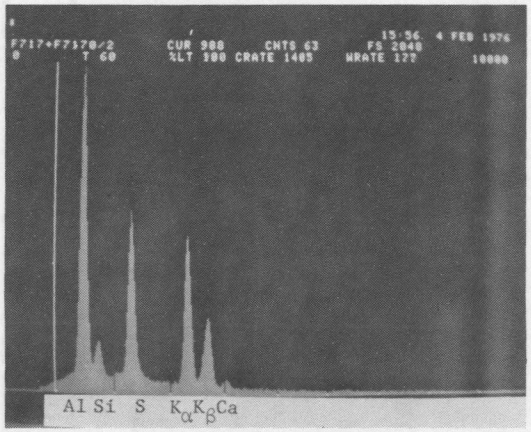

(a) An EDX Scan of Layer No. 5.

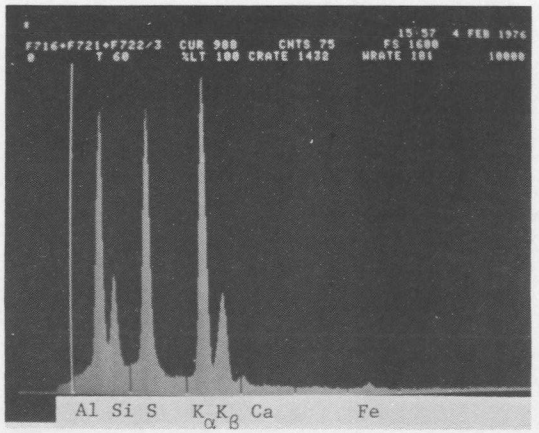

(b) An EDX Scan of Layer No. 6.

Figure 3.11. EDX Analysis of Layer at the Entrance of the Radiant Boiler.

also occurred in the slag coating on the walls of the radiant "boiler" in Test System I (B=0). Similarly, an EDX scan in Figure 3.12 shows the concentration of potassium and sulfur condensed on the wall.

Figure 3.13 depicts the layer separation in the slag coating of the splitter plate wall (which divides the flow into two cyclones). Layer six in Figure 3.14 at the side of the wall surface also indicates that a significant amount of K and S exists right at the wall, i.e. K_2SO_4 is condensed on the wall and thereby covered over by the slag deposit. It is believed that the seed material first deposits at the cold wall and then sulfur evaporates slowly as SO_2 through the slag deposit up to approximate plasma surface. This loss of K_2SO_4 would appear to occur one time during starting because samples viewed under the SEM are taken from the radiant "boiler" or splitter plate slag layer after many test runs have been made; this does not exhibit a K_2SO_4 layering effect. In order to determine if the loss of K_2SO_4 seed in the slag layer occurs by the mechanism suggested above, one could make a test run without seed and then with seed so there will be a smooth layer of unseeded slag before the seeded slag. Also, the overall potassium loss in the slag layer surface area is scale dependent.

Calculation of Equivalent Oxides

From chemical data obtained from the commercial laboratory, such as Table 3.4 (page 49), it is possible to compute the weight distributions of the various oxides formed in slag/seed material. For unseeded coal, it is commonly assumed that these compounds would consist of: SiO_2, Al_2O_3,

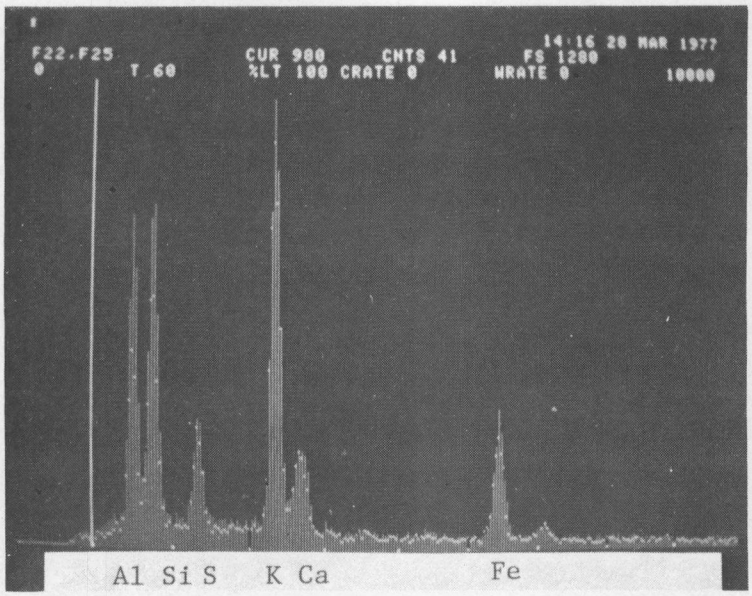

Figure 3.12. An EDX Analysis of a Radiant Boiler Slag Layer From Test System I.

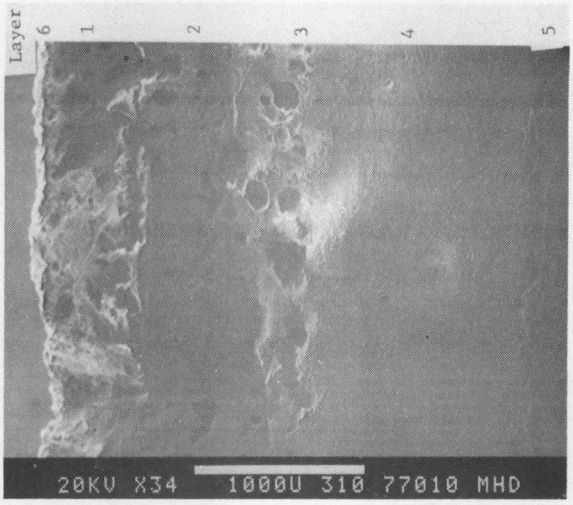

Figure 3.13. Layer Separation in the Slag Coating at the Splitter Plate Wall.

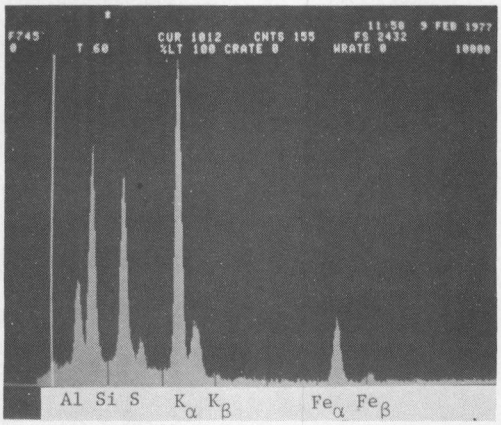

(a) An EDX Scan of Layer No. 6.

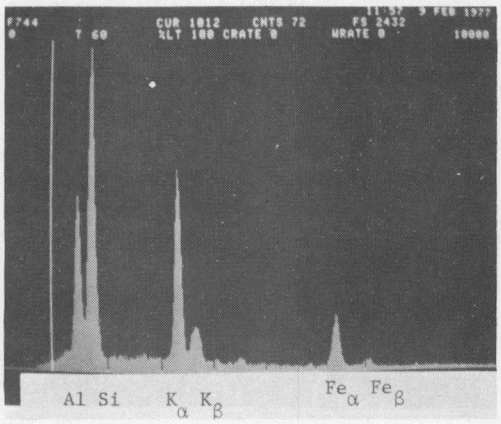

(b) An EDX Scan of Layer No. 5. (Side of the Flow.)

Figure 3.14. EDX Analysis of Slag Layer at the Splitter Plate Wall.

Fe_2O_3, MgO, CaO, Na_2O, TiO_2, P_2O_5. The commercial laboratory determined Si as SiO_2. Aluminum, iron, calcium, sodium and potassium were measured by atomic absorption, spectrophotographic methods and chemical methods. Gravimetric analysis was used to determine sulfate.

For the present case of seeded coal, it was assumed that potassium sulfate would form instead of K_2O. However, if a surplus of K over that needed for the total available sulfate existed, K_2O was assumed to form in addition to K_2SO_4. If an excess of sulfate existed, it was assumed that it would exist in some form of SO_4 (sulfate).

Tables 3.8 and 3.9 summarizes the calculated oxides and sulfates or carbonates for tests from Test System I and II and where potassium sulfate or potassium carbonate seed was employed. It should be noted that laboratory analysis on the samples from Test System I was not carried out for the elements (1) magnesium, (2) titanium and (3) phosphorus. These species are known to exist in the coal that was fired from other samples and are estimated here in the form of MgO, TiO_2, and P_2O_5 that would exist in the slag. It should also be noted that the moisture measurements were not always made on all samples from Test System I sent to chemical laboratory so they are estimated here. While these elements and moisture are estimated for tests from Test System I, they are also measured chemically for Test System II. This also suggests that these species indeed existed in coal that was fired and the assumption made for these elements was reasonable. X-ray analysis has also shown that in many of the samples these elements existed.

Inspection of these tables illustrates that for dust collected by the cyclone, the conventional composition accounted

TABLE 3.8. SLAG/SEED OXIDE AND SULFATE COMPOSITION CALCULATED FROM LABORATORY ANALYSIS WITH K_2SO_4 SEED FOR TEST SYSTEM I AND II

Specie Oxide	Dust From Cyclone		Chunk Material From Cyclone	
	I-1437	II-67	I-1437	II-67
SiO_2	23.56	24.98	40.42	38.93
Al_2O_3	14.00	13.32	27.00	21.97
Fe_2O_3	9.81	10.94	10.41	14.06
CaO	1.50	1.46	2.60	3.14
Na_2O	0.78	0.44	0.70	0.49
C	5.91	2.20	0.0	0.0
CuO	0.23	0.032	0.06	0.017
K_2SO_4	38.23	33.11	3.05	7.98
K_2O	0.0	5.99	0.05	15.09
SO_4	0.60	0.0	0.0	0.0
Moisture	0.50	0.38	0.1	0.0
MgO	3.0	1.04	5.0	1.33
TiO_2	0.8	1.00	1.00	0.12
P_2O_5	0.4	0.4	0.4	0.0
TOTAL	99.30	95.29	90.80	103.25

TABLE 3.9. SLAG/SEED OXIDE AND SULFATE COMPOSITION CALCULATED FROM LABORATORY ANALYSIS WITH K_2CO_3 SEED FOR TEST SYSTEM I AND II

Specie Oxide	Dust From Cyclone		Chunk Material From Cyclone	
	I-1440	II-58	I-1440	II-58
SiO_2	30.86	20.99	42.48	40.01
Al_2O_3	8.84	8.84	26.24	24.31
Fe_2O_3	12.01	20.86	13.01	15.29
CaO	2.60	1.64	3.50	3.88
Na_2O	0.62	0.27	0.57	0.32
C	8.20	2.60	0.10	0.00
CuO	0.23	0.024	0.11	0.009
K_2SO_4	29.45	32.03	2.68	4.79
K_2CO_3	0.0	7.68	0.0	23.27
SO_4	2.93	0.0	1.31	0.0
Moisture	0.2	1.14	0.10	0.0
MgO	3.0	0.90	5.0	0.74
TiO_2	0.8	0.10	1.0	0.17
P_2O_5	0.4	-	0.4	-
TOTAL	99.90	97.07	96.50	112.79

for about 99% of the weight of the dust sample from Test System I and 95% of the weight of the dust sample from Test System II. In the case of the chunk material collected by the cyclone, the calculation oxides accounted for about 90% of the total weight of the slag/seed chunk material from Test System I. It is possible to account for missing weight. From Test System II, the composition assumed accounted for more than 100% of the weight of the chunk material suggesting there are no missing oxides of the elements.

From these calculated oxide and sulfate composition it is evident that large amounts of potassium sulfate are formed in the system and the slag/seed separation cyclone served to separate potassium compounds from slag compounds.

Size Distribution

Particle size distribution obtained by measuring and counting particles on micrographs, such as Figure 3.4 and 3.5 (page 53) are shown in Figure 3.15. The figure compares the size distribution of dust collected by the cyclone in both test systems. It is noted that the cyclone collected dust has a most probable particle diameter of about ten microns in Test System I and about six microns in Test System II. One might expect that there could be an effect of particle size on the slag/seed interaction process which will be discussed in Chapter V. In the next chapter the particle size distribution of the flyash, which leaves the cyclone, will be given.

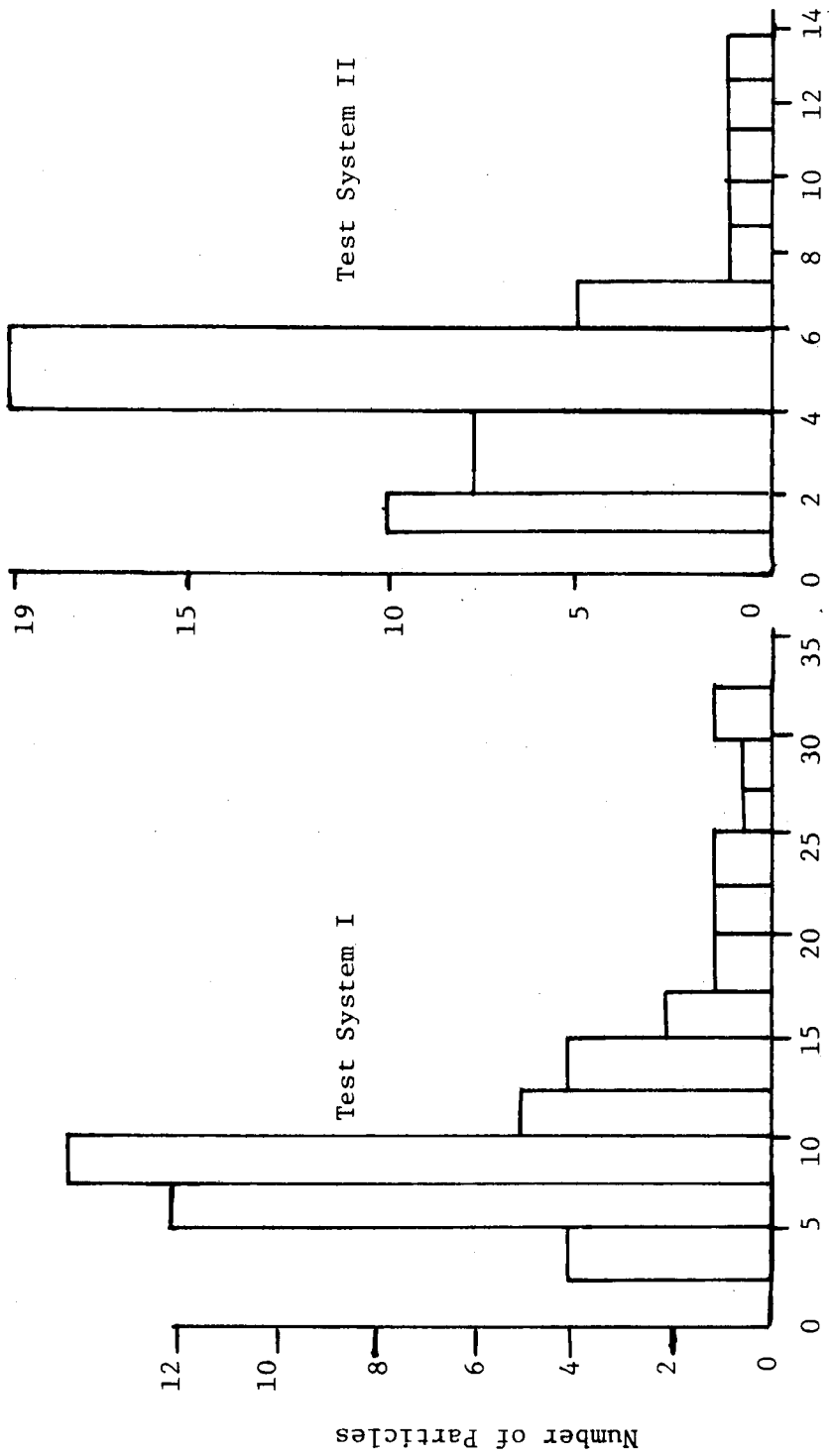

Figure 3.15. Size Distribution of Cyclone Collected Ash From Both Test Systems.

CHAPTER IV

EMISSIONS FROM THE CYCLONE SEPARATOR

Sampling Techniques and Sampling Calculations (13, 14)

Particulate concentration of the emissions from stacks were sampled during these tests to: (1) determine the chemical content in the flyash and recover potassium, (2) determine the effectiveness of the slag/seed separation equipment, (3) identify the pollutants (for example, sulfur dioxide in this experiment) in the atmosphere, and (4) determine the capability of additional equipment needed to reduce potassium loss and reduce the concentrations of the pollutants. Normal sampling measurements have been made at the cyclone exit during these tests.

Particulate Matter (15)

Since the particles in the flyash emitted from the exit of the cyclone stack are much larger than gas molecules, each time the flow direction of the gas stream changes, such as a bend in the sample tube or flow around an object, the larger particles tend to continue on their original path and are somewhat displaced from the new path of the gas stream as illustrated in Figure 4.1. Thus, it is necessary for all parts of the stream to be sampled and properly weighted to obtain a representative sample of the particle distribution in the whole stream.

One of the EPA source sampling requirements is isokinetic sampling which was used to obtain the particulate concentration profiles of cyclone emissions in the Test System II. Isokinetic sampling means that the gas

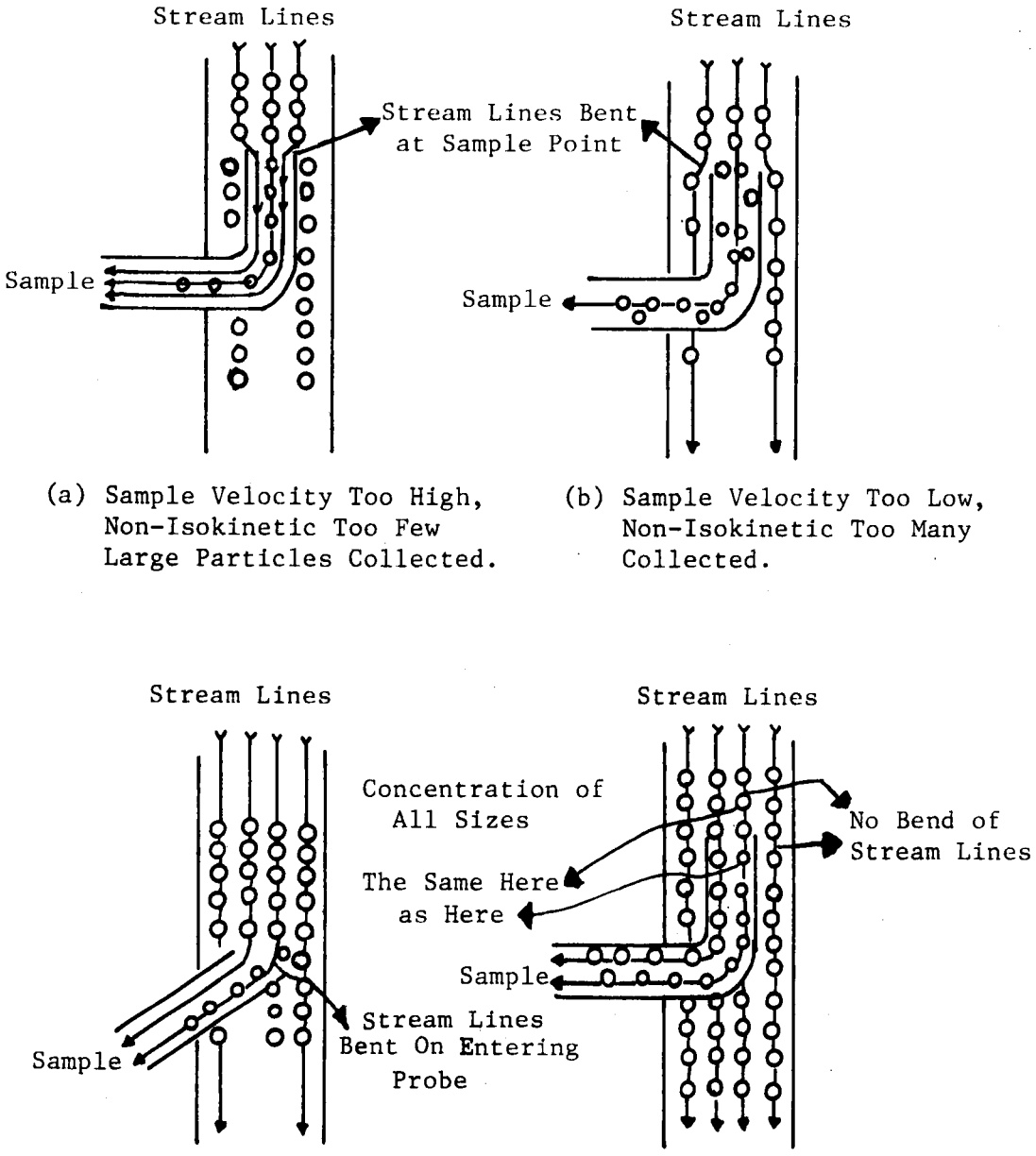

(a) Sample Velocity Too High, Non-Isokinetic Too Few Large Particles Collected.

(b) Sample Velocity Too Low, Non-Isokinetic Too Many Collected.

(c) Sample-Tube Not In Line, Non-Isokinetic Too Few Large Particles Collected.

(d) Illustration of Isokinetic Sampling.

Figure 4.1. Schematic Illustration of Isokinetic and Non-Isokinetic Sampling (Ref. 15).

sampling velocity (V_n) entering the probe tip, which extracts a portion of the gas sample from the stack and delivers it to the sampling probe, is equal to the stack gas velocity (V_s) at that point; so that the collected particles will be representative of the flow in that portion of the stream being sampled. Due to the unavailability of a complete EPA type sampling train for earlier tests in Test System I, the flow was not sampled isokinetically during the early experiments. In Test System I, the sampling probe (about 25.4 cm. long) was aligned with the vortex flow in the exhaust duct as described in Chapter II. Due to the vortex motion in the exhaust of Test System I, it was not possible to obtain uniform velocity in order to carry out isokinetic sampling which is more desirable. These difficulties were solved in Test System II where flow straightening vanes and an extended exhaust stack were used in order to have a smoothed flow and to allow the isokinetic sampling of the particulate emissions from the cyclone. The sampling probe used in this test system was about 1.91 meters long having replacable probe tips with diameters ranging from 0.89 cm. to 1.27 cm., while the probe tip to the sampling probe in the earlier tests had a fixed diameter of 0.95 cm.

If the gas sample is taken into the probe tip at a velocity, V_n, greater than the stack gas velocity, V_s, (Figure 4.1(a), page 69) then the measured particulate concentration, C_m, is less than the true concentration, C_t, due to the fact that the larger and heavier particles are unable to follow the flow streamlines, but the gas around them is drawn into the probe. Thus, fewer heavy or large particles are collected than should be. A similar situation occurs (Figure 4.1(c), page 69) when the sample

probe tip is not in line with the flow and if $V_n < V_s$, then a greater portion of large particles are sampled than should be (see Figure 4 (b)), so $C_m > C_t$. In these three cases the sample is said to be non-isokinetic. If the gas sampling rate is adjusted so that $V_n = V_s$ (Figure 4.1 (d), page 69) then an isokinetic sample is achieved.

Table 4.1 gives, for many of the tests described herein, the calculated values of the stack gas velocity and the nozzle velocity along with other parameters including the variation of percentage of isokinetic. Table 4.1 also shows higher volumetric flow rate for the runs in Test System I than for those of Test Sytem II. This may be due to the fact that in the first system the particulate matter was sampled in a vortex flow while it was sampled in the uniform flow in the second system. The same arguement follows for the results of the particulate emission rate.

It is not always necessary to use isokinetic sampling to obtain a reasonably good particulate sample. Experiments carried out in Test System I indicated that small particles (about 0.3 microns diameter and less) were being emitted from the stack of the cyclone. Since the particles are so small, the requirement for isokinetic sampling for efficient collection is lessened because inertial effects are minimized due to the small mass of particles.

Particulate Emission Calculations and Sampling Procedure

The sampling parameters of (1) velocity pressure ΔP, (2) pressure drop across the orifice meter ΔH, (3) inlet and outlet meter temperature T_m, (4) meter volume V_m, (5) sample time θ, and (6) stack temperature T_s

TABLE 4.1. SLAG/SEED CYCLONE EMISSIONS TESTS DOWNSTREAM OF THE MHD GENERATOR

Test System	Test Run	Stack Gas Temperature T_s °C	Stack Gas Velocity $V_s)_{avg}$ m/sec	Q_s std m^3/min	Nozzle Velocity $V_n)_{avg}$ m/sec	Particulate Emissions Rate Kg/min	Isokinetic %
I	1431*	227	NOT MEASURED	52.76	NOT MEASURED	1.89	N/A
I	1437*	227	NOT MEASURED	39.03	NOT MEASURED	1.20	N/A
I	1440*	227	NOT MEASURED	31.79	NOT MEASURED	3.17	N/A
I	1447	227	NOT MEASURED	39.29	NOT MEASURED	0.69	N/A
II	54	598	6.41	7.46	7.14	0.22	111
II	57	616	6.92	8.45	6.34	0.32	92
II	58	548	5.30	7.98	4.78	0.28	90
II	62	551	7.01	11.28	6.11	0.31	87
II	66	628	10.00	15.10	8.54	0.31	86
II	67	616	9.84	13.88	9.18	0.35	93
II	68**	808	16.89	19.21	11.42	0.74	68
II	69**	737	14.68	17.32	14.71	0.65	100
II	71	645	11.26	15.10	8.67	0.48	77

*With a Magnetic Field; **High Mass Flow Rate.

were measured for every traverse point used in obtaining the sample. The sampling time per traverse point was selected such that it was not less than two minutes and the total sampling time was greater than or equal to the minimum total sampling time required to collect significant amounts of particulate matter on the filter as specified by EPA. At the end of the sampling period, after the sampling probe has been removed from the stack, the sample train was disassembled. The volume of water condensed in the impingers was measured and sent for analysis to a chemical laboratory. The sum of the mass of water collected by the silica gel and the volume of water condensed in the impingers is the total amount of water of the sampled gas.

In Test System I, the first three impingers were water filled and the last one was kept empty in the manually assembled sample train, whereas for Test System II sampling, the first two impingers were filled about half with water, the third was dry and the last was filled with silica gel (about 200 grams) in order to absorb the carryover liquid. Figure 4.2 illustrates the ice bath for the impingers and the heated portion for the filter. This latter sampling arrangement is more consistent with recommended EPA procedures.

Prior to the test, the fiberglas filter (or thimble) was desiccated and dried to a constant weight ($\pm$ 0.2 mg.). After the sampling test, samples from the probe were removed by acetone washings and evaporated to dryness at ambient temperatures. Particulate matter from the filter and acetone washings are added to determine the total amount of particulate collected. Chapter II provides the detail diagram of the sampling train used in this experiment. (Figure 2.10, page 35).

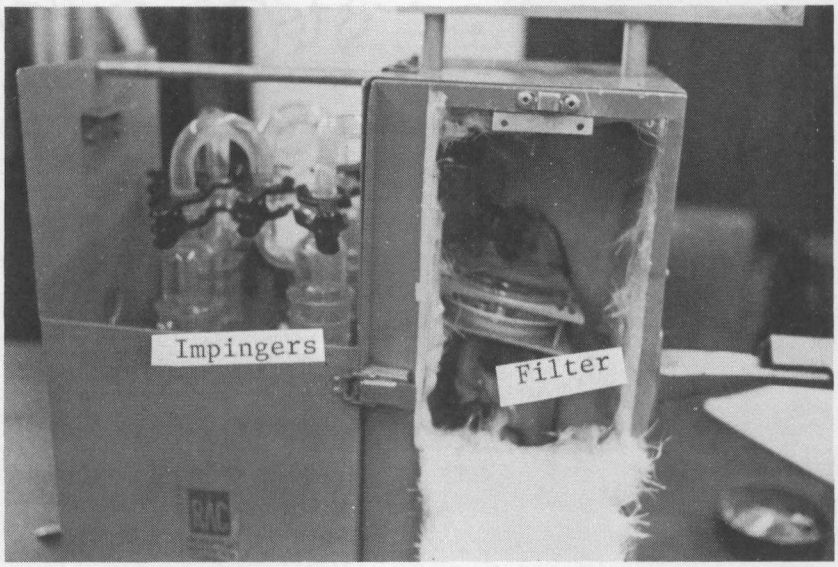

Figure 4.2. Sampling Box Assembly Showing Impingers and Filter - Test System II.

Velocity Measurement (EPA Method 2)

The velocity of the stack gas is determined from the gas density and from the measurement of the velocity head ΔP. The S-type (reverse-type) pitot tube is used primarily for stack testing since it is not easily clogged in a dust ladden gas flow and can be inserted through a small hole in the stack. It does not measure directly the average velocity of a gas stream but measures the local velocity at the traverse point at which it is located. Figure 4.3 shows a sketch of a duct and the location of the traverse points on a 35.6 cm. diameter duct. There were six traverse points. The table next to the figure gives the location distance of each traverse point. The measured ΔP is larger than that corresponding to a standard pitot-static tube.

The S-type pitot was calibrated by using a standard pitot tube according to the procedure in section four of Reference (14). The pitot tube coefficient C_p was calculated to be 0.85.

The equation to calculate the average stack gas velocity has the following form:

$$V_s = 34.97\ C_p\ (\Delta P)^{\frac{1}{2}}_{avg} \left[\frac{(T_s)_{avg}}{P_s M_s} \right]^{\frac{1}{2}} \qquad (4.1)$$

where,

P_s is the absolute stack gas pressure, mm of Hg, and M_s is the molecular weight of stack gas (wet basis),

$$M_s = M_d\ (1-B_{wo}) + 18\ B_{wo} \qquad (4.2)$$

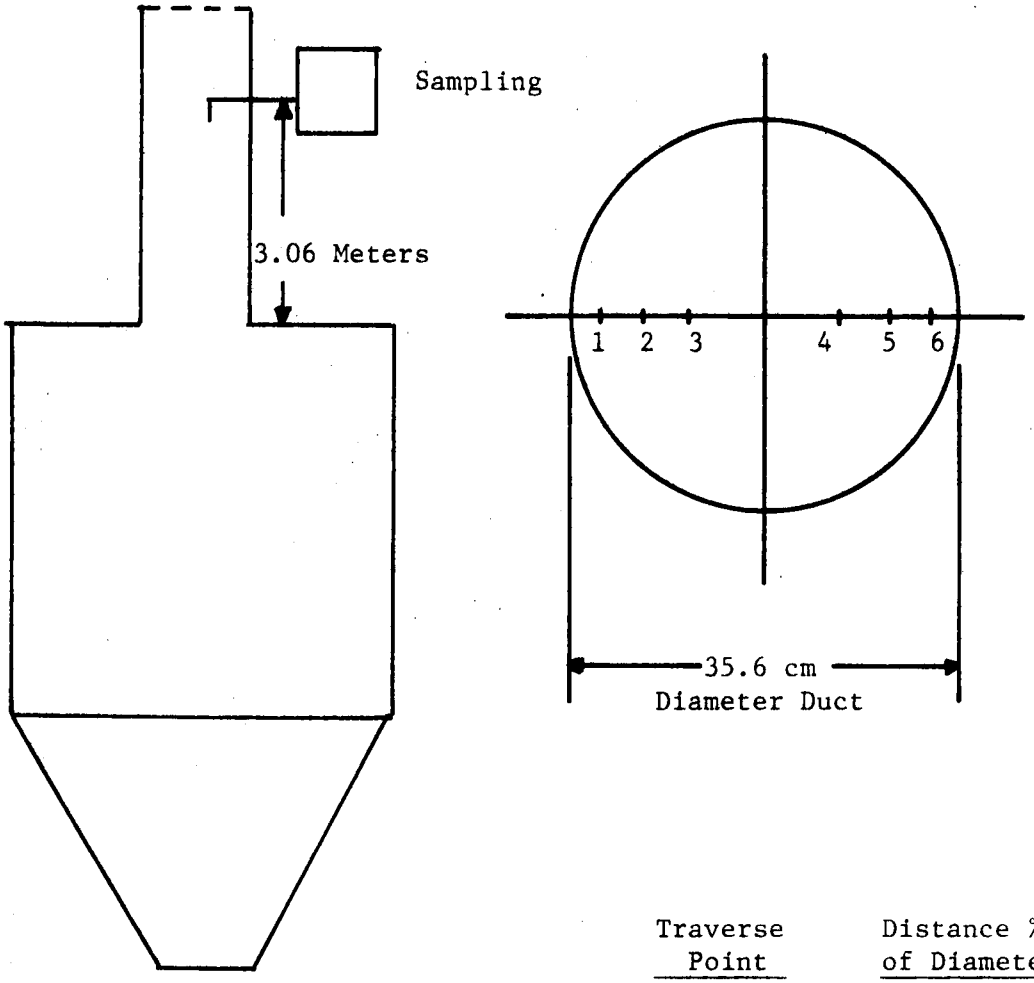

Location of Sampling Probe

Traverse Point	Distance % of Diameter
1	4.4
2	14.7
3	29.5
4	70.5
5	85.3
6	95.6

Figure 4.3. A Sketch Showing Circular Stack Divided Into Six Traverse Points According to EPA Rules.

M_d is the molecular weight of stack gas (dry basis) determined by the Orsat analyzer and found to be 44 g/g-mole in this experiment. The stack gases were found to have a very large amount of CO_2 and CO as a result the use of a molecular weight of 44 (that of CO_2) is justified.

Velocity measurements were made only in Test System II since in this test series uniform velocity profiles were obtained in the extended exhaust duct with flow straightening vanes.

Calculations

The calculated procedures used to determine the particulate emissions are summarized below. Further details may be found in Reference (14).

Volume of Dry Gas Samples

Sample volume measured by the dry gas meter V_m was corrected to standard conditions (20°C, 760 mm. Hg.) by the following equation:

$$V_{m_{std}} = V_m \left[\frac{T_{std}}{T_m}\right] \left[\frac{P_{bar} + \frac{\Delta H}{13.6}}{P_{std}}\right] \tag{4.3}$$

where,

P_{bar} is the barometric pressure at the outlet of the orifice meter, mm of Hg, ΔH is the average pressure drop across the orifice meter, mm of H_2O. T_m is the average dry gas meter temperature, °K, T_{std} is the standard absolute temperature, 293°K, and P_{std} is the standard absolute pressure, 760 mm Hg.

Volume of Water Vapor in the Stack Gas

The total volume of liquid collected in impingers and silica gel, $V_{lc}(ml)$ was measured and the volume of water vapor in the stack gas at standard conditions $V_{w_{std}}$ was calculated by using the Equation (4.4),

$$V_{w_{std}} = V_{lc} \left[\frac{\rho_{(H_2O)}}{M(H_2O)} \times \frac{R\, T_{std}}{P_{std}} \right] \qquad (4.4)$$

where,

ρ_{H_2O} is the density of water at standard conditions, 1.0 g./ml., M_{H_2O} is the molecular weight of water, 18 g/g-mole, R is the ideal gas constant, 0.06236 mm. Hg-$m^3/^oK$-g-mole.

Moisture Content of Stack Gas

A dimensionless factor B_{wo}, indicating the propertion by volume of water vapor in the gas stream was calculated by Equation (4.5),

$$B_{wo} = \frac{V_{w_{std}}}{V_{m_{std}} + V_{w_{std}}} \qquad (4.5)$$

where,

$V_{w_{std}}$ is calculated from Equation (4.4) and $V_{m_{std}}$ is calculated from Equation (4.3).

Particulate Emission Concentration

The concentration of particulate matter in the stack gas (dry basis) C_s' in grains/std m^3 was calculated by the following equation:

$$C'_s = (0.0154 \frac{\text{grain}}{\text{mg}}) \frac{M_n}{V_{mstd}} \quad (4.6)$$

where,

M_n is the total amount of particulate matter collected, mg, $V_{m_{std}}$ is calculated from Equation (4.3).

Stack Gas Volumetric Flow Rate (EPA Method 2)

The average volumetric flow rate at dry standard conditions Q_s (m^3/hr) was calculated using the following equation,

$$Q_s = 3600\ (1-B_{wo})\ V_s A \left[\frac{T_{std}}{T_s}\right]\left[\frac{P_s}{P_{std}}\right] \quad (4.7)$$

where,

B_{wo} is the dimensionless factor calculated from Equation (4.5), V_s is the average stack gas velocity calculated from Equation (4.1), m/sec, A is the cross-sectional area of stack, m^2, T_s is the average absolute stack gas temperature, ^oK and P_s is the absolute stack gas pressure, mm Hg.

The stack gas volumetric flow rate in Test System I was calculated by using the ideal gas law equation assuming the exhaust stack pressure to be atmospheric pressure and assuming stack gas temperature T_s (^oK) to be constant across the duct,

$$P\dot{V} = \dot{m}RT_s \quad (4.8)$$

where,

$\dot{V} = \frac{dV}{dt} = Q_s$ is the volumetric flow rate and $\dot{m}$ is the mass flow rate of the stack gas.

Isokinetic Variation

The average percentage isokinetic sampling ratio I was calculated by taking the ratio of the average probe inlet velocity V_n to the average stack gas velocity V_s. The equation used is,

$$I = (V_n/V_s) \quad x100 \tag{4.9}$$

where,

$$V_n = \frac{V_m T_s (P_{bar} + \frac{\Delta H}{13.6})}{T_m (1-B_{wo})\theta P_s A_n} \tag{4.10}$$

is the probe inlet velocity, independent of the velocity pressure measured in the stack,

where,

V_m is the volume of gas sample through the dry gas meter, m^3, θ is the total sampling time, sec., A_n is the cross-sectional area of the probe inlet, m^2, and V_s is calculated from Equation (4.1), m/sec.

Equations (4.3) and (4.6) were used to calculate the volume of dry gas sampled and the concentration of particulate matter in the stack gas in Test System I. All equations were used to calculate the particulate emissions in Test System II except where noted for Test System I.

A summary of the calculated results of the slag/seed cyclone emissions are tabulated in Table 4.1 (page 69) and Table 4.2.

TABLE 4.2. SLAG/SEED CYCLONE EMISSIONS TESTS DOWNSTREAM OF THE MHD GENERATOR

Test System	Test Run	Seed Type	Total Sampling Time, min θ	Moisture In Stack Gas B_{wo} %	Particulate Emissions Concentration C'_s grains/std m^3	Stack Gas Temperature T_s °C
I	1431	K_2SO_4	5.0	NOT MEASURED	550.1	227
I	1437*	K_2SO_4	4.0	NOT MEASURED	474.6	227
I	1440*	K_2CO_3	3.0	NOT MEASURED	1536.4	227
I	1447	NONE	6.0	NOT MEASURED	268.4	227
II	54	K_2SO_4	15.25	40.5	452.0	598
II	57	K_2SO_4	19.00	36.4	582.3	616
II	58	K_2CO_3	12.00	27.3	531.8	548
II	62	K_2CO_3	17.00	22.0	424.4	551
II	66	K_2CO_3	14.00	19.9	317.8	628
II	67	K_2SO_4	10.00	26.5	394.4	616
II	68**	K_2SO_4	9.0	27.8	593.6	808
II	69**	K_2CO_3	12.00	30.4	579.1	737
II	71	K_2SO_4	12.00	27.1	486.2	645

*With a Magnetic Field; **High Mass Flow Rate.

Characteristic of Collected Particulate Matter at the Exit of the Cyclone

Chemical Analysis

This section discusses the chemical composition of the flyash collected by the sampling train at the exit of the cyclone from both test systems. Table 4.1 (page 72) and Table 4.2 (page 81) give the values of particulate emissions concentration and flow conditions from both test systems.

Table 4.3 shows the chemical composition of the flyash collected by the sampling probe at the exit of the cyclone from Test System I and II. These results were obtained with K_2SO_4 and K_2CO_3 seed with and without magnetic field. The temperature range for the runs on Test System I was $1350^{o}K$ - $1500^{o}K$ and for the runs on Test System II was $1600^{o}K$ - $1950^{o}K$.

The composition from flyash leaving the cyclone from Test System I shows lower percentage by weight potassium than that from Test System II, while the sulfate composition in both test systems appears to be equal. This could be due to the fact that the temperatures at the entrance of the slag/seed separation cyclone and the stack gas temperatures in Test System I were lower than in Test System II. In addition, these two systems had different flow train geometries mainly because of differences in the radiant "boiler." In the inclined radiant "boiler" (Test System I) the temperature axial gradiant was higher than in the straight radiant "boiler" flow duct employed in Test System II. This may be the cause of variation in the composition of two test systems where the same kind of coal was fired.

TABLE 4.3. COMPOSITION OF THE SAMPLED FLYASH AT THE EXIT OF THE CYCLONE FROM TEST SYSTEM I AND II (WITH K_2SO_4 AND K_2CO_3)

Specie	Cyclone Discharge				
	K_2SO_4 Seed			K_2CO_3 Seed	
	Thimble		Filter	Thimble	Filter
	B=0 I-1431	B≠0 I-1437	B=0 II-67	B≠0 I-1440	B=0 II-58
K	15.77	14.53	23.70	14.18	31.5
Si	9.70	8.81	12.03	9.07	8.06
SO_4	35.23	33.80	34.58	40.61	38.55
K_2SO_4	35.22	32.45	52.82	31.61	69.92
Al	3.22	4.20	1.48	2.58	1.70
Fe	7.13	6.69	2.98	6.43	2.07
Cu	0.08	0.14	0.019	0.14	0.011
Ca	1.12	0.92	0.49	2.12	0.62
Na	0.27	0.30	0.27	0.29	-
Wt.	1.9183 gms	1.6794 gms	1.4043 gms	3.133 gms	0.3959 gms

Numbers Are In Percent-By-Weight.

To illustrate the degree of repeatability Table 4.4 presents a comparison of the cyclone discharge for two different runs at the same test conditions. One comparison with K_2SO_4 seed and the other with K_2CO_3 seed, for both test systems with and without a magnetic field. Inspecting these data, it can be said that there are no essential differences in the chemical composition of the flyash leaving the cyclone when carbonate seed was used separately in two systems. About 14% to 15% by weight of the dust collected by the sampling probe at the cyclone exit was potassium in Test System I when the magnetic field was energized. While in Test System II where B=0, the filter dust collected at the exit of the cyclone contained about 31% to 35% by weight potassium which is twice that of the potassium in the dust collected in the cyclone (see Table 4.4). It is expected that the magnetic field has an influence on the slag/seed interaction.

The composition of the sampled flyash from the thimble filter at the exit of the cyclone, with K_2SO_4 seed with and without the presence of a magnetic field in Test System I from Table 4.3 (page 83) and 4.4, indicates about the same percentage by weight K and sulfate (SO_4). This suggests for the same geometry of the flow train there was no significant difference in the thimble filter when the system was operated with or without a magnetic field.

It is also seen in Table 4.5 that large amounts of potassium and sulfate are recovered by the impingers while the potassium content of the flyash collected at the exit of the cyclone is decreased in the presence of the magnetic field. The amount of material collected in the cyclone

TABLE 4.4. COMPARISON OF COMPOSITION OF COLLECTED FLYASH AT THE EXIT OF THE CYCLONE WITH K_2SO_4 AND K_2CO_3 SEED IN TEST SYSTEM I ($B \neq 0$) AND TEST SYSTEM II ($B=0$)

Specie	Cyclone Discharge			
	With B-Field		Without B-Field	
	K_2SO_4 Seed	K_2CO_3 Seed	K_2SO_4 Seed	K_2CO_3 Seed
K	14.53	14.18	34.90	31.50
Si	8.81	9.07	8.20	8.06
SO_4	33.80	40.61	36.64	38.55
K_2SO_4	32.45	31.67	66.45	69.92
Al	4.20	2.58	6.92	1.70
Fe	6.69	6.43	6.87	2.07
Cu	0.14	0.14	0.009	0.011
Ca	0.92	2.12	0.52	0.62
Na	0.30	0.29	-	-

TABLE 4.5. POTASSIUM AND SULFATE CONCENTRATION OF SAMPLES IN TEST SYSTEM I (B≠0) AND TEST SYSTEM II (B=0) FOR K_2SO_4 AND K_2CO_3 SEEDING

Sample	Test System I (B-Field)		Test System II (No B-Field)	
	K Run 1437 (K_2SO_4)	SO_4	K Run 71 (K_2SO_4)	SO_4
Impinger #1	690ppm	2581ppm	40ppm	384ppm
Impinger #2	108ppm	1494ppm	55.5 ppm	570ppm
Impinger #3	54ppm	950ppm	4.52ppm	407ppm
	%K	%K	%K	%K
Cyclone Discharge	14.53	33.80	28.50	2.98
Impinger #1	152ppm	1090ppm	1.64ppm	29ppm
Impinger #2	46ppm	809ppm	1.85ppm	184ppm
Impinger #3	52ppm	21ppm	-	-
	%K	%K	%K	%K
Cyclone Discharge	14.18	40.61	31.5	38.55

emissions depends upon the stack gas velocity, its temperature, moisture content and the duration of sampling. The amount of potassium (K) that passes through the filter is approximately twice that collected by the thimble filter in Test System I when B≠0. When B=0, the amount of K collected in the impingers is much less. This suggests that the magnetic field would decrease slag/seed interaction and may enhance the potassium seed recovery as the effect of the magnetic field produced small size particles (0.3 microns retention) in the particulate matter. However, other possibilities also exist; (1) the geometry of the flow train may effect the potassium distribution, (2) the flat filters may be more effective than the thimble filters used in Test System I tests, and (3) the method of sampling at the exit of the cyclone and the length of the sampling probe in the sampling train may make a difference in collecting the particulate emissions effectively.

Analysis by Use of SEM and EDX

A micrograph of the particulate matter emitted by the cyclone at 1000X and its EDX scan is given in Figure 4.4. This material was collected on a fiberglas thimble which had a high retention for particles over 0.3 microns in Test System I and corresponding to K_2SO_4 seeding and with B-field. Comparison of the micrographs in Figures 3.4 (page 53) and 4.4 illustrates that the particles leaving the slag/seed separation cyclone are smaller than those collected by it. Figure 4.5 contains a SEM photo of the fiberglas filter collected dust leaving the cyclone from Test System II with K_2SO_4 seeding and without B-field. The EDX scan in Figures 4.4 and 4.5 show potassium

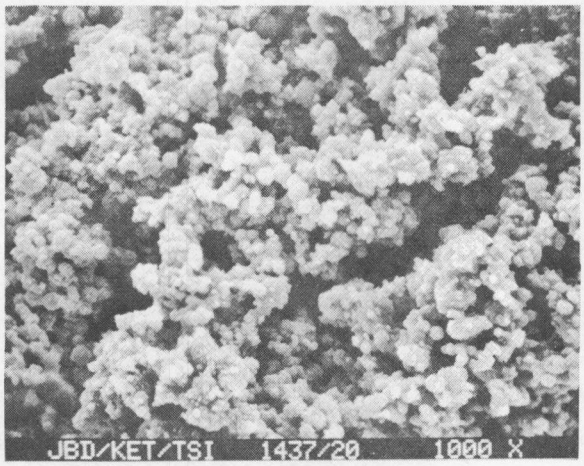

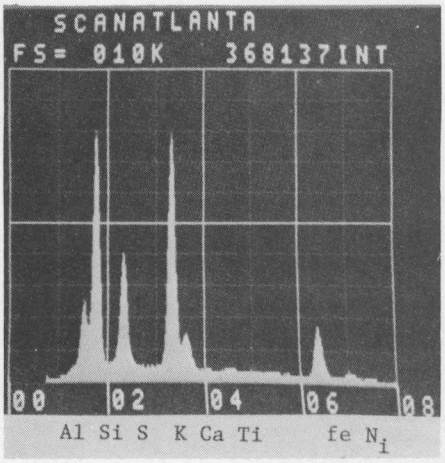

(a) SEM Photo of Dust Leaving Cyclone, 1000X.

(b) EDX Scan.

Figure 4.4. Particulate Dust Formed Under MHD Conditions and Collected at the Exit of the Cyclone by a Fiberglas Filter, Unwashed (Run 1437).

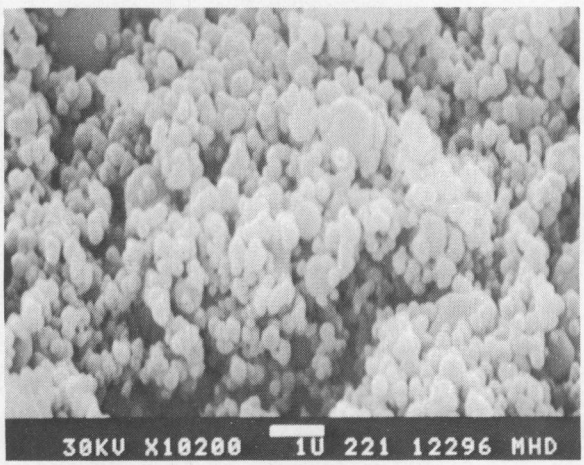

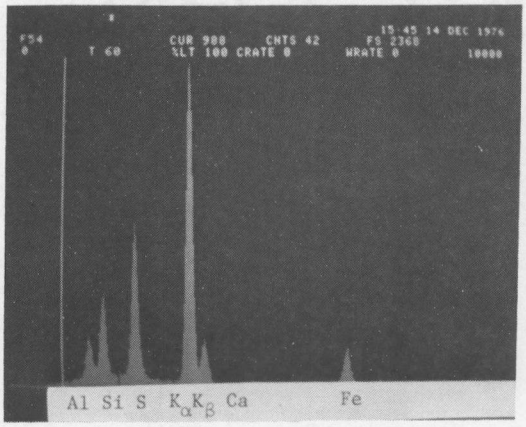

(a) SEM Photo of Dust Leaving Cyclone, 10200X.

(b) EDX Scan.

Figure 4.5. Particulate Dust Collected at the Exit of the Cyclone by a Fiberglas Filter, Unwashed (Run 54) Test System II.

and sulfur exist in the dust leaving the cyclone. Comparison of the SEM photos in Figures 4.4 (page 88) and 4.5 (page 88) indicates that the particles leaving the cyclone and collected on the fiberglas filter having retention of 0.3 microns were smaller when the magnetic field was not applied. This suggests that the flat fiberglas filter used in Test System II collected the particulate matter more effectively than the tube-like thimble used in Test System I.

Figures 4.6 (a) and 4.6 (b) corresponds to particulate matter leaving the cyclone from Test System I and Test System II when K_2CO_3 seed was used. These EDX scans are not different than the EDX scan when K_2SO_4 seed was used. In the sense that these samples contain the same elements as Al, Si, S, K, Fe, etc., chemical analysis showed that there was no significant difference in the chemical composition when two different seed materials were used.

Calculations of Equivalent Oxides

It is possible to compute the weight distributions of the various oxides formed in the slag/seed material discharged from the cyclone in the form of particulate matter as was done in Chapter III for the cyclone collected material. Tables 4.6 and 4.7 summarizes the calculated slag/seed oxides and sulfates or carbonates from laboratory elemental analysis for the fine particulate at the cyclone exit for both test systems. The same assumptions are made here as was in calculating the equivalent oxides of the dust and chunk material collected by the cyclone in Chapter III.

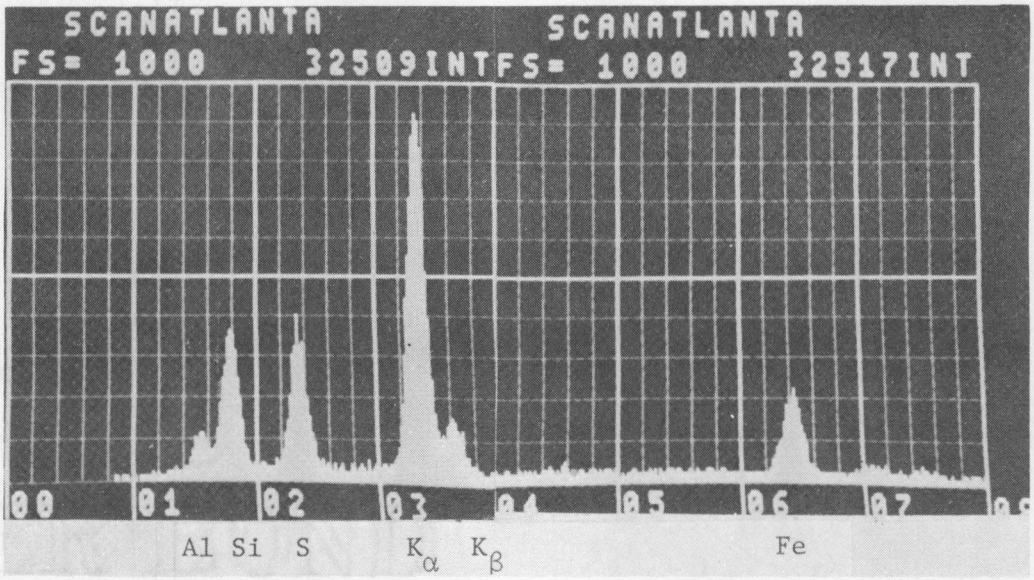

(a) Test System I (Run 1440).

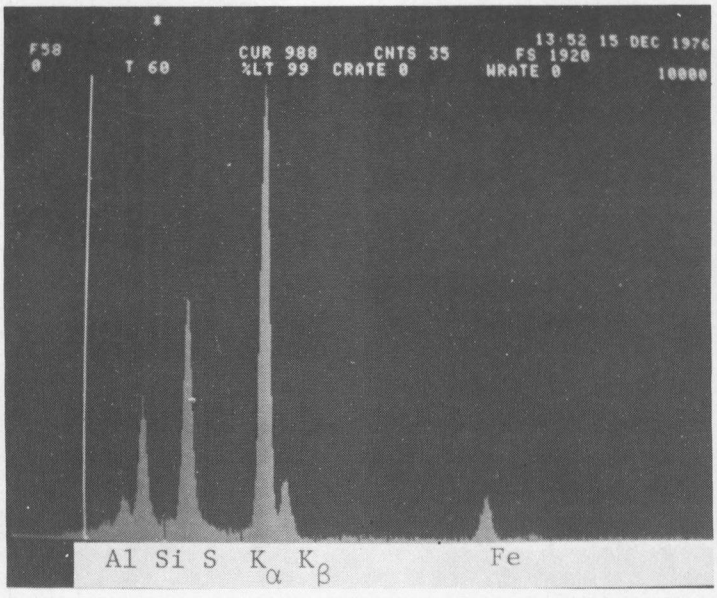

(b) Test System II (Run 58).

Figure 4.6. EDX Analysis with K_2CO_3 Seed for Particulate Collected at the Cyclone Exit.

TABLE 4.6. SLAG/SEED OXIDE AND SULFATE COMPOSITION CALCULATED FROM LABORATORY ANALYSIS WITH K_2SO_4 SEED FOR TEST SYSTEM I AND II

Specie Oxide	Fine Particulate at Cyclone Exit	
	I-1437	II-67
SiO_2	18.87	25.75
Al_2O_3	7.93	2.80
Fe_2O_3	9.56	4.26
CaO	1.29	0.69
Na_2O	0.40	0.36
C	1.20	-
CuO	0.18	0.024
K_2SO_4	32.45	62.68
K_2O	-	-
SO_4	16.50	-
Moisture	0.5	0.36
MgO	3.0	0.15
TiO_2	0.8	0.03
P_2O_5	0.4	-
TOTAL	93.08	97.10

TABLE 4.7. SLAG/SEED OXIDE AND SULFATE COMPOSITION CALCULATED FROM LABORATORY ANALYSIS WITH K_2CO_3 SEED FOR TEST SYSTEM I AND II

Specie Oxide	Fine Particulate at Cyclone Exit	
	I-1440	II-58
SiO_2	19.43	17.25
Al_2O_3	4.87	3.21
Fe_2O_3	9.19	2.96
CaO	2.97	0.87
Na_2O	0.39	0.46
C	3.11	0.0
CuO	0.18	0.014
K_2SO_4	31.63	70.04
K_2CO_3	23.11	0.18
SO_4	-	-
Moisture	0.5	1.06
MgO	3.0	1.04
TiO_2	0.8	0.67
P_2O_5	0.4	-
TOTAL	99.6	97.75

By inspecting these tables it is seen that for the fine particulate collected at the cyclone exit with composition assumed, accounted for about 93% of the weight of the sample from Test System I. This is lower than the accounted 99% of the weight of the collected dust sample at the bottom of the cyclone but still accounts for a very significant part of the material mass. For Test System II, the conventional composition assumed was accounted for about 97% of the weight of the sample which almost equals the accounted composition of the collected dust sample.

Size Distribution

Figure 4.7 compares the size distribution of the flyash leaving the cyclone in both test systems which is collected by the sampling probe filter. It is observed that at the cyclone exit very few particles, above 5 microns, are collected and the most probable diameter of the particles is about 2 microns in Test System I and about 0.5 microns in Test System II. Details of the particle size influencing the recovery of seed will be found in Chapter V. It is believed, however, that the filter did not collect particles less than 0.3 microns with high efficiency and as a result, the size distribution of particles leaving the cyclone is shifted to lower particle size than the result shown here.

Possible Collection Methods

There is a significant amount of K_2SO_4 in the form of fine particles leaving the cyclone and as discussed in the introduction all of the seed has to be recovered. In order to account for all the potassium emitted by the cyclone and to remove the solid sulfur compounds, an effective device could be used.

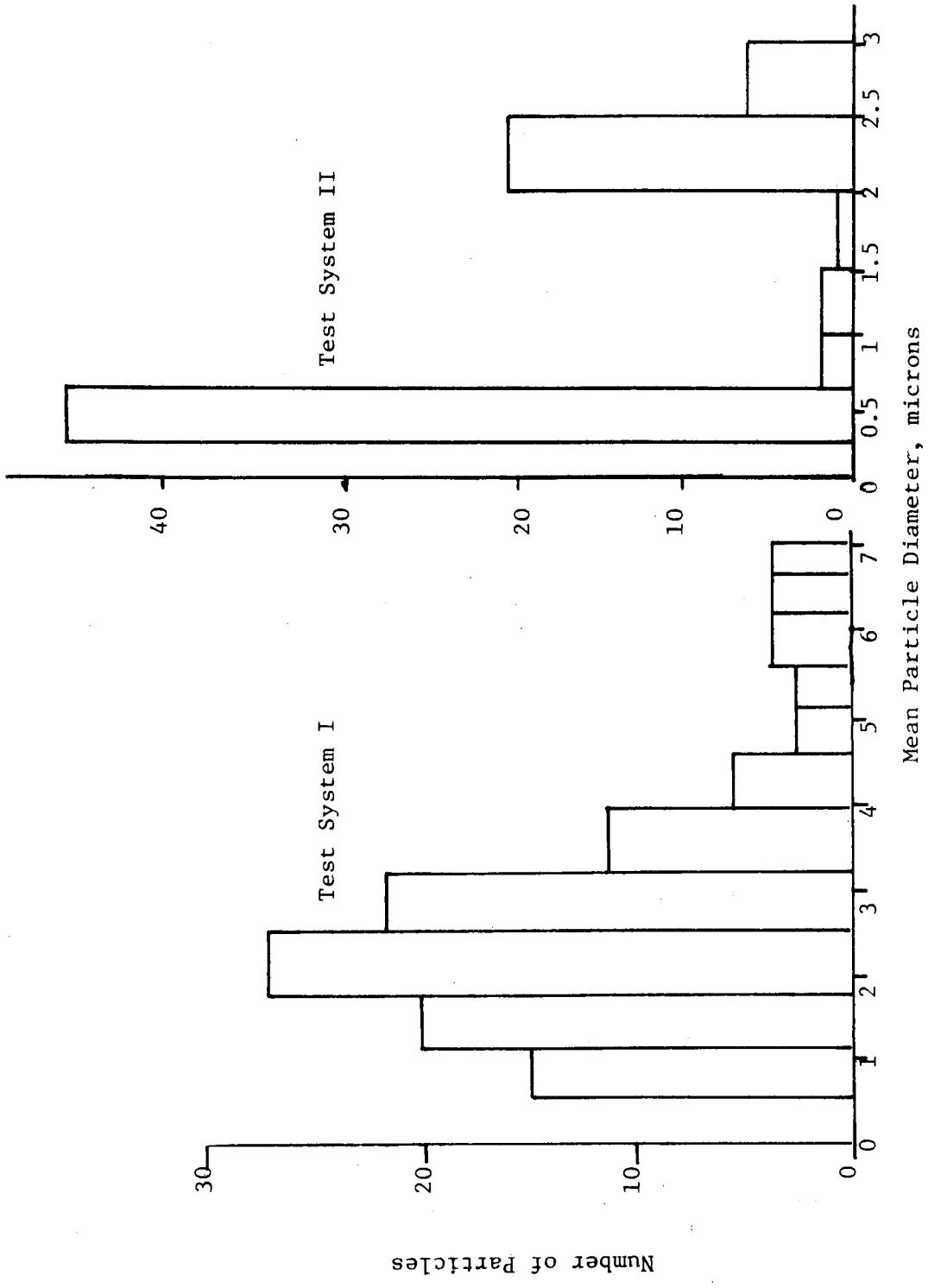

Figure 4.7. Size Distribution of Flyash Leaving the Cyclone.

There are several types of devices that could be operated for controlling different particulate emissions. Of these, a baghouse and venturi scrubber will be connected to the slag/seed separation cyclone and evaluated in seed recovery at the University of Tennessee MHD laboratory.

A baghouse is in the form of a long cylindrical (fabric) bag, closed at the top and supported over a wire frame, mounted vertically so that air introduced through the open bottom is forced to pass outward through the side. The bag may be shaken by a mechanical device to dislodge the trapped particles which can be collected in a hopper at the bottom permitting the baghouse to be operated continuously.

A water scrubber operates on the principle that contact with a liquid can remove certain gaseous and particulate matter from an air stream.

Electrostatic precipitators are often employed at the exhaust of the power plant to collect particulate matter. In these devices, the waste gases before entering the stack passes between an array of alternating wires maintained at high positive or negative electrical potential and plates, which are at ground potential. Electrons are collected by wires when the wire is at high positive potential, but the positively charged ions are accelerated toward plates. Some of the ions, while moving, strike the particles such as flyash in the effluent and remove electrons. Due to this continuing process, the particles themselves become positively charged and build up a deposit on the plates. When the wires are at negative potential, electrons while migrating toward plates get attached to neutral molecules and subsequently after collision with particles

transfer their charge and the plates get deposited with ash. The sulfur dioxide (SO_2) produced in the combustion process is important in the electrostatic precipitation because of its effect on the resistivity of the flyash[16]. Most of the SO_2 condenses on the flyash particles so that the amount found in the flue gas is less and the non-conductive deposits form on the plate. The voltage drop across the layer increases as the resistivity increases and the current gets interrupted and the precipitation ceases. Due to this, the collection efficiency of the ESP (electrostatic precipitator) decreases and since SO_2 removal becomes a major problem, ESP is not advisable to use in this experiment.

CHAPTER V

SEED RECOVERY

Introduction

MHD power generation involves burning coal at high temperatures at about 3000°K. At these temperatures, the slag species could chemically interact with seed material forming slag species like Al_2O_3, Fe_2O_3, SiO_2, which may interact with the seed material forming complex compounds such as K_2SiO_3, $K_2Al_2O_3$ as well as K_2SO_4 as previously summarized in Chapter I. With the slag/seed separation process being carried out for this experiment and from the details of the chemical analysis and the energy dispersive x-ray (EDX) analysis given in Chapters III and IV, it appears that large percentages of potassium as potassium sulfate might be recoverable. This chapter considers the recovery of K_2SO_4 and the loss of potassium to other compounds.

Experimental Measurements

Potassium recovery by water extraction of the particulate matter has been investigated because of its simplicity. Some of the collected samples were treated by two 80°C water washings to determine what portion of the slag would be soluble in water without extensive treatment. When the wash water was evaporated to recover the soluble component in the dust or chunks or fine dust from the filter at the exit of the cyclone, a white or colorless crystal-like material was obtained which, in weight, nearly equalled the weight loss produced by water washing. Table 5.1 contains results of the water solubility of the dust and chunk material collected

TABLE 5.1. PERCENTAGE OF WATER SOLUBLE COMPONENT FROM COLLECTED SLAG AND FLYASH SAMPLES

		% Water Soluble Compound									
		Test System			Test System			Test System	Test System		No Seed System	
Table	Sample	I-1437	II-54	II-57	II-67	II-68	II-71	I-1440	II-58	II-62	I	II
3.3	Cyclone Collected Washed Chunks	2.47	5.23	1.09	2.36	3.40	5.88	6.37	1.82	3.6	0.256	1.34
3.3	Crushed Washed Chunks	1.97	-	-	-	-	-	5.60	0.087	-	-	-
3.3	Washed Dust	35.62	27.83	22.11	32.79	34.77	26.9	36.62	29.58	23.30	9.0	5.97
4.3	Particulate Leaving	54.6	58.11	57.16	56.44	53.97	55.1	61.00	63.07	76.05	-	3.82

by the cyclone and the particulate leaving the cyclone from Test System I and II. With potassium sulfate or potassium carbonate seed, approximately 36% of the dust material from Test System I is water soluble and the component recovered is found to be potassium sulfate as determined by x-ray and chemical analysis. Only about 2% to 6% of the chunk like material is soluble in water. On the other hand, about 60% of the fine particulate matter emitted by the cyclone is water soluble. Thus, the dust has higher concentrations of K and S and is much more water soluble than the chunk material. With unseeded coal it is observed that less than 10% of particulate matter collected by the cyclone in Test System I is water soluble and less than 1% of the chunks are water soluble. Solubility of the particulate matter collected from Test System II is in the range of about 20% to 35% for dust material, 1% to 6% for chunk material and 50% to 75% for the particulate emitted by the cyclone. Thus, the solubility is about the same for particulate matter from both tests. It is observed that the soluble component has a concentration of K and S which could be K_2SO_4. In the case of unseeded coal, there was not enough potassium to react with the sulfur to form K_2SO_4 and, therefore, the water solubility of the particulate matter is low. Similarly, the water solubility of the chunk material shows low values. In these instances with a deficit of K to form K_2SO_4, the sulfur compounds were emitted from the system as SO_2 and SO_3.

Potassium Sulfate (K_2SO_4) Seeding

Figure 5.1 (page 101) contains a scanning electron micrograph of the dust sample after warm water washing and drying. This sample was taken from

the tests made in Test System I with K_2SO_4 seed and with a magnetic field. An SEM photo of the unwashed dust from Test System I, under the above conditions with an EDX scan, is shown in Figure 3.5 in Chapter III (page 53). Comparison of the EDX scan in Figures 3.5 and 5.1 illustrate the chemical change of the dust sample brought about by water washing. Similar results are shown in Figures 3.6 (page 55) and 5.2 which represents the unwashed and washed dust samples from the bottom of the cyclone in Test System II with K_2SO_4 seeding and no magnetic field, but, at a higher temperature at the entrance of the cyclone than for Test System I.

It is observed that water washing has almost eliminated the sulfur peak and the potassium peak is greatly reduced in both cases. Following washing, the wash water was slowly evaporated to recover the soluble component. Figure 5.3 contains a micrograph of the soluble material removed from the dust by water washing. It is clearly seen that the soluble material is crystalline in nature. EDX scans in Figures 5.3 and 5.4 as well as chemical analysis seen in Table 5.3 of the next section (page 123) show that this material consists primarily of potassium and sulfur and small amounts of calcium, silicon and aluminum. This offers strong evidence that the water soluble component of the ash collected by the cyclone (dust and chunks) is in the form of K_2SO_4. Figure 5.5 gives an EDX scan of the soluble filter dust from Test System II. The potassium and sulfur peaks seen in this figure also indicate the presence of recovered K_2SO_4 from the flyash emitting the cyclone for tests in the second system.

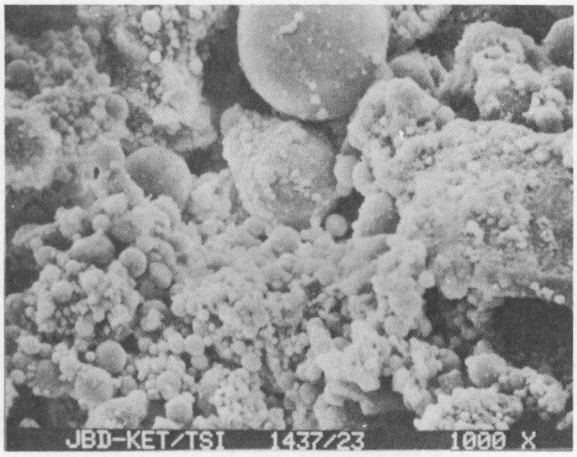

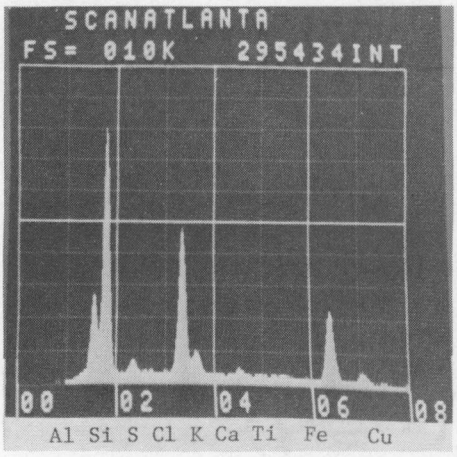

(a) SEM Photo of Dust From Bottom of Cyclone, 1000X.

(b) EDX Scan.

Figure 5.1. Particulate Dust From Bottom of Cyclone After Warm-Water Washing (Run 1437).

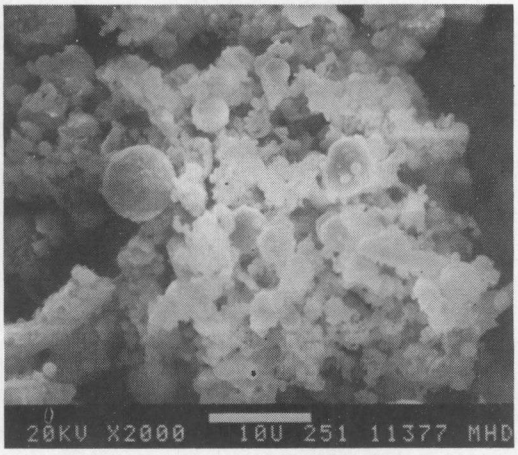

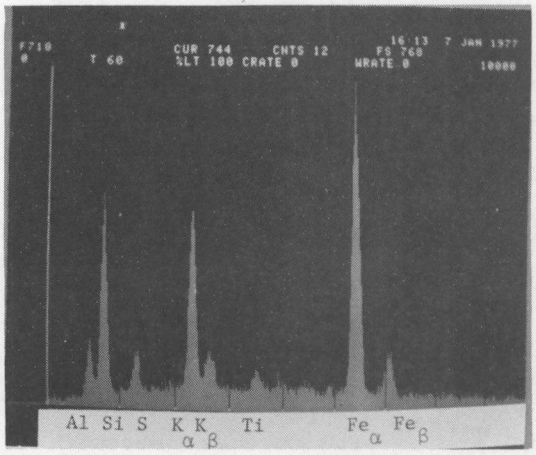

(a) SEM Photo of Dust From Bottom of Cyclone, 2000X.

(b) EDX Scan.

Figure 5.2 Particulate Dust From Bottom of Cyclone After Warm-Water Washing (Run 71).

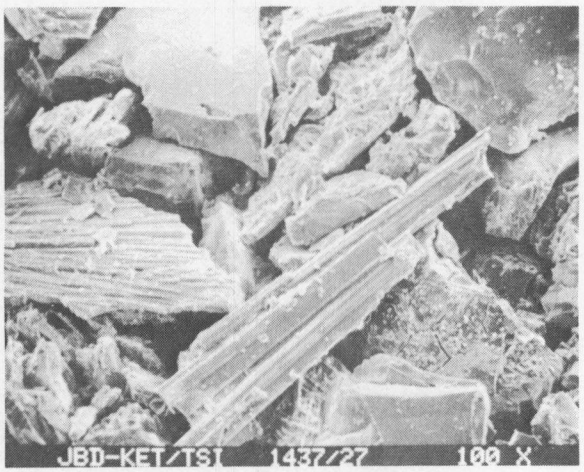

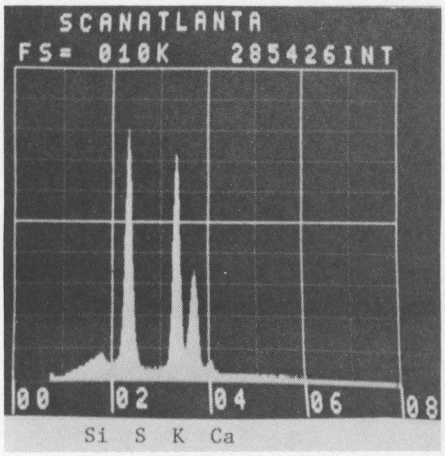

(a) SEM Photo of Soluble Portion of Dust, 100X.

(b) EDX Scan.

Figure 5.3. Solid Material Resulting From Water Washing of Dust Taken From Bottom of Cyclone (Run 1437).

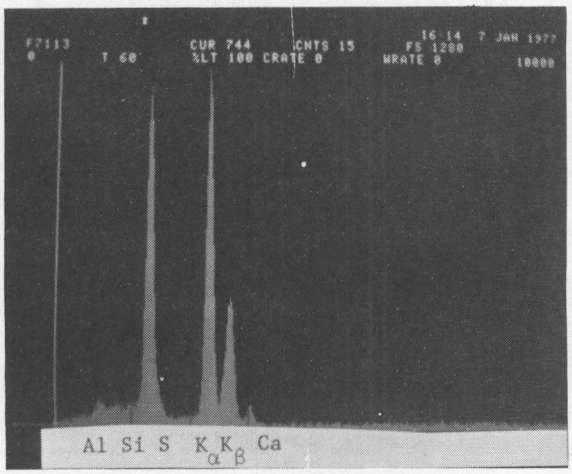

Figure 5.4. EDX Scan of Soluble Dust Taken From Bottom of Cyclone (Run 71) Test System II.

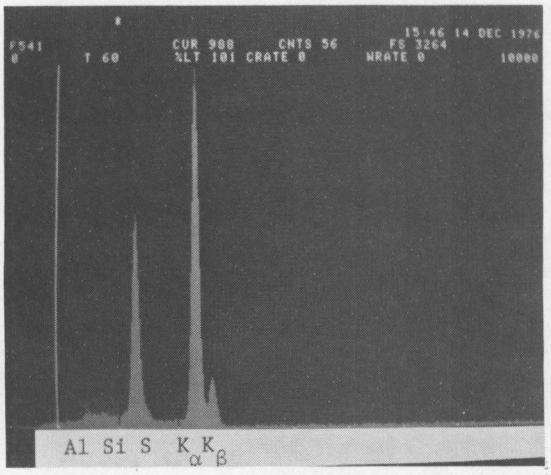

Figure 5.5. EDX Scan of Soluble Dust at the Cyclone (Run 54) Test System II.

Potassium Carbonate (K_2CO_3) Seeding

Energy dispersive x-ray analysis of particulate matter collected with K_2CO_3 seeding in both test systems is given in Figures 5.6 and 5.7. Figures 4.6 (a) (page 90) and 3.8 (a) (page 58) correspond to particulate matter leaving the cyclone and collected by the cyclone from Test System I and demonstrates significant potassium and sulfur peaks. Similar results are shown in Figures 4.6 (b) (page 90) and 3.8 (b) (page 58) from Test System II samples. When this dust material is warm water washed (Figures 5.6 (a) and 5.7 (a)) the sulfur peak again almost disappears and the potassium peak is also greatly reduced. Figures 5.6 (b) and 5.7 (b) show the dissolved material totally consists of potassium and sulfur which chemical analysis viewed as K_2SO_4 (Table 3.4, page 49, and Table 4.4, page 85). It is clear now that when K_2CO_3 seed is used in the combustor products, the potassium compound formed in the exhaust is again K_2SO_4. Thus, K reacts with SO_x produced during combustion to form K_2SO_4 and reduces the sulfur emissions thus controlling pollution from this coal-fired MHD plant.

One reaction which may take place is;

$$K_2CO_3 + SO_2 + \tfrac{1}{2}O_2 \rightleftharpoons K_2SO_4 + CO_2 \qquad (5.1)$$

Fletcher and Gibson[17], studied the reaction of SO_2 with sodium chloride (NaCl) using radioactive sulfur and showed that sodium sulfate can be formed from SO_2 particularly in the presence of Fe_2O_3 (iron oxide). Figure 5.8 shows the rate of formation of sodium sulfate (Na_2SO_4) under

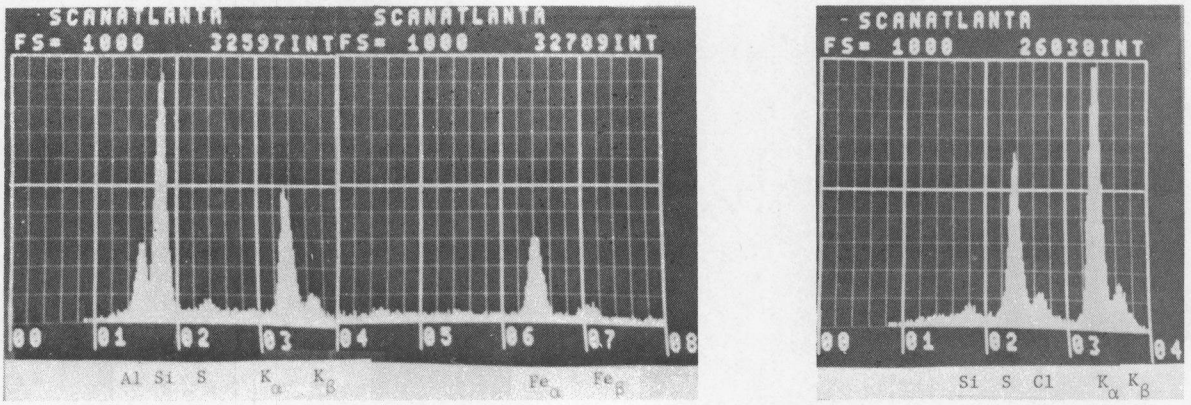

(a) Washed Dust Collected by Cyclone. (b) Soluble Component of Dust.

Figure 5.6. EDX Analysis with K_2CO_3 Seed for Particulate Collected From the Bottom of the Cyclone (Run 1440) Test System I.

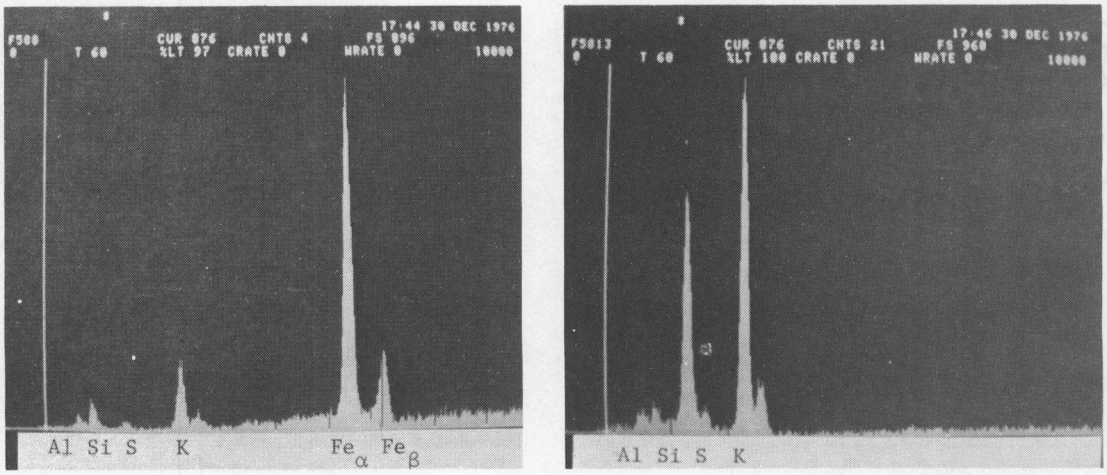

(a) Washed Dust Collected by Cyclone. (Test System II.) (b) Soluble Component of Dust (Test System II).

Figure 5.7. EDX Analysis With K_2CO_3 Seed for Particulate Collected at the Bottom of Cyclone (Run 58).

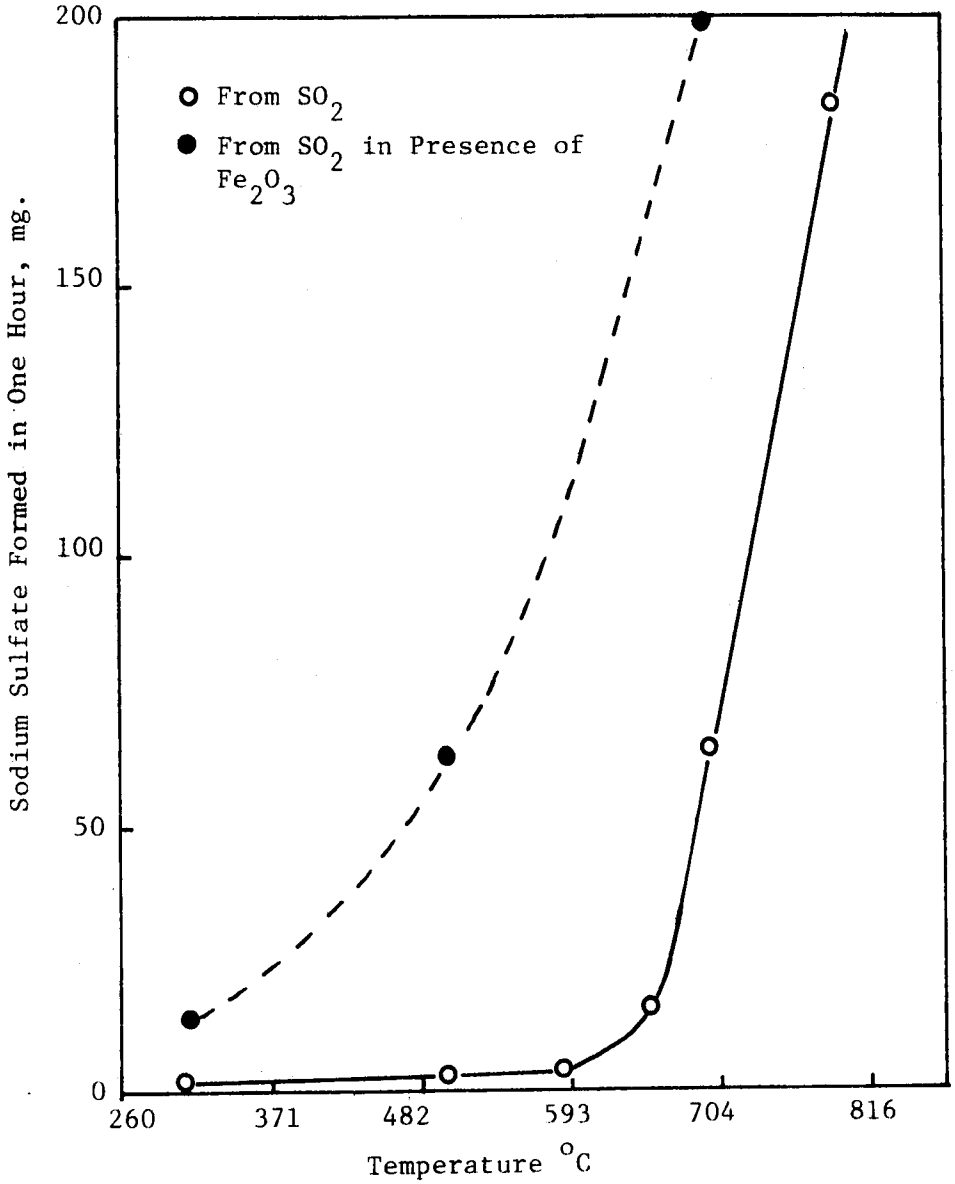

Figure 5.8. Formation of Sodium Sulfate From Sodium Chloride and Sulfur Dioxide (Ref. 17).

various conditions. It is observed that above 900°K, the rate of sulfate formation from SO_2 increased rapidly with temperature. The reaction in this case is;

$$2\ NaCl + SO_2 + \tfrac{1}{2}O_2 + H_2O \longrightarrow NaSO_4 + 2\ HCl + 51\ Kcal \qquad (5.2)$$

From the above discussion it is suggested that the rate of formation of potassium sulfate in the slag/seed interaction at a temperature above 1300°K is rapid and it increases rapidly with increasing temperature. Sodium has a slightly higher ionization potential than potassium and sodium sulfate melts before potassium sulfate.

Figure 5.9 shows the energy distribution of molecules at temperatures T_1 and T_2 where $T_2 > T_1$. It is seen from the diagram that the fraction of all the molecules possessing the minimum energy to produce reaction at T_1 is given by the area N_1. When the temperature is raised to T_2 this energy is given by the area N_2 which is larger than that of N_1. It is only these high energy molecules that participate in the reaction and the fraction of the collisions that are effective at the higher temperature and is greater than at the lower temperature.

An increase in the rate of reaction at higher temperature is due to an increased number of collisions and to the larger fraction of high energy molecules at the higher temperature.

Effect of Temperature Variation

Temperature at the entrance of the slag/seed separation cyclone was in the range of 1350°K to about 1500°K in Test System I and 1600° to

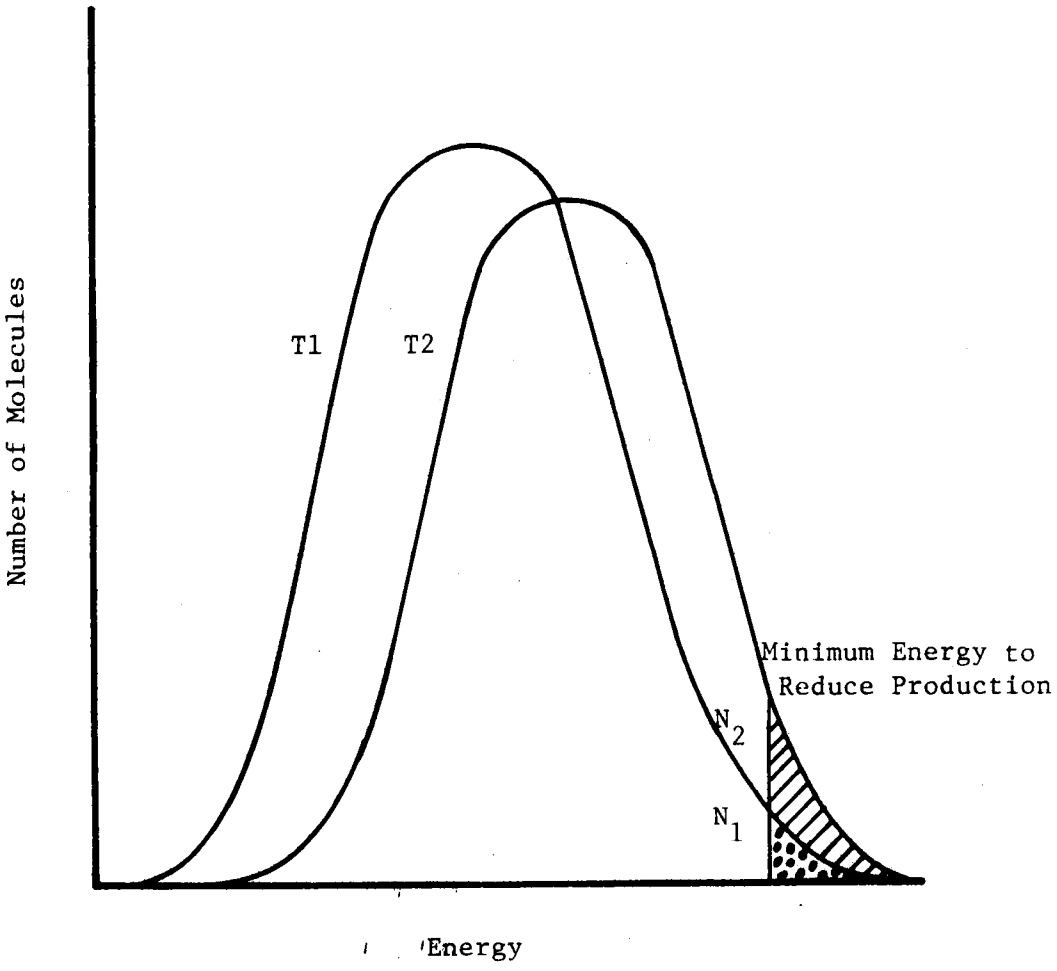

Figure 5.9. Energy Distribution of Molecules.

1950°K in Test Sytem II. The temperature was varied by inserting different lengths of constant area diffusers between the channel and the radiant "boiler." A measured and calculated temperature distribution through the system for a typical run is shown in Figure 3.2 in Chapter III (page 41). It is not possible to isolate the effect of temperature as the mass flow rate of coal/seed and oxygen changes, so does the temperature and the stack gas velocity. Table 5.2 shows the comparison of the composition of collected slag/seed samples from Test Systems I and II treated with warm water washing. These tests were made with potassium sulfate seed and without magnetic field. The sample composition from Test System I shows lower percentage by weight K than from Test Sytem II while sulfate composition in both test systems is equal. This may be due to the fact that in the first system the temperature at the entrance of the slag/seed separation cyclone was lower than in the second system as well as these two test systems that have different flow train geometries which could cause this variation. In addition, these two systems carried different sampling procedures at the exit of the cyclone in order to sample the particulate matter leaving the cyclone.

The amount of potassium recovered from the dust material collected at the bottom of the cyclone and from particulate collected by the filter in the sampling train at the exit of the cyclone, at different temperatures, are given in Figures 5.10 and 5.11. Figure 5.10 indicates the results of potassium recovery for K_2SO_4 seed runs for both test systems with and without magnetic field. Similarly, Figure 5.11 illustrates the results of K recovery for K_2CO_3 seed runs for both test systems with and

TABLE 5.2. COMPARISON OF COMPOSITION OF COLLECTED SLAG/SEED FROM TEST SYSTEM I AND II (WITH K_2SO_4 SEED AND NO B-FIELD)

Specie	Dust Sample - Cyclone Collected					
	Unwashed		Washed		Evaporated	
	Run 1431 (1360°K)	Run 67 (1700°K)	Run 1431	Run 67	Run 1431	Run 67
K	12.65	19.8	6.05	11.1	41.25	39.5
Si	11.5	11.67	15.76	14.55	0.06	0.05
SO_4	19.14	18.25	1.88	2.82	53.75	49.75
K_2SO_4	28.19	33.11	3.41	5.12	91.93	88.03
Al	8.78	7.05	14.18	7.61	0.05	0.32
Fe	9.24	7.66	11.48	6.19	1.12	0.02
Cu	0.13	0.025	0.18	0.002	0.01	0.005
Ca	1.75	1.04	1.75	0.96	1.86	0.39
Na	0.50	0.33	0.38	0.33	0.50	0.38
Wt. gms.	15.07	44.3455	10.3694	30.5518	4.7354	14.0794
	Chunk Sample - Cyclone Collected					
K	6.70	16.10	6.50	15.10	43.80	41.9
Si	16.26	18.20	16.30	19.78	0.014	0.39
SO_4	1.77	4.40	0.15	1.20	55.16	52.77
K_2SO_4	3.21	7.98	0.27	2.18	97.62	93.38
Al	17.06	11.63	15.13	11.14	0.03	0.42
Fe	11.76	9.84	11.62	9.19	0.28	0.25
Cu	0.04	0.014	0.06	0.013	0.01	0.002
Ca	3.07	2.24	3.75	1.91	0.57	1.32
Na	0.32	0.36	0.32	0.24	0.48	0.66

	Cyclone Discharge Unwashed	
	Thimble (Run 1431)	Filter (Run 67)
K	15.77	23.70
Si	9.41	12.03
SO_4	35.23	34.58
K_2SO_4	35.22	52.82
Al	3.22	1.48
Fe	7.13	2.98
Cu	0.08	0.019
Ca	1.12	0.49
Na	0.27	0.27
Wt. gms.	1.9183	1.6794

Numbers Are In Percent-By-Weight. Run 1431 - Test System I.
Run 67 - Test System II.

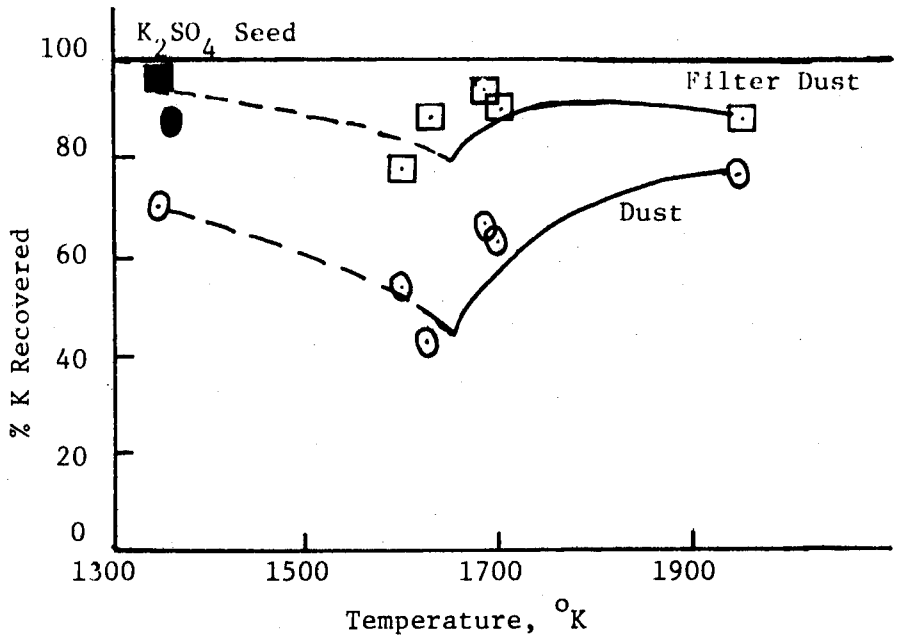

Figure 5.10. Effect of Temperature on Potassium Seed Recovery. Solid Symbols - B-Field, Open Symbols - No B-Field (K_2SO_4).

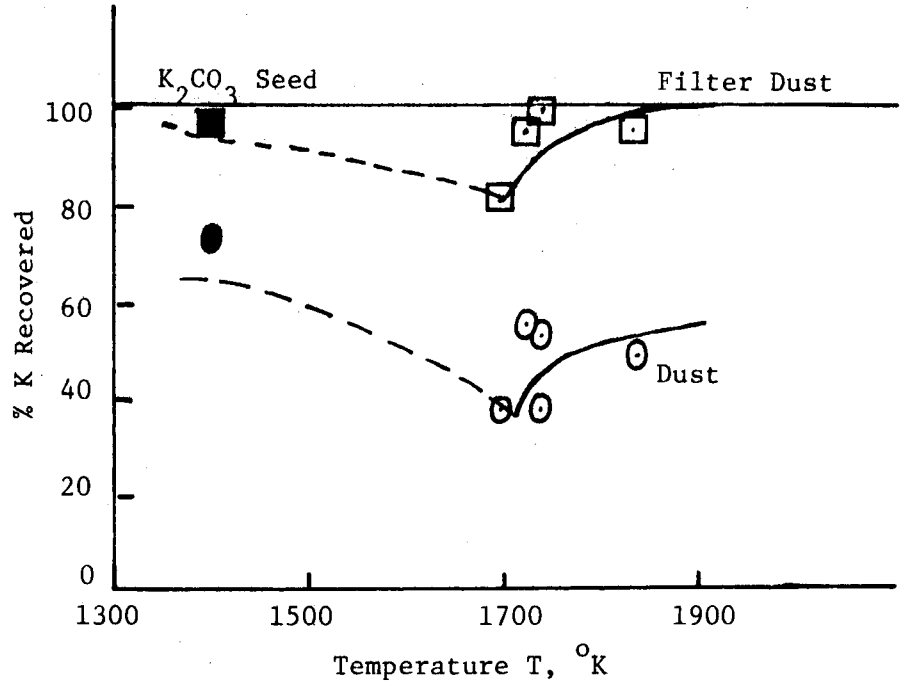

Figure 5.11. Effect of Temperature on Potassium Seed Recovery. Solid Symbols - B-Field, Open Symbols - No B-Field (K_2CO_3).

without magnetic field. These figures do not include the percentage K recovered in the case of chunk material as this material is essentially detached from the walls of the flow train and the slag layer thickness on the walls primarily depends upon temperature. As a result, when the high temperature tests were made, the cyclone collection and potassium recovery efficiencies, greater than 100%, were obtained (see discussion in Chapter III, page 36). Due to this, the effect of temperature on K recovery from chunks could not be documented and hence is not shown. Observations made on the wall deposit are described in Chapter III. Figures 5.10 and 5.11 depict that temperature variation of potassium recovery follows the trends suggested by equilibrium theory[2]. Figures 5.10 and 5.11 show that the magnetic field has certain affect on potassium recovery as the percentage K recovered is greater when the magnetic field was on in both types of seed runs as K_2SO_4 and K_2CO_3. It is noteworthy to say that the highest potassium recovery obtained is from the flyash leaving the cyclone and the lowest is from the large chunk pieces.

Figure 5.12 indicates the comparison of the experimental results from both test systems with the calculated equilibrium results by the Bureau of Mines[2]. The experimental results obtained from Test Systems I and II considers the ratio of potassium lost to that available from the system only in the case of the dust material and the flyash leaving the cyclone since, as explained above, the chunk material is not included. Though the results are scattered, it demonstrates lower potassium absorption by the slag material than predicted by equilibrium theory.

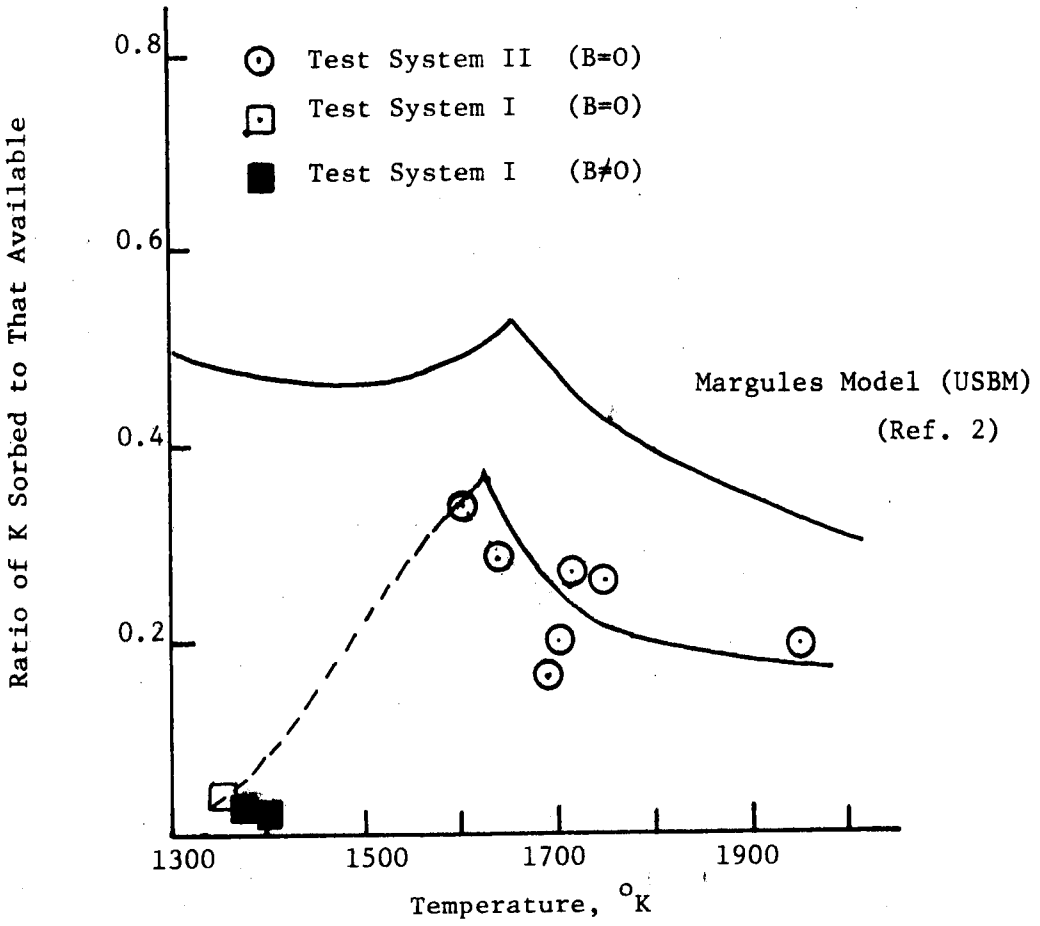

Figure 5.12. Comparison of Experimental Results With the Predicted Equilibrium Model.

The equilibrium model produced by Spencer et al.[2] in Figure 5.12 (page 112) and Figure 1.3 (page 9) shows a peak in temperature range of $1600^{o}K$ - $1700^{o}K$, which quantitatively agrees with the peak obtained in the experimental results (Figures 5.10, 5.11 and 5.12, pages 110 and 112).

Effect of Magnetic Field

It is noteworthy to say that the presence of a magnetic field may reduce the potassium absorption to lower values than with no magnetic field (Figures 5.10, 5.11, and 5.12, pages 110 and 112).

Table 5.3 gives the comparison of the composition of dust and chunk material taken from the cyclone and fine dust collected at the exit of the cyclone when it was water washed. Results were obtained in both test systems. It is observed that the presence of the magnetic field results in the potassium content of the chunk material is being decreased by a large amount as is the sulfate. It is also seen that large amounts of K and SO_4 were recovered by the impingers while the potassium content of the flyash collected at the exit of the cyclone is decreased for $B \neq 0$. The amount of K that passes through the filter is larger for $B \neq 0$, than when $B=0$. This says that the amount of K collected on the filter is considerably larger and that collected in the impingers is much less when $B=0$. This suggests two possibilities: (1) a suppression of turbulence in the MHD generator when the magnetic field is present, decreases slag/seed interaction and (2) the second sampling method in collecting particulate matter leaving the cyclone with a flat filter and longer sampling probe may be more effective than the thimble with a short sampling probe employed in Test Sytem I. The first possibility is believed to be the most probable.

TABLE 5.3. COMPARISON OF COMPOSITION OF COLLECTED SLAG/SEED FROM TEST SYSTEM I (B-FIELD ON) AND II (NO B-FIELD) WITH K_2SO_4 SEED

Specie	Dust Sample - Cyclone Collected					
	Unwashed		Washed		Evaporated	
	Run 1431 (1360°K)	Run 67 (1700°K)	Run 1431	Run 65	Run 1431	Run 67
K	17.20	15.0	3.80	6.99	42.70	38.5
Si	11.00	14.26	20.63	12.74	0.01	0.03
SO_4	21.09	16.08	5.12	0.28	53.75	51.60
K_2SO_4	38.26	29.15	8.47	0.51	95.16	93.53
Al	7.41	3.88	9.89	6.09	0.81	0.21
Fe	6.86	8.32	8.26	11.20	0.32	0.02
Wt. gms.	26.7808	26.0304	17.1847	18.6354	9.5407	7.0003
	Chunk Sample - Cyclone Collected					
K	1.42	15.2	1.23	9.98	42.70	39.40
Si	18.86	17.35	17.03	14.53	0.10	0.04
SO_4	1.68	15.78	0.56	4.62	52.02	54.90
K_2SO_4	3.05	28.60	1.02	8.37	94.38	99.51
Al	14.29	11.49	16.69	12.72	0.11	0.32
Fe	7.28	11.20	9.52	7.60	0.20	1.06
Wt. gms.	48.6582	51.4894	47.3530	48.3829	1.994	3.0256

	Cyclone Discharge		Impingers	
	Thimble (Run 1437 (B=2T)	Filter (Run 71) (B=0)	Run 1437	Run 71
K	14.53	28.50	0.085	0.01
Si	8.81	11.93		
SO_4	33.80	2.98	0.503	0.136
K_2SO_4	32.45	5.40		
Al	4.20	0.79		
Fe	6.69	2.93		
Wt. gms.	1.4043	2.2139		

Numbers Are In Percent-By-Weight. Run 1437 - Test System I.
Run 71 - Test System II.

Effect of Residence Time in the Flow Train

The difference between the experimental measurements on seed recovery and the equilibrium calculations are believed to be due in part to the fact that equilibrium was not reached in the slag/seed interaction process. For this reason, the effect of residence time in the system on the seed recovery was investigated in order to obtain some idea of the kinetic effects on this process.

Residence times of the combustion gas from the combustor to the cyclone entrance were calculated for tests in Test System II, by using the values of temperature, pressure and the mass flow rate. As the temperature and mass flow in the flow train increased, the residence time decreased. Figure 5.13 illustrates these results for both types of seed. It is observed from this figure that the potassium recovery decreases with increasing residence time of the flyash in the system and suggests that the approach to equilibrium may be slow.

Effect of Particle Size

The particles produced are of various sizes: chemical reactions taking place can alter their sizes; collisions in the gas stream can result in a growth or break-up of particles resulting in agglomeration or splitting of particles. The particle interaction controls which of these would occur. The rate of change of size of the particles depends upon the temperature and pressure of the gas as well as the concentration of particles. Shapiro and Ericksen[18] have presented analysis relating the mechanism of collision and the interaction of the particles to the variation in the particle size distribution along the direction of flow.

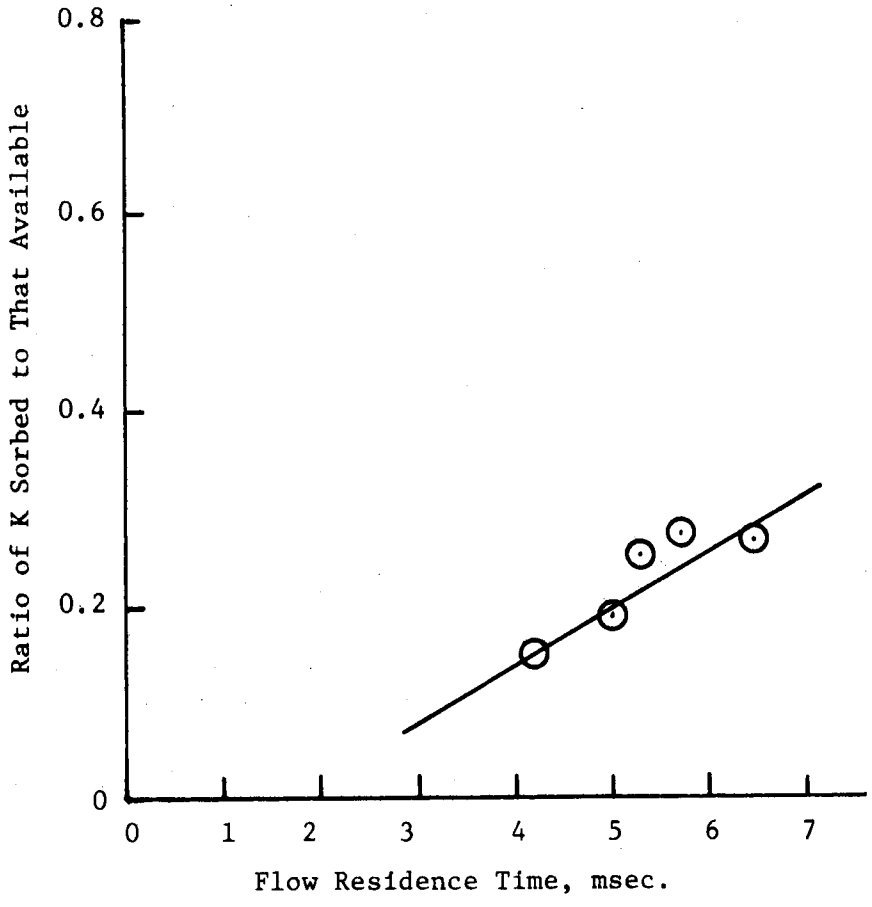

Figure 5.13. Effect of Flow Residence Time on Seed Recovery.

In collisions occurring between liquid-liquid, solid-solid and liquid-solid, agglomeration of particles may occur. The surface tension of the combustion products is an important property in determining this agglomeration. The agglomeration is less in solid particle collisions (as they result in loosely packed structures) than liquid particle collisions. There is little known about the collisions occurring between liquid and solid particles and it is likely to be an important one in the flow trains described here.

If the gaseous constituent is absorbed with the solid or liquid constituent, the molecule of the gas will disappear from the physical picture and there will be an effect on particle size. This phenomena is basically a function of collision frequency.

The rate at which the particles change size depends on the collision rate and the interaction between particles during collision which may be of a chemical or a physical nature producing a new chemical compound.

The previous section suggests that the rate of reaction increased when the temperature increased. This implies that the collision rate is high and the number of collisions is increased in order to form any product compound. As the collision rate increases, the rate of change of the particle size also increases.

Comparison of three different runs; (1) tests made with unseeded coal in Test Sytem II (SEM photo shown in Figure 5.14), (2) test made within seeded (K_2CO_3 or K_2SO_4) coal in Test System II at higher temperatures (SEM photo shown in Figure 3.6, page 55) and (3) test made with seeded coal with a magnetic field in Test System I (SEM photo shown in Figure 3.5, page 53) are instructive.

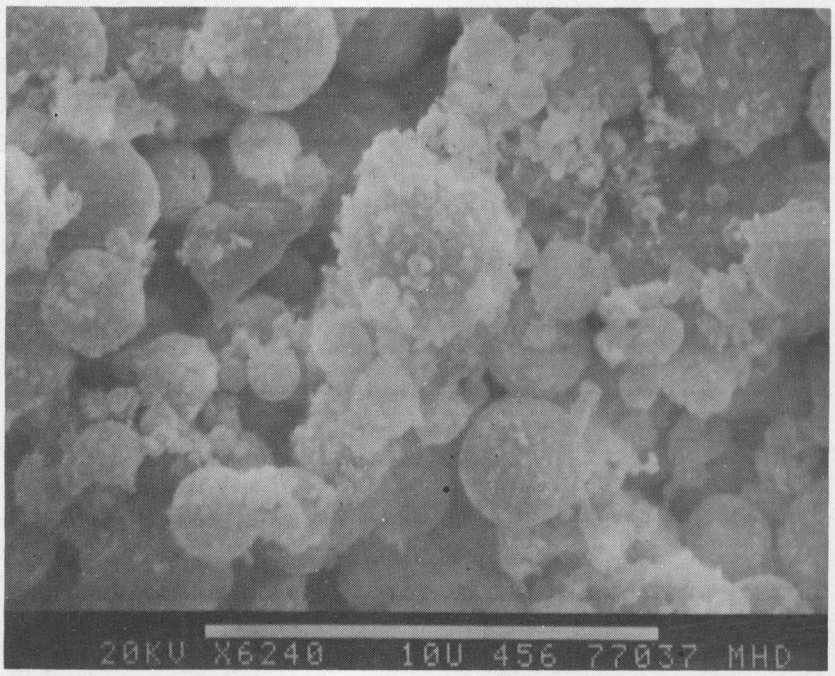

Figure 5.14. SEM Photo of Cyclone Collected Dust, 6240X (Unseeded Coal Run).

It is observed from an SEM micrograph of unseeded dust, which was collected from the bottom of the cyclone, that the particles are smooth and spherical and had a most probable particle diameter of about 2 microns. However, seeded coal (K_2SO_4 or K_2CO_3 seed) particles were covered with irregular patches of material and there was an agglomeration. Seeded dust collected from the bottom of the cyclone from Test System I had a most probable particle diameter of about 10 microns while the seeded dust from Test System II had a most probable particle diameter of about 6 microns. Size distribution of these materials is discussed in Chapter III. This size difference could be due to the presence of a magnetic field in Test Sytem I. The above discussion seems to indicate that the particle size has increased from 2 microns to about 10 to 6 microns from Test System I and II respectively. This suggests that the particle size of the slag sample may be strongly dependent upon the interaction mechansim between constituent particles.

Inspection of the calculated results from these tests show a higher percentage of potassium recovery in the dust which was collected by the cyclone from Test System I (26%) when the large size particles were formed than when smaller size particles were formed from Test Sytem II (13%). It is noticed from the above discussion that one cannot isolate the effect of particle size since it is related with the effect of temperature, magnetic field, residence time and the flow train geometry.

Potassium Balance

With this concept and the chemical analysis presented previously, it is easy to calculate the recovered potassium by assuming that all of the water soluble component is K_2SO_4.

The highest potassium recovery was obtained in the test with potassium carbonate seed under the influence of a magnetic field and the 86.3% as shown in Figure 5.15.

The potassium recovered from the dust material, which was collected at the bottom of the cyclone, corresponded to 0.86 kilograms while 0.15 kilograms of K was obtained from a single water washing from the chunks. The chunk material, after being washed once, was crushed and washed a second time. From the second washing, 0.14 kilograms of K was obtained. A large portion of the potassium leaving the cyclone separator was collected. Summing these potassium recoveries indicates that small amounts of potassium is recovered from the chunk material. However, there is a large portion of potassium which can be recovered from the dust collected by the cyclone and leaving the cyclone.

The potassium that is "lost" to the slag was greater in the dust material than the chunk material which was collected at the bottom of the cyclone. As a result, approximately 11.4% of the added potassium was lost to the slag.

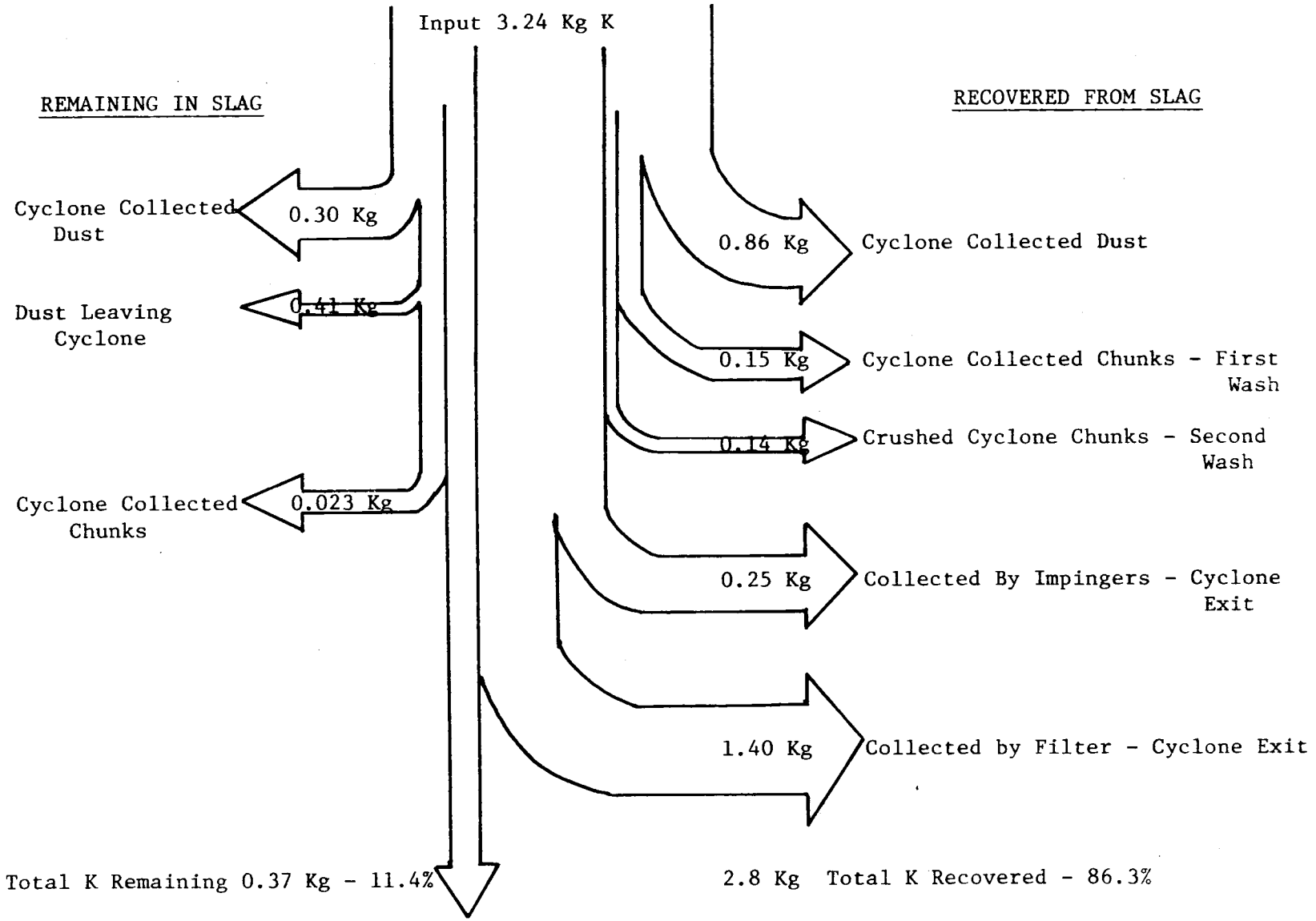

Figure 5.15. Potassium Recovery at 1400°K, K_2CO_3 Seed With Magnetic Field.

CHAPTER VI

CONTROL OF SULFUR DIOXIDE EMISSIONS

Introduction

The direct coal-fired open-cycle MHD power plant offers a unique means of recovering sulfur from its effluent gases because the potassium seed material in the combustion products interacts with SO_2 resulting from a sulfur impurity from a fuel forming potassium sulfate.

This chapter describes the sulfur dioxide (SO_2) removal efficiency determined from experimental data obtained during these tests.

Sulfur Balance

Sulfur balance data obtained in Test System I and II are given in Table 6.1. Run 1440 corresponds to Test Sytem I and Runs 58, 62, 64 and 69 are from Test System II. The sulfur input was based on sulfur analysis of the coal used in the runs and the calculated coal firing rate. The sulfur output was determined from sulfate content in the impingers and the measured sulfur in the particulate matter collected by the cyclone and the flyash leaving the cyclone. The sulfur content of the ash was in most cases much higher than that of the gas. Sulfur removal ranged from 34% to 87%.

Sulfur Dioxide (SO_2) Reduction

Table 6.2 gives the values of SO_2 in the combustion gas for Test System I and II for K_2CO_3 seeded runs. The K_2CO_3 added to coal amounted to 9% that of the coal flow rate. Table 6.2 also gives the percentage of SO_2 reduced during each test run and illustrates that 34% to 87% of the

TABLE 6.1. SULFUR BALANCE (K_2CO_3 SEED)

Test System	Test Run	Sulfur Input Kg/min	Sulfur Removed Kg/min
I	1440	0.28	0.20
II	58	0.39	0.13
II	62	0.11	0.086
II	64	0.13	0.12
II	69	0.40	0.25

TABLE 6.2. REMOVAL OF SULFUR COMPOUNDS IN MHD GENERATION WITH K_2CO_3 SEED

Test System	Test Run	SO_2 in Combustion Gas Kg/min	SO_2 Reduction %	Stoichiometric Sulfur Removal %
I	1440	0.56	64	78
II	58	0.77	34	80
II	62	0.21	81	77
II	64	0.26	87	97
II	66	0.85	18	93
II	69	0.81	60	76

SO_2 formed during coal combustion was removed from the gas and believed to be trapped as sulfate compounds. Based on the K_2SO_4 reaction and partial loss of seed in the slag, the percentage of the stoichiometric removal of sulfur was calculated and is given in Table 6.2. Coal containing about 2.5% to 4.5% sulfur was used in this experiment. For low sulfur content coal (< 3% S) sulfur emissions reduced to about 20% when K_2CO_3 seed is not used (no seed run). In all tests a large portion of the sulfur that could react with potassium did so.

Figure 6.1 plots the percentage of K against percentage of S from coal samples from each run. Theoretical results are calculated for the stoichiometric ratio to form K_2SO_4 from potassium and sulfur. Observing the agreement between the experimental and theoretical values, it can be said that the stoichiometry is approached in this experiment.

Figure 6.2 illustrates the dependance of temperature on the percentage of SO_2 reduced for K_2CO_3 seeded runs. It is noted that as temperature increases, the SO_2 emission decreases for both ranges of coal sulfur content shown. Also, the percentage of SO_2 reduced in the case of high content of sulfur (> 3% S) coal is low as would be expected since insufficient K was added to react the sulfur present.

Figures 6.3 and 6.4 are the plots of the percentage SO_2 reduction against the residence time in the system up to the entrance of the cyclone and against the stack gas velocity. Residence time was calculated by using the values of temperature, pressure and the total mass flow rate (coal/seed and oxygen). For low sulfur content coal (< 3%), the sulfur emissions were reduced 60% to 85% when the normal amount of K

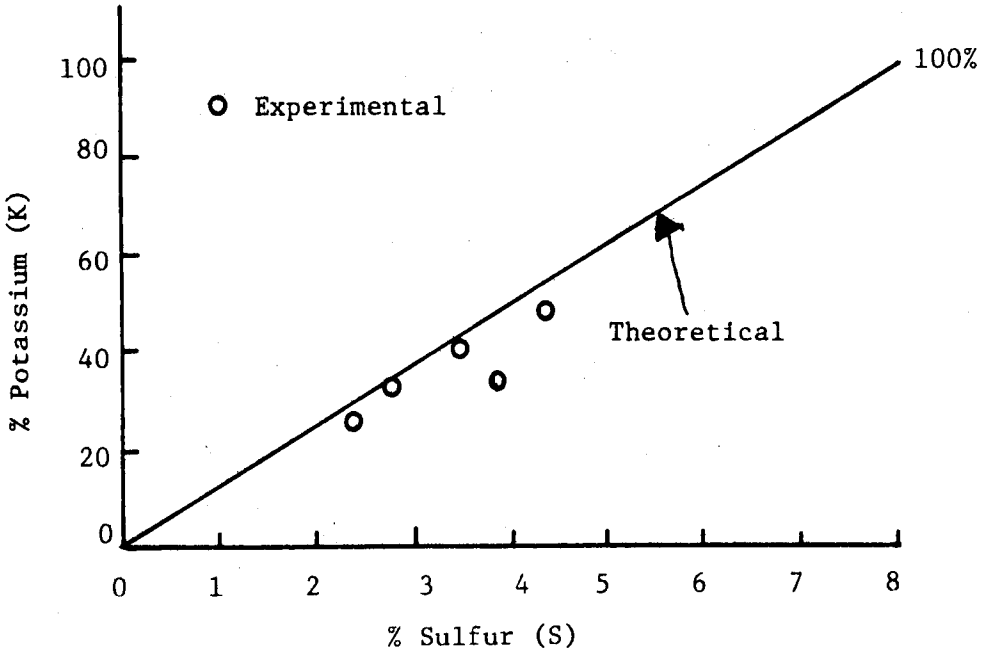

Figure 6.1. Variation of K With S.

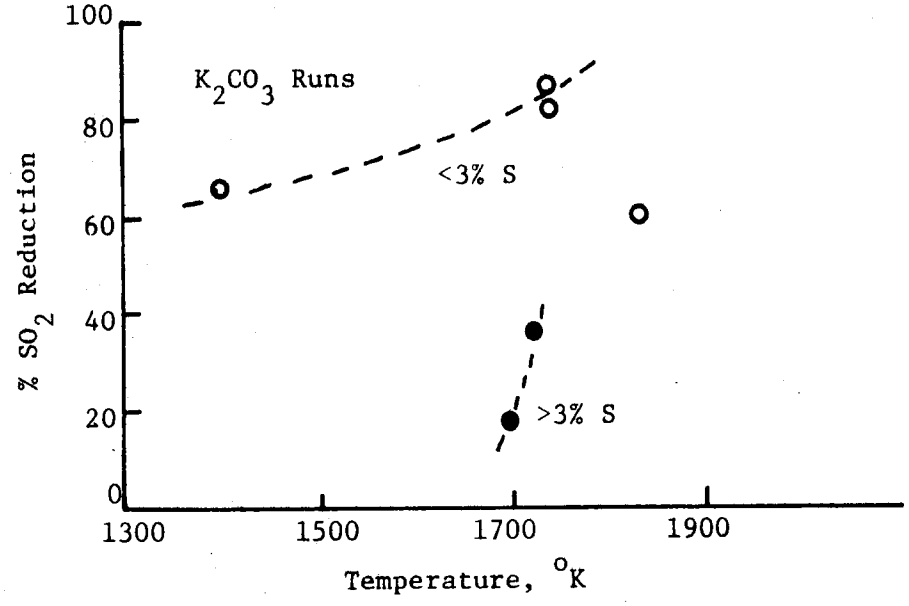

Figure 6.2. Effect of Temperature on SO_2 Control, Test System II.

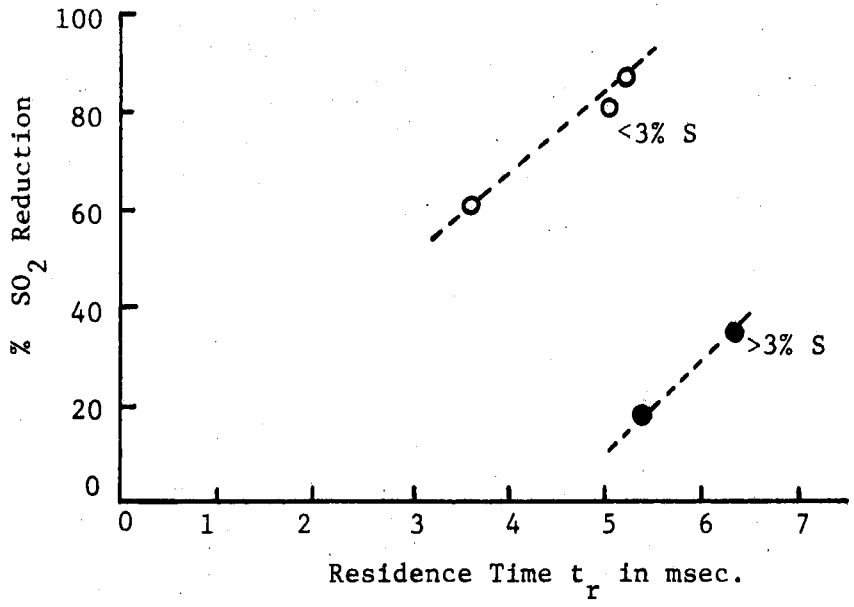

Figure 6.3. Reduction of SO_2.

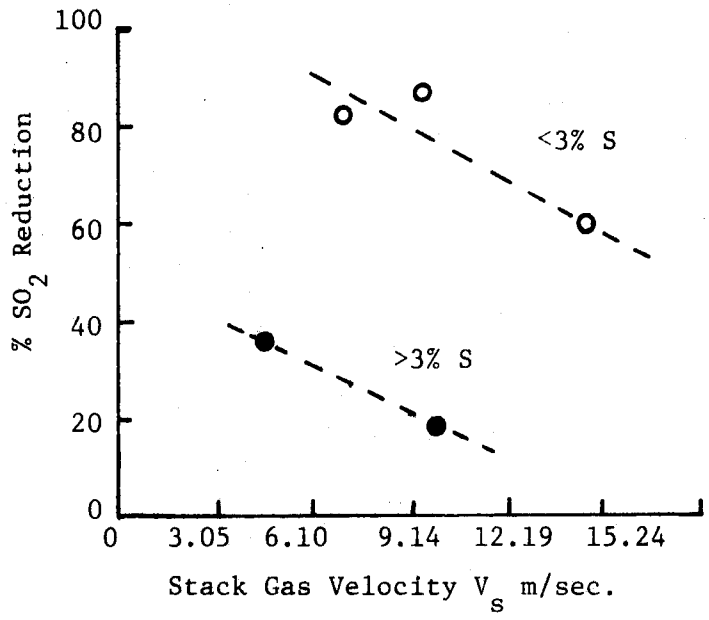

Figure 6.4. Effect of Velocity on SO_2 Reduction.

was present in the flow to produce the σ needed in MHD power generation. For high sulfur content (> 3%), the sulfur emissions increased significantly as expected because insufficent K was available to completely react the sulfur present. This seems to agree well with Figure 6.4 (page 126) which illustrates that the higher the stack gas velocity, the higher the sulfur dioxide emission. The residence time is inversely proportional to the velocity.

Completely definitive conclusions cannot be made from these few data. However, in accordance with Figures 5.10 and 5.11 in Chapter V (page 110), it is noteworthy to say that potassium seed recovery and sulfur removal depend upon many parameters and it is very difficult to isolate one effect of the parameter when the other parameters vary.

Observing the effective removal of SO_2 one can say that the open cycle MHD power generation offers a unique means of controlling air pollution and environmentally suitable means of energy conversion.

One percent of K added in the flow is in the normal seeding range required to achieve the necessary electrical conductivity in the plasma and is sufficient to react the sulfur impurities from coal less than 3% sulfur for test operations such as described herein. For coal, K_2CO_3 offers good prospects for seed material when the sulfur content of coal is about 2%. When low sulfur content coal (< 3%) is used, it is advantagous to use a combination of K_2SO_4 and enough K_2CO_3 seed to react all the sulfur compounds with potassium and form potassium sulfate. However, when high sulfur content coal (> 3% to the conditions of these tests) is used, greater amounts of K_2CO_3 seed than needed for MHD should

be added to the flow in order to remove all the sulfur impurities in the coal by reacting with potassium to form K_2SO_4.

The conventional boiler temperatures are lower than that of a MHD generator. As seen above, potassium compound added to the flow interacts with the sulfur impurities from a fuel and forms K_2SO_4 which can easily be removed. Potassium carbonate (K_2CO_3) dissociates at about 1164°K and potassium sulfate (K_2SO_4), sodium sulfate (Na_2SO_4) and calcium sulfate ($CaSO_4$) melt at 1342°K, 1157°K and 1723°K respectively which are achievable temperatures in the boilers and the potassium would react with sulfur compounds to form K_2SO_4 thus controlling SO_2 emissions from a conventional power plant. Alkali salts such as sodium (Na), calcium (Ca), and potassium compounds can be used as an additive using this process of chemical reaction in order to control SO_2 emissions in flue gas in conventional power plants.

CHAPTER VII

DIFFUSION OF POTASSIUM (K) IN SLAG

Some of the differences between the experimental measurements on seed recovery and the equilibrium calculations may be due to the fact that equilibrium was not reached in the slag/seed interaction process. The kinetics of the slag/seed sorption process appear to play an important role. The actual flow and chemical processes may be far from equilibrium.

Little is known about the details of the dynamics of the complex interaction between the surface of coal slag and the potassium seed. Experimental data presented here, indicate that the seed material absorbed on the surface of the slag droplets is in the form of K_2SO_4 (potassium sulfate). However, the slag surface could absorb K_2SO_4 and/or a new chemical compound could form which may diffuse into slag. In order to provide a better understanding of the slag/seed absorption process both from an equilibrium and the kinetic view points, this process of diffusion of K into slag is studied here.

Very little information on diffusion of metals in liquid slag could be found.

McCallum and Barrett[19] using platinum crucibles and a technique of measuring the refractive index of the quenched glass to find the change in concentration, determined the diffusion coefficient of CaO (lime) in 37.5% CaO - 10% Al_2O_3 - 52.5% SiO_2 (lime-alumina-silica) slag. D_{CaO} was found to be 9.6×10^{-6} $cm^2/sec.$ at 1723^oK and 12.25×10^{-6} $cm^2/sec.$ at 1773^oK giving an activation energy of 29 Kcalories.

Derge, Philbrook, and Goldman [20] determined the diffusion coefficient of sulfur D_s in a slag. They melted a slag having 2% sulfur over an identical sulfur free slag in a blast furnace and suggested that D_s is of the order of 10^{-6} cm^2/sec.

Johnson, Bristow, and Blau [21] found the diffusion coefficient of sodium (Na) in silicates (in glassy state) at about $1273^{\circ}K$ to be between 10^{-6} and 10^{-7} cm^2/sec. They used Na^{24} as a radioactive tracer for their diffusion studies.

Towers and Chipman [22] developed a simple radioactive tracer technique for the measurement of the diffusion coefficient of calcium (Ca^{45} tracer) and silicon (Si^{31} tracer) in a 38.5% CaO - 20.9% Al_2O_3 - 40.5% SiO_2 slag. Ca^{45} tracer was added to the slag in the form of $Ca^{45}O$. Graphite crucibles were used and a microdensitometer record of a film made from a diffusion specimen was used to calculate the diffusion coefficient of calcium. The particulate solution of the diffusion equation they used was:

$$\frac{2C}{C_o} - 1 = - \left(\text{erf} \frac{x}{2(Dt)^{\frac{1}{2}}}\right) \qquad (7.1)$$

this was the case of a semi-cylinder, where C_o is the initial concentration of Ca^{45} in the active slag (as is called when the tracer is added to slag) and C its concentration at distance x from the interface after time t.

They obtained Si^{31} by deuteron bombardment of finely ground high-purity silicon in cyclotron to study the diffusion coefficient of Si^{31} in liquid slag. The isotope Si^{31} emits β rays of maximum energy 1.8 Mev

and has a half-life of about 2.7 hours. Due to its short half-life, measurement of silicon diffusion was difficult.

Their results are shown in Figure 7.1. Average values of D_{Ca} at $1623^{o}K$, $1773^{o}K$ and $1813^{o}K$ resp. were found to be 3.5×10^{-7}, 2.1×10^{-6} and 3.4×10^{-6} $cm^2/sec.$ giving the energy of activation to be 70 K cal. Average values of D_{Si} at $1638^{o}K$ and $1703^{o}K$ are 4.7×10^{-8} and 1.05×10^{-7} $cm^2/sec.$ Results for D_{Ca} found earlier was in good agreement with this.

Absorption of Potassium (K) Into Slag

The isotope K^{43} emits β rays of maximum energy 1.8 Mev and has a half-life of about 22.4 hours. This half-life is short in order to carry the diffusion coefficient measurement in slag, but as seen in the above literature for Si^{31} diffusion, diffusion study of K could be possible. This experiment involving the radioactive tracer technique is beyond the scope of this dissertation.

Reviewing the literature on the diffusion, it is possible to say that the activation energy for potassium diffusion in slag could range between 50 K cal. to 70 K cal. Calcium in the periodic table is just one atomic number above potassium. Their atomic weights also differ by a factor of one. It is believed that the diffusion coefficient for K in slag would range from 10^{-6} to 10^{-8} $cm^2/sec.$ in accordance with above theory.

The residence time τ or the time of adsorption given by Equation (1.4) $\tau = \tau_o$ Exp (Q/RT) is calcualted for different temperatures, by assuming the activation energy to be 60 K cal. Table 7.1 represents the

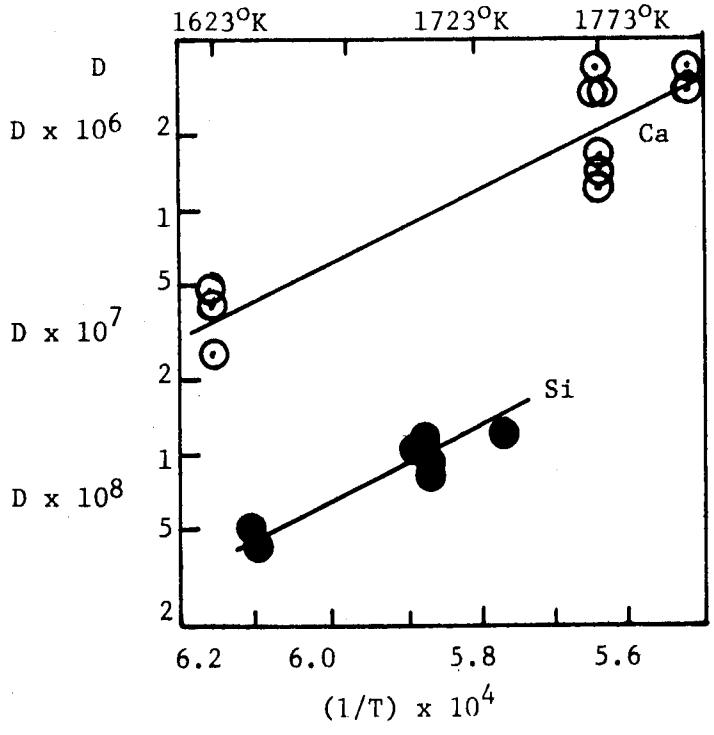

Figure 7.1. Diffusion Coefficients of Calcium and Silicon in a Slag (Ref. 22).

TABLE 7.1. DEPENDENCE OF TEMPERATURE T ON RESIDENCE TIME τ FOR 60 K CAL ENERGY OF ACTIVATION

Temperature T ^{o}K	Residence Time In Sec. for 60 Kcal
1300	1.22×10^{-4}
1400	2.33×10^{-5}
1500	5.53×10^{-6}
1800	1.93×10^{-7}
1900	7.98×10^{-8}
2000	3.61×10^{-8}
2100	1.76×10^{-8}

calculated values of τ suggesting the higher the temperature the lower the residence time, so there will be less absorption. Assuming that the surface absorbed potassium sulfate or a new chemical compound formed from it diffuses into slag, the Figure 7.2 indicates the mean concentration of the diffused species $\bar{c}$ in the spherical droplet of the slag calculated for different times of adsorption. Equation 1.1 from Chapter I (page 10) is used to calculate $\bar{c}$ by assuming the value of 10^{-7} cm^2/sec. for the diffusion coefficient. It is observed from this plot that as the time of adsorption or the residence time decreases which corresponds to the higher temperature, the diffusion of any substance into the spherical droplet of slag is less as predicted. Similarly, the calculations of the $\bar{c}$ (Equation (1.4) page 14) for diffusion into two-dimensional wall layer show less diffusion for higher temperatures (Figure 7.3). That is to say at the wall temperatures in the MHD generator flow train, potassium sulfate may have more opportunity to diffuse into slag or large chunk pieces blown from the walls of the system. The overall potassium seed recovery becomes scale dependent. Full scale MHD plant will have large volume to the cooled-surface area ratios and, therefore, the seed recovery will be higher than would be experienced in these experiments.

Figure 7.4 indicates that the experimental results lies in the range of diffusion coefficient 10^{-6} to 10^{-8} cm^2/sec. Lower limit in this data gives the flow residence time up to the entrance of the cyclone and upper limit is the flow time of the system including the cyclone. This is the residence time potassium molecule has to adsorb on the surface of slag particles or diffuse into it. Slag compounds are solidified at about

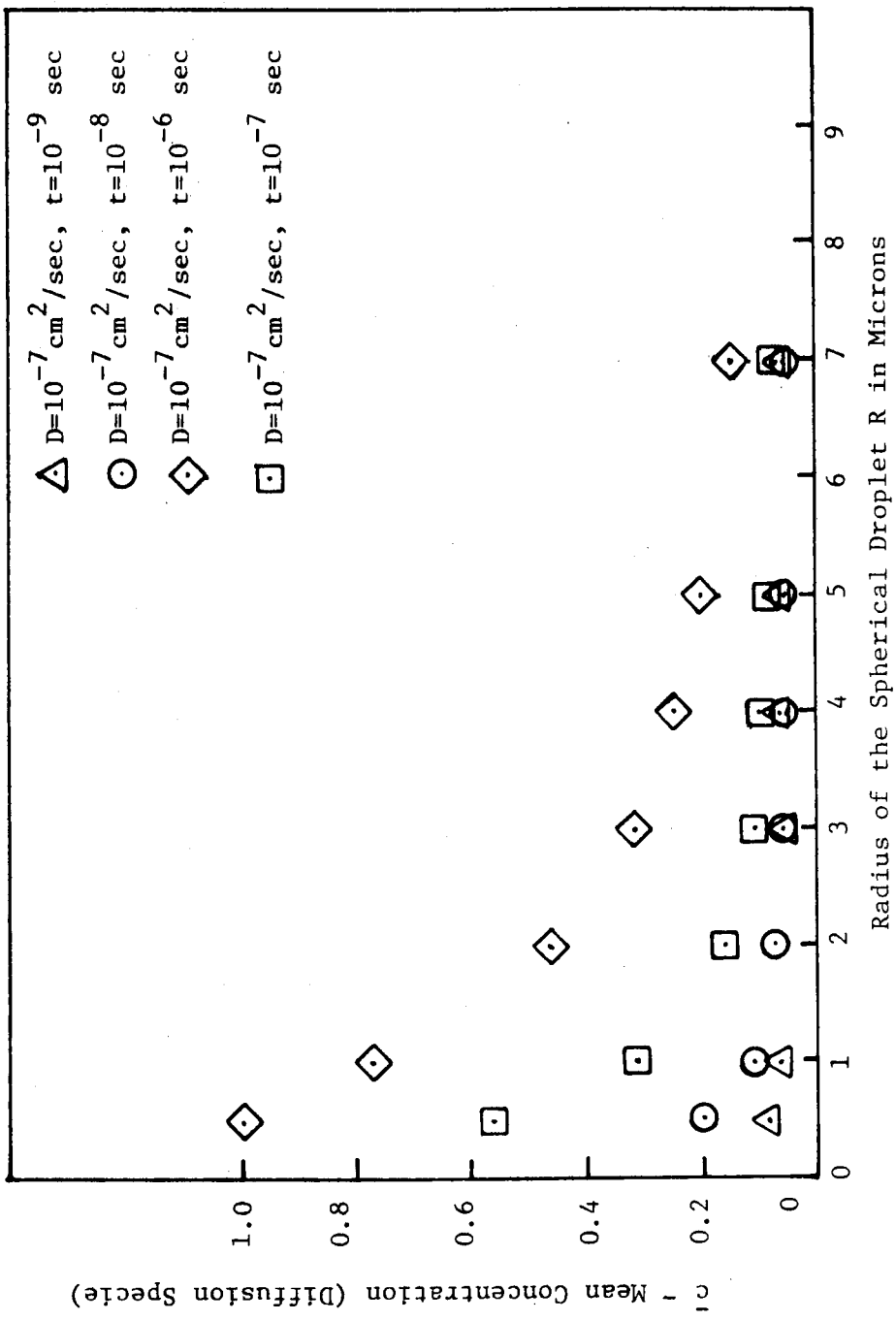

Figure 7.2. Diffusion Into Spherical Droplet.

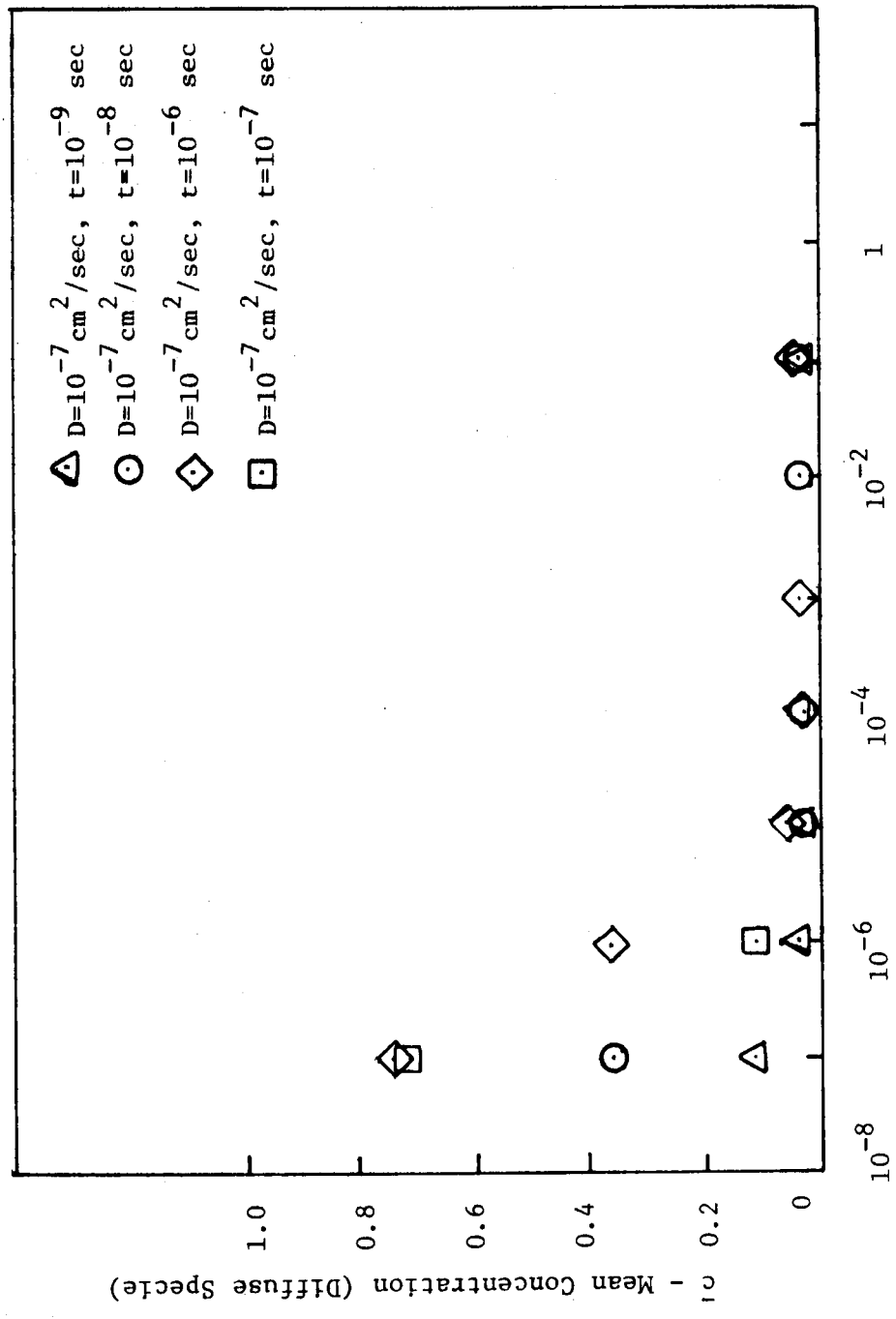

Figure 7.3. Diffusion Into Two-Dimensional Wall Thickness.

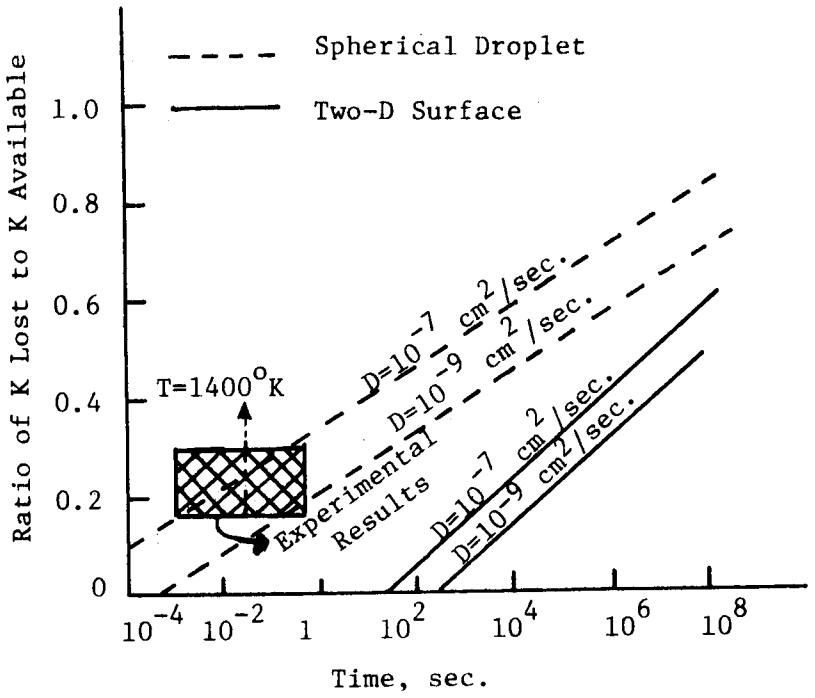

Figure 7.4. Diffusion Times Into Spherical and Two-Dimensional Surface.

1700°K to 1900°K and the potassium sulfate (K_2SO_4) becomes solid at about 1400°K. Above this temperature (1400°K) there will actually be no diffusion. Residence time would be less than the upper limit shown in Figure 7.4, (page 137). All this discussion leads to conclusion that diffusion constant for potassium compounds into slag compounds will be around $10^{-7} cm^2/sec$.

Table 7.2 summarizes the ratio of the experimental values for potassium lost in the MHD system to that of the calculated equilibrium value taken from Reference (2). It shows the experimental results are 30% to 60% lower than the predicted equilibrium results.

TABLE 7.2. COMPARISON OF EXPERIMENTAL RESULTS WITH EQUILIBRIUM CALCULATIONS FOR POTASSIUM LOSS

Temperature ^{o}K	$\frac{\text{(K Lost) Experimental}}{\text{(K Lost) Equilibrium}}$
1400*	0.023
1630	0.54
1690	0.29
1700	0.38
1720	0.57
1740	0.58
1950	0.59

*Test Runs With A Magnetic Field From Test System I.

CHAPTER VIII

SUMMARY AND CONCLUSIONS

The principal conclusion from this experimental work is that the slag/seed separation cyclone performed well and served the purpose of separating potassium compounds from slag compounds, yielding useful information on the slag/seed interaction and separation process with high-ash carryover through the generator. Test results indicate the collection efficiency of the slag/seed separation cyclones varied from about 70% to 95% with the materials having sizes of 5 microns and above over a wide range of test conditions.

Analysis of Material Collected From Cyclone

The particulate matter collected by the cyclone consisted of about 50% fine dust and 50% "chunk-like" pieces. In general, the chunk material had lower percentage by weight of potassium than the dust material. Test results indicated that the composition of the dust material from Test System I had a slightly lower percentage by weight of potassium than that of Test System II. However, the potassium content in the chunk material taken from Test System II when K_2SO_4 seed was used, was three times greater than that which was taken from Test System I. While K_2CO_3 seeding test results indicate the difference between the composition of chunk material from both test systems varied by a factor of 13 to 15. This could be due to the presence of the magnetic field in Test System I and/or the geometry of the MHD flow train. Dust material viewed under SEM and EDX indicated the existence of the elements such as aluminum (Al),

silicon (Si), sulfur (S), potassium (K), calcium (Ca), iron (Fe), titanium (Ti) and some traces of chlorine (Cl) which confirmed the chemical analysis.

Wall samples from the system were investigated under the scanning electron microscope and with EDX analysis and chemical analysis, in order to determine potassium seed loss into slag layer. These results indicate the K_2SO_4 seed loss to the slag layer probably occurs during the start-up. The losses measured would not continuously occur during running the MHD plant (i.e. the slag layer loss may be a one-time start-up effect).

Test results of the composition of the cyclone effluent sampled according to an EPA requirements, indicated that the flat filters used in the sampling train of Test System II may be more effective than the "tube-like" thimble used in Test System I. Potassium content in the particulate emissions concentration in Test System I ($B \neq 0$) was greater than that of Test System II ($B=0$). It was concluded from these results that the presence of magnetic field strength may influence the potassium seed recovery due to the suppression of flow turbulence.

Seed Recovery

Particulate matter collected by the cyclone was weighed and water washed in order to recover the soluble component K_2SO_4. This experimental result obtained showed that there are several factors which influence the potassium seed recovery in a direct coal-fired open-cycle MHD power generator. It was found that increasing (1) the magnetic field strength,

(2) temperature at the entrance of slag/seed separation cyclone and (3) plant scale will influence the absorption of potassium into slag and result in an increase of the seed recovery. It was also note in accordance with Reference (17) that the rate of formation of potassium sulfate in the slag/seed interaction at high temperature is fast and the potassium will diffuse more easily into the spherical droplets than into the slag layer on the walls. This supports the above conclusion that K losses to wall layers are associated with the facility start-up. It was found that the formation of large particles in the dust tends to increase the seed recovery. A peak observed in predicted seed loss calculations in the temperature range of $1600^{o}K$ to $1700^{o}K$ in the equilibrium model by Spencer et al.[2] is found to be in agreement with the peak found in the experimental results at lower potassium absorption by slag than for equilibrium model. Experimental results show lower K absorption than predicted by equilibrium theory by a factor of 50% to 70%.

Sulfur Dioxide (SO_2) Control

Sulfur dioxide (SO_2) emissions were investigated indicate for low sulfur content coal (less than 3%) the combination of K_2SO_4 and K_2CO_3 seed in MHD generator is suitable (1) to chemically react all sulfur present in coal with K (potassium) from seed and form potassium sulfate which through chemical transformation can be recycled and (2) to achieve the necessary electrical conductivity of plasma. For high sulfur content coal (greater than 3%) an additional K_2CO_3 seed is needed than that required to achieve the electrical conductivity of the coal seeded MHD plasma. About 60% to 85% of SO_2 was recovered for low sulfur content

coal during these runs suggesting MHD power plant to be an environmentally acceptable form of energy conversion.

Discussion presented on diffusion coefficient of metals into slag indicated the diffusion coefficient for K into slag based on this experimental data is in the range of 10^{-6} cm^2/sec. to 10^{-8} cm^2/sec.

Recommendation for Future Work on the Absorption of Potassium Seed by Slag Compounds

(1) Future tests in Test System II should be with the EPA type sampling equipment at the cyclone exit and conducted in the presence of a magnetic field to obtain more information concerning its effect on seed recovery.

(2) X-ray diffraction may be used to analyze the slag samples in detail for complex chemical compounds such as K_2SiO_3, $K_2Al_2O_3$ or $KAlSi_3O_8$, etc.

(3) Diffusion coefficients for potassium compounds into slag compounds may be found by a radioactive tracer technique and would be useful in future tests to reduce seed losses.

(4) The first test run should be made on unseeded coal to better understand the start-up seed losses.

(5) Various kinds of coal should be tested to determine the effect of ash and sulfur content of coal on seed recovery.

(6) Means of removing and analyzing a slag sample on-line before the cyclone entrance and at the exit of the cyclone should be developed in order to find the reaction rate.

(7) Extend this work to lower combustion gas temperature so that the slag/seed separation process can be investigated in a range where diffusion coefficients will decrease with decreasing separation temperature.

(8) Since the radiant boiler used in this investigation operated at temperature higher than conventional radiant boilers it would be desirable to have data at the conventional radiant boiler temperatures.

BIBLIOGRAPHY

BIBLIOGRAPHY

1. Bienstock, D., et al., "Air Pollution Aspects of MHD Power Generation," Proceedings of Thirteenth Symposium Engineering Aspects of MHD, March 26-28, 1973.

2. Spencer, F. E., et al., "A Ternary Margules-Type Model for Plasma/Slag Equilibrium in Potassium Seeded Coal Combustion for Magneto-hydrodynamic Power Generation: Calculations and Comparisons With Experiments," Sixth International Conference on Magnetohydrodynamic Electrical Power Generation, Vol. II, June 9-13, 1975.

3. Hals, F., Keefe, L., and El Binden, A., "Studies of Seed Recovery and Corrosion in Coal-Fifed MHD Power Plant," ASME Paper 64-WA/ENER-5, ASME Winter Annual Meeting, Nov.-Dec., 1964.

4. Dicks, J. B., et al., "The Direct Coal-Fired MHD Generator System," Proceedings of Fourteenth Symposium on Engineering Aspects of MHD, April 8-10, 1974.

5. Styrikovich, M. A., et al., "Ionizing Additive Input and Output in the U-25," High Temperature, Vol. 12, No. 2, March-April, 1974 (Nov. 1974).

6. Crawford, L., Tempelmeyer, K., Martin, J., Muehlhauser, J., "Investigation of Slag Deposits and Seed Absorption in a Direct-Fired MHD Power Generator," Sixth International Conference on MHD Electrical Power Generation, Vol. II, June 9-13, 1975.

7. Heywood, J. B., and Womack, G. J., Open Cycle MHD Power Generation, Pergamon Press, Oxford, 1969.

8. Carslaw, H. S., and Jaeger, J. C., Conduction of Heat in Solids, Clarendon Press, Oxford, 1959.

9. Jost, W., Diffusion in Solids, Liquids, Gages, Academic Press, Inc., New York.

10. deBOER, J. H., The Dynamical Character of Adsorption, Clarendon Press, Oxford, 1953.

11. Mori Yasuo and Hijikata Kunio, "Theoretical Study of Diffusion and Condensation of Seeded Potassium Salt on Cooled Wall," Fifth International Conference on Magnetohydrodynamic Electrical Power Generation, Vol. I, April 19-23, 1971.

12. Dicks, J. B., "Design and Operation of Open Cycle Hall Current Neutralized MHD Accelerators and Generators With Diagonal Conducting Strip Walls," Proceedings of 5th Symposium on Engineering Aspects of MHD, MIT, Cambridge, Massachusetts, April 1964.

13. Brenchley, D. L., Turley, C. D., Yarmac, R. F., Industrial Source Sampling, Ann Arbor Science Publishers, Inc., Michigan.

14. Federal Register, Part II, Environmental Protection Agency - Standards of Performance for New Stationary Sources.

15. Inter Society Committee, Methods of Air Sampling and Analysis, American Public Health Association, Washington, D. C.

16. White, H. J., "Electrostatis Precipitation of Flyash," Journal of the Air Pollution Control Association, Vol. 27, No. 2, February 1977.

17. Fletcher, A. W., and Gibson, E. J., "The Use of Carbon-14 and Sulfur-35 in Chemical Problems of Fuel Research," Radioisotope Conference, Oxford, Vol. II, 40-8, (1954).

18. Shapiro, A. H., and Ericksen, A. J., "On the Changing Size Spectrum of Particle Clouds Undergoing Evaporation; Combustion or Acceleration," Trans. ASME, 79, p. 775, 1957.

19. McCallum, N., and Barrett, L. R., "Some Aspects of the Corrosion of Refractories," Trans. Brit. Ceram. Soc. 51, p. 548, 1952.

20. Derge, G., Philbrook, W. O., and Goldman, K. M., "The Mechanism of Sulfur Transfer Between Carbon-Saturated Iron and $CaO-SiO_2-Al_2O_3$ Slags," Trans. AIME, 188, p. 1119, 1950.

21. Johnson, J. R., Bristow, R. H., and Blau, H. H., "Diffusion of Ions in Some Simple Glasses," Journal Amer. Ceram. Soc., 34, p. 165, 1951.

22. Towers, H., and Chipman, J., "Diffusion of Calcium and Silicon in a Lime-Alumina Silica Slag," Trans. AIME, June 1957.

APPENDICES

APPENDIX A

CHEMICAL ANALYSIS METHODS

1. Moisture - Oven at 105°C gravimetric.

2. K-Atomic Absorption ± 0.5%.

   Nitric/HCl dissolve and analysis.

3. SiO_2

   HCl Method for SiO_2 ±0.1%

   (a) Dehydr. and dissolve in HCl/Nitric Acid.
   (b) Evap. to dryness.
   (c) Redissolve in HCl.
   (d) Filter and Wash.
   (e) Ash in Pt crul. 1000°C and Wt.
   (f) Add dry H_2SO_4 and HCl evaporate.
   (g) Reheat and get weight loss.

4. SO_4 Precipatate as $BaSO_4$ by treatment with BaCl, filter on Whatman 40, wash, ash and weight.

5. Al and Fe

   (1) Precipitate with NH_3OH get Al and Fe as NH_3OH group.
   (2) Ash at 1000°C.
   (3) Weight $Al_2O_3 + Fe_2O_3$.
   (4) Dichloremate method (Titrate for Fe_2O_3)
   (Calcium to Fe)
   (5) Use value of Fe_2O_3 to get Al_2O_3 from total, Calcium Al.

6. Cu, Ca, Na — Atomic absorption using same nitric and HCl acid solutions as for K ±.5%.

7. Total Sulfur w/Leakco furnace, titrator — combustion → SO_2

$$S_{free} = S_{Tot} - S_{SO_2}$$

8. Carbon-ash and measure weight change.

Impinter Solutions

1. SO_2 BACl $BaSO_4$ ash and weight — very accurate 0.1%.
2. K-atomic absorption 0.5%.

report as mg/liter of solution

APPENDIX B

THE SCANNING ELECTRON MICROSCOPE

The scanning electron microscope produces images of specimens using secondary electrons emitted from the specimen. The electron signal is collected by a phosphorescent detector and changed to a current signal by a photomultiplier tube. The photomultiplier output is used to produce an intensity modulated image on the screen of a cathode ray tube. The sample can be of any size and thickness that will fit in the evacuated sample chamber of the instrument.

The electrons are emitted from a heated tungsten wire and accelerated through a 20,000 volt potential down a column. The electron beam is condensed (or attenuated), focused, shaped, and scanned across the specimen surface by a series of electromagnetic lenses and coils located in the column. The electron beam impinges upon the specimen and causes secondary electrons and x-rays to be generated within the specimen as well as primary electrons reflected or back-scattered from the specimen surface. The samples, which are the specimen used in this experiment, were dust and chunks in some runs. The x-rays and secondary electrons which escape the specimen are generated in a thin layer on the specimen surface. The energy of the x-rays is characteristic of the element from which the x-ray is emitted, and, therefore, can be used to identify the elements present at the specimen surface. A silicon disc with an applied voltage acts as the x-ray detector with the electrical conductivity of the silicon being varied in proportion to the energy of incident x-rays.

X-ray impulses are counted and stored in a multi-channel analyzer. The resulting x-ray energy spectra (EDX) are plots of number versus x-ray energy. After an appropriate counting time, the spectra will exhibit peaks whose centers are located at energies which can be correlated to atomic number of a particular element. The particulate samples were analyzed by the use of a scanning electron microscope (SEM) and EDX in the University of Tennessee Space Institute, Materials Laboratory, for Test System II and from other outside Laboratory for Test System I.

APPENDIX C

MEASUREMENT ACCURACIES

Water Temperature	± 1%
Coal Flow	± 1%
Oxygen Flow	± 1%
Cyclone Entrance Temperature	± 10%
Stack Gas Temperature	± 10%
Cooling Water Flow Rate	± 1 PSI
Chemical Analysis	
Potassium (K)	± 0.5%
Silica (SiO_2)	± 0.1%
Aluminum (Al)	± 0.1%
Iron (Fe)	± 0.1%
Copper (Cu)	± 0.5%
Calcium (Ca)	± 0.5%
Sodium (Na)	± 0.5%

VITA

The author, Latika S. R. Becker was born in Bombay, India, on November 26, 1946. She received the Bachelor of Science Degree and the Master of Science Degree in Physics from the University of Bombay in April 1966 and June 1969, respectively. From June 1966 to August 1970, she was a lab instructor in undergraduate physics at the University of Bombay. In September 1970, she entered the graduate school at Tennessee Technological University and in June 1972 received the degree of Master of Science in Electrical Engineering. She received the Doctor of Philosophy Degree in June, 1977, from The University of Tennessee, Knoxville.

The author is a member of The Institute of Electrical and Electronic Engineers, The American Physical Society, Federation of American Scientists and the Eta Kappa Nu.